Universidade do Minho
Escola de Engenharia

Catarina Gonçalves

Development of self-assembled dextrin nanogels

Maio 2010

Catarina Gonçalves **Development of self-assembled dextrin nanogels**

UMinho | 2010

Universidade do Minho
Escola de Engenharia

Catarina Gonçalves

Development of self-assembled dextrin nanogels

Tese no Programa de Doutoramento em Engenharia Biomédica

Trabalho efectuado sob a orientação do
Doutor Francisco Miguel Portela Gama

Maio 2010

Agradecimentos

Sem dúvida que a escrita desta tese não ficaria completa se não existisse uma palavra de gratidão a todos aqueles que de uma forma ou de outra contribuíram para que tudo o que ela implica acontecesse.

Começo por agradecer ao professor Miguel Gama, orientador principal deste trabalho, o conhecimento transmitido e a amizade. Quero agradecer de forma especial a sua rapidez na correcção dos documentos e dizer que muitas vezes pensei: “Era mesmo isto que queria dizer…”, quando lia as suas correcções.

Não podia deixar de referir os meus colegas de laboratório/departamento. Quero agradecer de forma especial à Paulinha, a sua ajuda preciosa, pois no tempo da minha licença de maternidade proseguiu com o trabalho de forma dedicada e empenhada. Su (A lutadora), Carlota (O exemplo), Vera (A paciente), Joana (A multifacetada), Neri (O optimista), Reinaldo (O conselheiro informático), Sílvia Ferreira (A trabalhadora), Sílvia Pedrosa (A bem disposta), Renata (A tranquila) e Fábia (A empenhada), gostava de dizer-lhes que é bom sair de casa de manhã e pensar que vamos encontrar aqueles que fazem de mais um dia, um dia feliz! Obrigada pela vossa amizade.

Aos meus familiares, e amigos de longa data, queria agradecer o incentivo e o apoio. Especialmente aos meus pais… quero dizer-lhes obrigada por tudo, a eles devo a pessoa que hoje sou. Obrigada pela educação, pelas palavras, pelos exemplos e pelo carinho. Ao meu marido… obrigada pelo amor, dedicação, e todas as palavras de incentivo. Á minha filha… que nasceu na fase final deste trabalho, quero dizer-lhe que os seus gestos e expressões muitas vezes me transmitiram tranquilidade.

Ao professores José Alberto Martins, Isabel Prata, Paula Gameiro, Margarida Bastos, Ana Maria Gil, Brian Goodfellow e à Engenheira Madalena Vieira, obrigada pelo conhecimento que me transmitiram e pelo apoio técnico.

Dedico esta tese
aos meus pais…

Abstract

Polymeric nanogels - also referred to as hydrogel nanoparticles, macromolecular micelles or polymeric nanoparticles - are emerging as promising drug carriers for therapeutic applications. These nanostructures hold versatility and properties suitable for the delivery of bioactive molecules, namely biopharmaceuticals. The polymer and the production methodology used are fundamental options. These systems may be obtained by incorporation of targeting moieties, detectable probes and/or degradable bonds allowing a controlled release in the physiologic environment which lead to smart systems reactive to physiologic stimuli, etc. A particular challenge in this field is the development of preparation procedures avoiding the use of organic solvents or surfactants.

Dextrin is a very promising biomaterial, available in medical grade and accepted by the *United States Food and Drug Administration* for application in humans. It is a polymer composed of α-(1-4) D-glucose units. In this work, dextrin was modified with long alkyl chains to produce an amphiphilic molecule. Dextrin-VA-SC_{16} ($dexC_{16}$) has a hydrophilic dextrin backbone with grafted acrylate groups (VA), substituted with hydrophobic 1-hexadecanethiol (SC_{16}). A versatile synthetic method was developed allowing control of the dextrin degree of substitution with the hydrophobic chains. Upon dispersion in water, $dexC_{16}$ self-assembles through association of the hydrophobic alkyl chains, originating nanoparticles. The hydrophobic chains, randomly distributed along the polymer backbone, promote the formation of hydrophobic domains within the nanoparticles. Colloidally stable nanoparticles were obtained. An average diameter of about 20 nm was determined by dynamic light scattering, atomic force microscopy and transmission electron microscopy. The critical micelle concentration, around 0.001 g/dL, was determined using pyrene as a fluorescent probe, and confirmed by dynamic light scattering. The influence of the degree of substitution on nanoparticles size, colloidal stability, density, aggregation number and nanoparticle weight was studied. The more substituted polymer forms more densely packed hydrophobic domains, such that the colloidal stability (in water or phosphate buffered saline solution) of nanoparticles is increased. Size distribution was also evaluated at different pH, urea concentration and ionic strength conditions. The nanoparticles have a slightly higher size when prepared in buffer (irrespective of the pH) or in the presence of a salt or urea (irrespective of the concentration).

The uptake of nanoparticles by cells of the mononuclear phagocytic system limits its use as colloidal drug carriers, reducing the blood circulation time and the ability to reach

biological targets. The interaction between dextrin nanoparticles and murine bone marrow-derived macrophages was evaluated *in vitro* by confocal laser scanning microscopy and fluorescence activated cell sorting. Fluorescein-labelled nanoparticles were used to assess the phagocytic uptake and blood clearance after intravenous injection. Cytotoxicity and nitric oxide production were studied, using the 3-(4,5-dimethylthiazol-2-yl)-2,5-diphenyl-tetrazolium bromide (MTT) assay and the Griess method, respectively. The results show that the nanoparticles are not cytotoxic and do not stimulate the production of nitric oxide by macrophages, in the range of concentrations studied. Nanoparticles are phagocytosed by macrophages and are detected inside the cells, concentrated in cellular organelles. The blood clearance study showed that the blood removal of the nanoparticles occurs with a more pronounced rate in the first 3 h after administration, about 30% of the material remaining in systemic circulation at this stage. The tissue distribution, after intravenous injection in Wistar rats, was evaluated using functionalized nanoparticles with a 1,4,7,10-tetraazacyclododecanetetraacetic acid (DOTA) metal chelator and subsequently labelled with the γ-emitting $^{153}Sm^{3+}$ radioisotope. The blood clearance rate and organ biodistribution of radioactively labelled nanoparticles was analysed, using materials both with and without poly(ethylene glycol) surface coating. The dexC_{16} nanoparticles display a characteristic biodistribution profile, being mainly taken up by the organs of the mononuclear phagocyte system - liver and spleen. The blood circulation time extends to several hours – as observed using the fluorescein-labelled nanoparticles, although the concentration is halved in about 1 hour. The functionalization of the nanoparticles with PEG 5,000 in this formulation improves their circulation time in the bloodstream and reduces the accumulation in the liver and spleen.

In order to explore the ability of dextrin nanoparticles as a drug carrier, curcumin was used as a model hydrophobic drug. Curcumin is a natural polyphenol with anti-oxidative, anti-inflammatory and anti-cancer properties. However, its therapeutical potential is substantially hindered by the rather low water solubility and bioavailability. Dextrin nanoparticles were tested as a curcumin carrier, allowing its dispersion in water, improving stability, and controlling release profile. Incorporation of curcumin into nanoparticles did not compromise its cytotoxicity in HeLa cell line.

Resumo

Nanogéis poliméricos - também designados hidrogéis nanoparticulados, micelas macromoleculares ou nanopartículas poliméricas - têm-se revelado transportadores promissores de fármacos para aplicações terapêuticas. Estas nano-estruturas possuem versatilidade e propriedades adequadas para a libertação de moléculas bioactivas, nomeadamente biofármacos. A escolha do polímero e da metodologia de obtenção das nanopartículas é fundamental. Estes sistemas podem incorporar sondas para o seu direccionamento ou detecção e/ou ligações lábeis em ambiente fisiológico proporcionando uma degradação controlada constituindo assim sistemas inteligentes reactivos a estímulos fisiológicos. Um dos principais desafios neste campo é o desenvolvimento de procedimentos de preparação que não recorram a solventes orgânicos ou surfactantes.

O dextrino é um biomaterial, disponível em grau médico e autorizado pela *United States Food and Drug Administration* para aplicações em humanos. Trata-se de um polímero composto por unidades de glucose ligadas por ligações α-(1-4). Neste trabalho, o dextrino foi modificado com cadeias alquílicas longas obtendo-se assim uma molécula anfifílica. O dextrino-VA-SC_{16} ($dexC_{16}$) tem uma cadeia hidrofílica de dextrino com grupos acrilato enxertados (VA), por sua vez substituídos com a molécula hidrofóbica 1-hexadecanetiol (SC_{16}). Foi desenvolvido um método de síntese versátil que permite o controlo do grau de substituição do dextrino com cadeias hidrofóbicas. Ao ser disperso em água, o $dexC_{16}$ auto-organiza-se através da associação das cadeias alquílicas hidrofóbicas, originando nanopartículas. As cadeias hidrofóbicas, aleatoriamente distribuídas na cadeia polimérica, promovem a formação de domínios hidrofóbicos no interior das nanopartículas. Foram assim obtidas nanopartículas coloidalmente estáveis, com um diâmetro médio aproximado de 20 nm, confirmado por difracção dinâmica da luz e miscroscopia de força atómica e de transmissão de electrões. A concentração micelar crítica, igual a aproximadamente 0.001 g/dL, foi determinada usando pireno como sonda fluorescente e foi confirmada por difracção dinâmica da luz. Foi caracterizada a influência do grau de substituição no tamanho das nanopartículas, na estabilidade colloidal, densidade, número de agregação e peso das nanopartículas. O polímero com maior grau de substituição origina domínios hidrofóbicos mais densos, aumentando a estabilidade coloidal (em água ou solução PBS) das nanopartículas. A distribuição de tamanhos das nanopartículas foi também avaliada em diferentes condições de pH, concentração de ureia e força iónica. As nanopartículas apresentam um ligeiro aumento

de tamanho quando preparadas em tampão (independentemente do pH) ou na presença de sal ou ureia (independentemente da concentração).

A internalização das nanopartículas pelas células do sistema mononuclear fagocitário limita o seu uso como transportador coloidal de fármacos, uma vez que reduz o tempo de circulação no sangue e a possibilidade de atingirem os alvos biológicos. A interacção entre as nanopartículas de dextrino e macrófagos extraídos da medula óssea de ratinho foi avaliada *in vitro* por microscopia confocal e por citometria de fluxo. Nanopartículas marcadas com fluoresceína foram usadas para avaliar a internalização por fagocitose e a eliminação do sangue após injecção intravenosa. A citotoxicidade e a produção de óxido nitrico foram estudadas, usando o ensaio de MTT e o método de Griess, respectivamente. Os resultados mostram que as nanopartículas não são citotóxicas e não estimulam a produção de óxido nitrico pelos macrófagos, na gama de concentrações estudada. As nanopartículas são fagocitadas pelos macrófagos e foram detectadas no interior das células, concentradas em organelos celulares. O estudo da eliminação das nanopartículas do sangue mostrou que a sua remoção da corrente sanguinea ocorre de forma mais pronunciada nas 3 horas que seguem a administração, após o que cerca de 30% do material permanece em circulação. A distribuição nos tecidos, após injecção intravenosa em ratos Wistar, foi avaliada usando nanopartículas funcionalizadas com um agente complexante do tipo DOTA e posteriormente marcadas com o radioisótopo γ-emissor $^{153}Sm^{3+}$. A eliminação do sangue e a biodistribuição das nanopartículas marcadas radioactivamente foi analisada usando materiais cobertos e não-cobertos com polietilenoglicol. As nanopartículas de $dexC_{16}$ apresentam um perfil de biodistribuição característico sendo principalmente internalizadas pelos órgãos do sistema mononuclear fagocitário – fígado e baço. O tempo de circulação no sangue extende-se até algumas horas, apesar de a concentração ser reduzida para metade em cerca de 1 hora. A funcionalização das nanopartículas com polietilenoglicol 5000 aumenta o tempo de circulação no sangue e reduz a acumulação no fígado e no baço.

Com o objectivo de explorar o potencial das nanopartículas de dextrino como transportador de fármacos, a curcumina foi usada como um fármaco hidrofóbico modelo. A curcumina é um polifenol natural com propriedades anti-oxidativas, anti-inflamatórias e anti-cancerígenas. No entanto, o seu potencial terapêutico é comprometido pela reduzida solubilidade em água e biodisponibilidade. As nanopartículas de dextrino foram testadas como transportadores de curcumina permitindo a sua dispersão em água, melhoria da estabilidade e controlo do perfil de libertação. A incorporação da curcumina nas nanopartículas não comprometeu a sua citotoxicidade na linha celular HeLa.

Motivation and Main Goals

The development of biomaterials using natural polymers is an important and promissing field of research. The new technologies of tissue engineering, controlled drug delivery and regenerative medicine draw the need for new biomaterials - biocompatible, processable and degradable. Dextrin, a glucose polymer – unexpensive, available in medical grade and in large amounts - has been basically ignored as an option for these applications. However, its properties make it, in our view, a serious candidate for the production of biomaterials. As compared to starch, dextrin is much more soluble. Having a very low molecular weight, it may be easily excreted – it is also degradable *in vivo* – therefore it will not accumulate in the tissues, having excellent resorbability/excretability. The good solubility improves its potencial for modification, exploiting the reactivity of the hydroxyl groups.

In this work, the production of nanogels made of dextrin was successfully exploited. The chemical reactivity of dextrin was further improved through grafting of acrylic groups. Other parallel ongoing projects include the development of dextrin injectable hydrogels. Thus, different applications of dextrin in the biomedical field are being exploited. Self-assembled nanogels are promissing nanobiotechnological tools with potencial application in the drug delivery and diagnostics. Exploiting the natural ability of biomolecules to self-organize is a biomimetic approach being developed in several laboratories world wide. Much remains to be done in this field. This work attempts to develop new self-assembled nanogels, and the characterization of its properties, namely regarding the interaction with biological systems (cells and organisms) and unveiling aspects of the structural organization of these materials.

Publications

This thesis is based on the following original research or review articles:

Chapter 1: Gonçalves, C., Pereira, P., Gama, F.M. **Self-assembled hydrogel nanoparticles for drug delivery applications.** *Materials* 2010, *3*, 1420-1460.

Chapter 2: Gonçalves, C., Martins, J.A., Gama, F.M. **Self-assembled nanoparticles of dextrin substituted with hexadecanethiol.** *Biomacromolecules* 2007, *8*, 392-398.

Chapter 3: Gonçalves, C., Gama, F.M. **Characterization of the self-assembly process of hydrophobically modified dextrin.** *European Polymer Journal* 2008, *44*, 3529-3534.

Chapter 4: Gonçalves, C., Torrado, E., Martins, T., Pereira, P., Gama, F.M. **Dextrin nanoparticles: Studies on the interaction with murine macrophages and blood clearance.** *Colloids and Surfaces B: Biointerfaces* 2010, *75*, 483-489.

Chapter 5: Gonçalves, C., Pereira, P., Schellenberg, P., Coutinho, P.J.G., Gama, F.M. **Dextrin nanoparticles as a curcumin delivery system; Studies on the stability of self-assembled nanoparticles.** *Submitted.*

Chapter 6: Gonçalves, C., Ferreira, M. F. M., Santos, A.C., Prata, M.I.M., Geraldes, C.F.G.C., Martins, J.A., Gama, F.M. **Studies on the biodistribution of dextrin nanoparticles.** *Submitted.*

Table of Contents

List of Figures

CHAPTER 1

CHAPTER 2

CHAPTER 3

CHAPTER 4

CHAPTER 5

CHAPTER 6

List of Tables

CHAPTER 1

CHAPTER 2

CHAPTER 3

CHAPTER 5

CHAPTER 6

List of Schemes

CHAPTER 2

CHAPTER 6

Abbreviations

A_2	Second virial coefficient
A549	Lung Cancer Cells-bearing mice
AFM	Atomic Force Microscopy
APCs	Antigen-Presenting Cells
AWBP	Artery Wall Binding Peptide
BBB	Blood-Brain Barrier
BMDM	Bone marrow-derived macrophage
BMPs	Bone Morphogenetic Proteins
BP	Betamethasone Disodium 21-Phosphate
C	Concentration
C_{16}	Hydrophobic chains
C2C12	Mouse myoblast Cells
CCL	Core-crosslinked
CHP	Cholesterol-Bearing Pullulan
CM	Curcumin
CMC	Critical micelle concentration
COS-1	Monkey kidney cells
CPB	Cetylpyridinium Bromide
CyA	Cyclosporin A
Cys	Cysteine
DAPI	4',6-diamino-2-phenylindole
DCs	Dendritic Cells
$DexC_{16}$	Hydrophobically modified Dextrin
DexVA	Dextrin-VA
DLS	Dynamic Light Scattering
DMEM	Dulbecco`s modified Eagle`s medium
DMSO	Dimethyl sulfoxide
DNA	Deoxyribonucleic acid
dn/dc	Differencial refractive index increment
D_2O	Deuterium Oxide
DOTA	1,4,7,10-tetraazacyclododecanetetraacetic acid
DS	Degree of Substitution
DS_{C16}	Degree of substitution of dextrin with alkyl chains
DS_{VA}	Degree of substitution of dextrin with acrylate groups
DU145	Prostate Carcinoma Cells
ECV304	Human Vein Endothelial Cells
EDTA	Ethylenediamine tetraacetic acid
EGF	Epidermal Growth Factor
EPR	Enhanced Permeability and Retention
$EuCl_3$	Europium (III) chloride

FACS	Fluorescence activated cell sorting
FDA	Food and Drug Administration
FGF	Fibroblast Growth Factor
FRET	Fluorescence Resonance Energy Transfer
GAD	Glutamic Acid Decarboxylase
GI	Gastrointestinal
HA	Hemagglutinin
HBsAg	Hepatitis B surface Antigen
HBSS	Hanks` balanced salt solution
HCl	Hydrochloric Acid
HCT116	Human Colon Carcinoma Cells
HeLa	Human Cervix Epithelial Carcinoma Cells
HepG2	Human Hepatocellular Carcinoma Cells
HGC	Hydrophobically Modified Glycol Chitosan
IFN-γ	Interferon-gamma
IL	Interleukin
IRF	Instrument Response Function
JE	Japanese Encephalitis
Jurkat	Human T Cell Leukemia
K	Optical constant
KBM-5	Human Chronicmyeloid Leukemia
L929	Mouse Fibroblast Cells
LHRH	Luteinizing Hormone- Releasing Hormone
LMWC	Low Molecular Weight Chitosan
Ln	Lanthanide
LNCaP	Prostate Epithelial Cells
LPS	Lipopolysaccharide
MCF-7	Breast Carcinoma Cells
MD	Microdomains
MDA-MB-231	Breast Adenocarcinoma Cells
mPEG-*b*-p(HEMAm-Lac$_n$)	*N*-(2-hydroxyethyl)methacrylamide-oligolactates
MPS	Mononuclear Phagocyte System
MTS	3-(4,5-dimethylthiazol-2-yl)-5-(3-carboxymethoxyphenyl)-2-(4-sulfophenyl)-2H-tetrazolium
MTT	3-(4,5-dimethylthiazol-2-yl)-2,5-diphenyltetrazolium bromide
M_w	Molecular weight
n_0	Solvent refractive index
N_A	Avogadro`s constant
NaCl	Sodium Chloride
N_{agg}	Aggregation Number
NaOH	Sodium Hydroxide
$NaPO_4$	Sodium Phosphate
NCL	Non-crosslinked

NMR	Nuclear Magnetic Resonance
NO	Nitric oxide
NP	Nanoparticle
NP_w	Weight-average Nanoparticle Weight
ODNs	Oligonucleotides
PBS	Phosphate Buffered Saline
PdI	Polydispersity Index
PE	Phosphatidylethanolamine
PEI	Polyethylenimine
PEG	Poly(ethylene glycol)
PEG-PHDCA	Poly methoxypolyethyleneglycol cyanoacrylate-co-n-hexadecyl
PEG-SH	*O*-[2-(3-Mercaptopropionylamino)ethyl]-*O'*-methylpolyethylene glycol 5,000
PGA	Poly(glycolic acid)
γ-PGA	Poly(γ-glutamic acid)
PLA	Poly(D,L lactic acid)
PLGA	Poly(D,L-lactic-co-glycolic acid)
PLL	Poly-L-lysine
Py	Pyrene
Q	Quencher
QSY-7	QSY-7 amine hydrochloride
R_θ	Rayleigh ratio
RGD	Arg-Gly-Asp
R_H	Hydrodynamic radius
rmIL-12	Recombinant murine interleukin-12
RNA	Ribonucleic acid
RSV	Respiratory Syncytial Virus
SAMSA-F	SAMSA (5-((2-(and-3)-S-(acetylmercapto) succinoyl) amino) fluorescein
SC_{16}	Alkyl chain
SCC7	Squamous Cell Carcinoma Cells
SEG-1	Human Esophageal Adenocarcinoma Cells
siNPRA	Short interfering ribonucleic acid for natriuretic peptide receptor A
siRNA	Short interfering ribonucleic acid
SKOV-3	Epithelial Ovarian Cancer Cells
SLS	Static Light Scattering
Sm	Samarium
$SmCl_3$	Samarium (III) chloride
SW480	Human Colon Carcinoma Cells
SW-1990	Pancreatic Cancer Cells
3T3	Mouse Fibroblasts
TCSPC	Time Correlated Single Photon Counting
TEA	Triethylamine
TEM	Transmission Electron Microscopy
THP-1	Human Monocyte/Macrophage Myelomonocytic Cells

TMC	Trimethyl Chitosan
UV-vis	Ultraviolet-Visible
VA	Vinyl Acrylate
VEGF	Vascular Endothelial Growth Factor
VIP	Vasoactive Intestinal Peptide
z-avg	mean hydrodynamic diameter
λ_0	Laser wavelength
ϕ_H	Average polymer density
τ	Average life time

1. General Introduction: Self-assembled hydrogel nanoparticles for drug delivery applications

Adapted from **Materials** (2010) 3, 1420-1460

Nanotechnology is the source of exciting progresses in the drug delivery field, offering suitable means for site-specific and time-controlled delivery of small molecular weight drugs, proteins, peptides, oligosaccharides, vaccines and nucleic acids (Dubernet*, et al.*, 2002, Jain*, et al.*, 2009, Moghimi*, et al.*, 2001, Panyam*, et al.*, 2003a, Sun*, et al.*, 2008). Overall, drug delivery is the method of administering a bioactive compound to achieve a therapeutic effect, in humans or animals. Drug delivery systems are formulations that modify the drug release profile and the ability to cross biological barriers, the biodistribution and pharmacokinetics, improving its efficacy and safety, as well as the patient compliance. Nanoformulations for drug delivery include numerous architectural designs in terms of size, shape, and materials. Several types of nanoparticles have been tested as potential drug delivery systems, including hydrogel nanoparticles (also known as polymeric nanogels or macromolecular micelles), dendrimers (Nanjwade*, et al.*, 2009), nanospheres (Arias*, et al.*, 2007), nanocapsules and liposomes (Iinuma*, et al.*, 2002). Each kind of formulation has characteristic drug loading capacity, particle and drug stability, drug release rates, and targeting ability. This review highlights the use of self-assembled hydrogel nanoparticles for drug delivery applications. Hydrogels are polymeric networks with three-dimensional configuration that absorb large quantities of water or biological fluids. Their water affinity is attributed to the presence of hydrophilic groups - such as ether, amine, hydroxyl, sulfate and carboxyl - in the polymer chains. Hydrogels can be formulated as macroscopic networks, or confined to smaller dimensions. When their size is in the submicron range, they are known as nanogels

(Vinogradov*, et al.*, 2004). Nanogels, or hydrogel nanoparticles, have gained considerable attention as one of the most promising nanoparticulate drug delivery systems, owing to their unique properties that combine the characteristics of hydrogel systems (e.g., rather high water content) with a very small size (nanosize). Hydrogel nanoparticles are outstanding drug delivery systems:

1. The particle size and surface properties can be manipulated to avoid rapid clearance by phagocytic cells, allowing both passive and active drug targeting;

2. Controlled and sustained drug release at the target site, improving the therapeutic efficacy and reducing side effects. Drug loading is relatively high and may be achieved without chemical reactions; this is an important factor for preserving the drug activity;

3. Ability to reach the smallest capillary vessels, due to their tiny volume, and to penetrate the tissues either through the paracellular or the transcellular pathways;

4. Potential for administration through various routes, including oral, pulmonary, nasal, parenteral, intra-ocular etc.

Self-assembled hydrogel nanoparticles in this context refer to nanogels formed from amphiphilic or polyionic polymers. The main properties of nanoparticles, the method and materials for their production, and the main applications will be reviewed.

1.1 Materials, properties, methods

1.1.1 Materials

A wide range of materials may be used for nanogels preparation. Biodegradability is essential to avoid organ accumulation, potentially leading to toxicity and other undesirable side effects (Peracchia*, et al.*, 1999, Plard*, et al.*, 1999). Hydrogel nanoparticles are made either from natural or synthetic polymers. The former possess a high variety of functional groups, which allow chemical and biochemical modification, resulting in many kinds of biopolymer-based materials. Among these, polysaccharides are the more often used. Polysaccharides are naturally occurring carbohydrate-based polymers, formed of repeating units (monosaccharides) joined together by glycosidic bonds. They may be obtained from algal (alginate), plant (cellulose, starch) and animal (chitosan) sources, exhibit quite variable structures and properties, different reactive

groups, a wide range of molecular weights and variable chemical composition. Polysaccharides can be divided into non-polyelectrolytes (dextran, dextrin, pullulan) and polyelectrolyte. Polyelectrolyte polysaccharides may be further divided into positively (chitosan) and negatively (heparin, hyaluronic acid) charged. Polysaccharides are highly stable, safe, non-toxic, hydrophilic and biodegradable. They are, in addition, abundant natural resources and may be processed at low cost.

Among the more often used synthetic polymers, block copolymers consist of two or more segments of simple polymers (blocks) joined in some arrangement. Block copolymers are further classified by the number of blocks each molecule contains: two, three, or more blocks correspond to diblocks, triblocks, or multiblocks, respectively. Biodegradable and biocompatible poly(D,L lactic acid) (PLA), poly(glycolic acid) (PGA) and their copolymer poly(D,L-lactic-co-glycolic acid) (PLGA) have been extensively used in controlled drug delivery and have been approved by the United States Food and Drug Administration (Hans*, et al.*, 2002).

1.1.2 Properties

The ability of nanodelivery systems to overcome physiological barriers is determined by properties such as particle size, surface charge and hydrophobicity. Physiological barriers are biological structures or physiologic mechanisms that hinder nanoparticles from reaching their targets, therefore compromising the therapeutic efficacy. Nanoparticulate systems able to overcome these biological barriers should be capable of: efficient extravazation through the vasculature, prolonged vascular circulation time, improved cellular uptake and endosomal escape.

The endothelial wall in the vasculature presents reduced permeability and constitutes the primary barrier for nanoparticles. The nanosize may facilitate the penetration of nanoparticles across the endothelium. It is well known that extravazation of nanoparticles into the brain, across the blood-brain barrier, represents a particular difficult challenge for nanomedicine. Small drugs may diffuse through the capillary walls into the tissues. Otherwise, nanoparticles transport occurs through compromised endothelial barrier or mediated by specific transport systems. Tumor tissues have an increased capillary permeability, which allows a high rate of nanoparticles accumulation, based on the “enhanced permeability and retention” (EPR) effect (Matsumura*, et al.*, 1986). Nanoparticles circulating in the bloodstream are normally able to penetrate the tissues through a paracellular path only at restricted sites, where the capillaries have open

fenestrations, as in the sinus endothelium of the liver, in the tumor neovasculature (Brannon-Peppas*, et al.*, 2004) or when the endothelial barrier is altered by inflammatory processes (e.g., rheumatoid arthritis, infections) (Moghimi*, et al.*, 2005).

Surface charge is important as it determines the stability of nanoparticles, hence its propensity to aggregate in the bloodstream or interact with the cell membranes. The zeta potential is commonly used to characterize and measure the surface charge: the larger the absolute value of the zeta potential, the larger the charge on the surface. In a sense, the zeta potential represents an index for particle stability. For charged particles, as the zeta potential increases the repulsive interactions becomes larger, leading to stable particles, likely to have a more uniform size distribution. A nanosuspension stabilized by electrostatic repulsion must have a minimum zeta potential of ±30 mV (Muller*, et al.*, 2001). This stability is important in preventing aggregation (Hornig*, et al.*, 2009). When a surface modifier like PEG is added, the negative zeta potential is lowered, although increasing the nanoparticles stability due to steric effects and hydration forces (Vila*, et al.*, 2002).

Long circulation time increases the odds for the nanoparticles to reach their target. The Mononuclear Phagocyte System (MPS) efficiently eliminates nanoparticles from the bloodstream, unless they are modeled to escape recognition. Opsonization is the process whereby a foreign organism or particle becomes covered with opsonins, thereby making it “visible” to phagocytic cells. This process typically occurs in the bloodstream and can take anywhere from a matter of seconds to many days to complete. Binding of opsonins onto the nanoparticle surface acts as a bridge between nanoparticles and phagocytes. Minimizing protein binding is the key point for developing long circulating time formulations. Together, these two processes – opsonization and phagocytosis - constitute the main blood clearance mechanism for particles larger than the renal threshold limit. There are no absolute rules or methods available to completely block opsonization, but research over the last 30 years yielded useful trends and methods to increase the blood circulation half-life and the effectiveness of “stealth” devices. For instance, it is well established that hydrophilic polymers provide steric stabilization and confers “stealth” invisibility for the body´s natural defense system (Storm*, et al.*, 1995). As a general rule, the opsonization of hydrophobic particles, as compared to hydrophilic ones, has been shown to occur quicker, due the enhanced adsorption of blood serum proteins (Luttmann*, et al.*, 2006). A correlation between surface charge and opsonization has also been demonstrated *in vitro*; neutral particles performing better than charged ones (Roser*, et al.*, 1998). Therefore, a widely used method to slowdown opsonization relies on the use

of shielding groups which can block electrostatic and hydrophobic interactions that help opsonins binding the nanoparticle surfaces. These groups are typically long hydrophilic polymer chains and non-ionic surfactants. Examples of effective shielding groups include polysaccharides, polyacrylamide, poly(vinyl alcohol), poly(*N*-vinyl-2-pyrrolidone), poly(ethylene glycol) (PEG), and PEG-containing copolymers such as poloxamers, poloxamines, polysorbates, and PEG copolymers (Owens*, et al.*, 2006, Storm*, et al.*, 1995). Among the polymers tested to date, the most effective and most used are PEG and PEG-containing copolymers, typically very flexible, highly hydrophilic and not charged, altogether properties lessening the protein binding.

The high mobility of nanoparticles in the smallest capillaries allows for efficient uptake and selective drug accumulation at target sites (Panyam*, et al.*, 2003b). Indeed, cell uptake of nanoparticles is relatively high, when compared to microparticles (> 1 μm) (Akagia*, et al.*, 2007). Specific cell internalization can be improved by surface decoration with targeting ligands (peptide, sugar molecule, antibody, vitamins), which are recognized by target cells/tissues. The release of bioactive molecules into the cytoplasm or nucleous compartments can be a challenging problem. Internalized particles are initially within endosomes but are trafficked rapidly to lysosomes, where they are degraded enzymatically, preventing their action. To avoid lysosomal trafficking, smart polymers with specific chemical groups have been designed.

Although nanogels are indeed rather promising, it must be stressed that their development as products for clinical applications still requires further knowledge on its physico-chemical properties, knowledge on the interaction with cells and tissues, nanotoxicology and safety. Generally, nanoparticles that have a mean diameter of approximately 100 nm, bearing a neutral and hydrophilic surface, exhibit prolonged blood circulation and an increased level of tumor delivery (Brannon-Peppas*, et al.*, 2004).

1.1.3 Methods

The self-assembly process, defined as the autonomous organization of components into structurally well-defined aggregates, is characterized by numerous beneficial attributes; it is cost-effective, versatile and facile; the process occurs towards the system's thermodynamic minima, resulting in stable and robust structures. Molecular self-assembly is characterized by diffusion followed by specific association of molecules through non-covalent interactions, including electrostatic and/or hydrophobic associations (Figure 1.1). Individually, such interactions are weak, but dominate the structural and

conformational behavior of the assembly due to the large number of interactions involved (Zhang, 2002). While oppositely charged polysaccharides associate readily as a result of electrostatic attractions (Rinaudo, 2006), interactions among neutral polysaccharides tend to be weaker, or nonexistent, a modification with chemical entities able to trigger assembly being necessary. A convenient strategy consists on linking hydrophobic grafts to e.g., a highly water-soluble polysaccharide, inducing the formation of nanoparticles via hydrophobic interactions. This kind of amphiphilic polymers can be constructed by three routes: hydrophobic chains grafted to a hydrophilic backbone, hydrophilic chains grafted to a hydrophobic backbone (grafted polymers) or with alternating hydrophilic and hydrophobic segments (block polymers). Upon contact with an aqueous environment, amphiphilic polymers spontaneously form self-aggregated nanoparticles, via intra- or intermolecular associations between the hydrophobic moieties, primarily to minimize the interfacial free energy. The important feature, from the physicochemical point of view, is that the molecule is able to orient itself to expose the hydrophilic regions to the polar environment (normally the aqueous medium) and the hydrophobic segments aggregates in the internal core of the material. The concentration above which the polymeric chains aggregate is called the critical micelle concentration or the critical aggregate concentration. Several strategies for the preparation of nanoparticles have been used, including direct dissolution, solvent evaporation/film formation, dialysis, emulsion, and co-solvent evaporation.

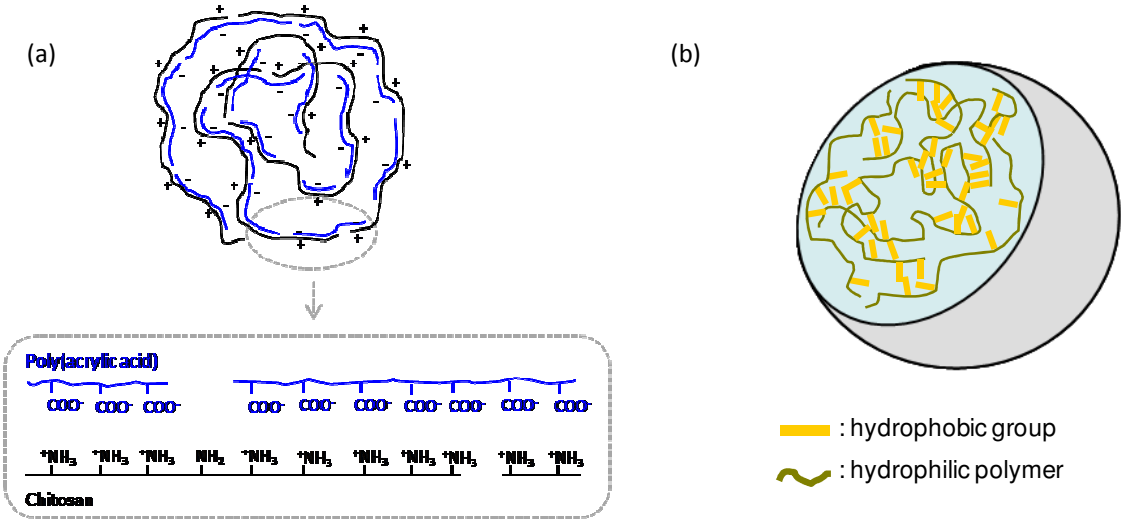

Figure 1.1. Schematic representation of intermolecular interactions driving self-assembly processes (a) electrostatic interactions or (b) hydrophobic association.

The commercialization of nanodevices obtained using these technologies is limited due to the employment of potentially toxic organic solvents and surfactants, often not acceptable, at least for parenteral administration. For example, polymer based nanoparticles may be prepared by the well-known solvent evaporation method, in which the droplets of a nanoemulsion are composed of a volatile organic solvent in which the polymer is solubilized (Soppimath*, et al.*, 2001). Traces of solvent are very difficult to eliminate, even using very sophisticated and time consuming methods such as ultradialysis, ultracentrifugation or ultrafiltration. In general, the currently available nanotechnologies are not able to meet the severe requirements enacted by the public health agencies for medicines. Therefore, there is an urgent need to develop new concepts and ideas to overcome these technological issues by proposing preparation procedures avoiding the use of organic solvents and surfactants. In this view, direct dissolution in pure water is the most suitable strategy to obtain nanogels (Gonçalves*, et al.*, 2007).

1.2 Drug loading, targeting and release

1.2.1 Drug loading

Nanogels are widely used as carriers of therapeutic agents. A successful nanodelivery system should have a high drug-loading capacity, thereby reducing the required amount of carrier. Therapeutic agents can either be physically entrapped into the polymeric matrix or covalently bound to the polymer backbone. Polysaccharides, for instance, contain hydroxyl groups that allow direct reaction with drugs containing carboxylic acid function, producing ester linkages. Drugs lacking a carboxylic acid group require activation before the reaction takes place (Mehvar, 2000, Shrivastava*, et al.*, 2009). Physical drug entrapment is by far the more often used loading method for drug delivery applications. The best incorporation strategy for an efficient entrapment must be selected according to the physicochemical characteristics of the pair drug-carrier. Several methods have been used for drug loading, such as dialysis, nanoprecipitation, solvent displacement/evaporation, desolvation or direct dissolution. The encapsulation efficiency is different for each specific nanosystem; for example, the anti-cancer taxol is

encapsulated with 100% and 20% efficiency on poly(lactide-co-glycolide) (Mu*, et al.*, 2003) and poly(ε-caprolactone) (Kim*, et al.*, 2001) nanodevices, respectively.

The incorporation of biomolecules without compromising its bioactivity constitutes a fundamental goal. Physical drug loading can be performed by incorporating the drug while producing the nanoparticles, or by incubating a concentrated drug solution with the already formed nano-carrier. Drug loading and entrapment efficiency depend on the solubility in the polymeric matrix, which is in turn related to the polymer composition, molecular weight, drug-polymer interactions, and the presence of functional groups (i.e., ester or carboxyl) (Govender*, et al.*, 2000, Govender*, et al.*, 1999, Panyam*, et al.*, 2004).

1.2.2 Targeting

Drug delivery mediated by nanoparticles can be either an active or passive process. Passive delivery refers to the transport through leaky capillary fenestrations, into e.g., tumor interstitium and cells, by passive diffusion (Zambaux*, et al.*, 1999). Selective accumulation of nanoparticles and drug then occurs by EPR effect. Active targeting involves the use of peripherally conjugated targeting moieties, for enhanced delivery to a specific site, based on molecular recognition. One such approach is to surface-coat nanoparticles with an antibody, which can interact with its specific antigenic target cell site. According to some authors, antibody targeting does not increase tumor localization, instead increasing internalization (Hatakeyama*, et al.*, 2007, Kirpotin*, et al.*, 2006). The targeting moieties may help cellular uptake. Thus, long circulation times will allow for effective transport of the nanoparticles to the tumor site through the EPR effect, the targeting molecule then enabling endocytosis of the nanoparticles (Figure 1.2). The internalization of the nanoparticle is important for effective delivery of bioactive agents, especially in gene delivery, gene silencing, and other biotherapeutics. Sophisticated strategies to control the intracellular trafficking of nanoparticles are being developed (Tarragó-Trani*, et al.*, 2007, Watson*, et al.*, 2005). Such advanced drug carriers can be intelligently designed based on the inherent properties of the target site such as pH, presence of enzymes or specific tissue markers. After internalization by endocytosis, nanoparticles end up in endosomes and then lysosomes, where the pH values of about 5.5 (endosomes) and 4–5 (lysosomes) are found (Shen*, et al.*, 2009). Thus, pH sensitive constructs may be used as a smart trigger system for drug release.

For optimal therapeutic effect, the drug concentration must be maintained at an effective dose at the target site for the appropriate time-frame, with minimal dose

accumulation at off-target sites. For these purposes, careful design of multifunctional drug carriers with nano-dimensions has become a popular research subject.

Antibody fragments containing only the variable region of the antibody – that governs the recognition specificity - are now more commonly used for active targeting of therapeutics, avoiding the presence of the constant Fc effector region. This region may trigger the complement activation or undesirable interaction with other cells, potentially leading to premature phagocytosis of the drug delivery system (Chapman, 2002). In addition, the smaller size of antibody fragments may be an important factor in the development of an actively targeting nanoparticle. Antibodies, or antibody fragments, are conjugated either directly to the nanoparticle surface or through linker molecules such as PEG. The conjugation reaction is commonly carried out using carbodiimide-mediated chemistry, which creates stable amide bonds between carboxylic acid groups in the nano-carrier and primary amine groups, including lysines and the N-terminus amine, in the antibody or antibody fragment (Chapman, 2002).

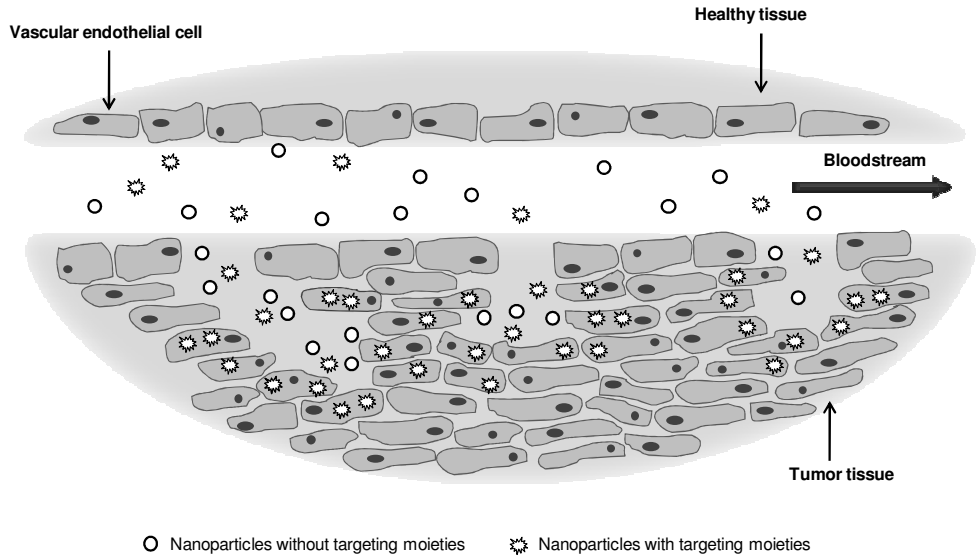

Figure 1.2. Targeting strategies for cancer therapy. Passive targeting can be achieved by EPR, an effect involving leaky vascular structures. Active targeting mediated by targeting ligands specifically localizes drug carriers at desired cells or tissues. The decoration of the nanoparticles with ligands improves its internalization by endocytosis.

Cell-specific ligands have been popularly employed to confer tissue- or cell-specificity to drug delivery systems. Specific interaction between a targeting ligand and its cellular receptor generally enhances the cellular uptake of nano-carriers by a mechanism called

receptor-mediated endocytosis. Therefore, increasing the specific cellular uptake significantly improve the therapeutic efficacy achieved with a much lower dose (Schiffelers*, et al.*, 2004). A variety of targeting ligands have been used in drug delivery systems, including galactose and lactose to target hepatocytes, mannose for dendritic cells, RGD peptide to target integrins on cell surfaces and lactoferrin for bronchial epithelial cells.

Different targets may be addressed for cancer therapy purposes. Targeting angiogenesis has become a major area of focus. The growth of solid tumors is dependent upon the ability to generate an adequate blood supply. Anti-angiogenesis approaches are effective in limiting tumor growth, the transformed endothelial cells of the neovasculature becoming a preferential target. Main angiogenic targets are the vascular endothelial growth factor receptors, $\alpha_v\beta_3$ integrins, matrix metalloproteinase receptors, and vascular cell adhesion molecule-1. Cell proliferation markers are another important target for cancer therapeutics, as many of them are highly overexpressed by certain tumor cells. Actively targeting nanoparticles to cell proliferation receptors may be achieved using monoclonal antibodies. The selection of monoclonal antibodies for cancer targeting is based on four basic criteria: (1) the antigen of interest is overexpressed by tumor cells, (2) the antigen participates as a principle component in the progression of the disease, (3) the antigen, present on the tumor cell surface must be stable, and (4) the antigen is expressed by a large percentage of tumor cells and a large variety of tumors. The most established cell proliferation targets used by actively targeting nanoparticles include human endothelial, transferrin and folate receptors. Targeting highly expressed antigens is a promising area that can ensure the elimination of malignant tumors and metastatic cells that have not become large enough to induce angiogenesis.

1.2.3 Drug release

The nanoparticles made of biodegradable materials allow sustained drug release over periods of days or even weeks. Biodegradation should not only modulate the release of drugs for a desired period of time, but also enable the removal of the empty device. Drug release is affected by the particle size. Smaller particles have a larger surface-to-volume ratio, therefore most of the drug is at or near the particle surface, leading to faster drug release. In contrast, larger particles allow more drug encapsulation in the inner cores, providing a slower release. Thus, control of particle size provides a means of tuning the drug release rates. The release mechanism can be modulated also by the molecular

weight and the copolymer composition used. It has been shown that the higher the polymer molecular weight, the slower the *in vitro* release of drugs (Mittal*, et al.*, 2007, Zambaux*, et al.*, 1999). The release mechanism is a complex function of three main processes, i.e., drug diffusion, matrix swelling, and chemical reactivity of the drug/matrix. Recent studies focuses on biopolymers responsive to physiological changes such as pH, temperature and external stimuli such as light, that can trigger a control release of the therapeutic agent.

1.3 Applications

1.3.1 Small molecular weight drug delivery

The sustained delivery of small drugs from polymer formulations has broad application in the treatment of several diseases – namely and noteworthy, the case of cancer. Biomaterial-mediated delivery schemes offer a unique method to deliver this kind of drugs. This section summarizes the polymer-based delivery systems for small drugs described in the literature, namely studies *in vivo* or using cell lines (Table 1.1).

Table 1.1. Nano-carriers for small molecular weight drug delivery

Polymer	Therapeutic agent	Ligand	Cell line	Drug binding	Stimuli	References
azo-dextran	aspirin	--	COS-1	simple mixing and irradiation with UV light	UV–vis light	(Patnaik, *et al.*, 2007)
carboxymethyl chitosan-linoleic acid	adryamycin (anti-cancer)	--	HeLa	direct dissolution	--	(Tan, *et al.*, 2009)
pullulan acetate	adriamycin (anti-cancer)	vitamin H (biotin)	HepG2	dialysis method	--	(Na, *et al.*, 2003a)
pullulan acetate/sulfonamide	adriamycin (anti-cancer)	--	MCF-7	dialysis method	pH	(Na, *et al.*, 2003b)
poly[(maleilated dextran)-*graft*-(*N*-isopropylacrylamide)]	camptothecin (anti-cancer)	--	L929	dialysis method	pH, temperature	(Li, *et al.*, 2009a)
poly(N-isopropylacrylamide)/ chitosan	camptothecin (anti-cancer)	--	SW480	direct dissolution	pH	(Li Fan, 2008)
poly[2-(*N,N*-diethylamino)ethyl methacrylate]-*block*-PEG	cisplatin (anti-cancer)	--	SKOV-3 *In vivo*	solvent displacement method	pH	(Xu, *et al.*, 2006)
poly (lactide-co-glycolide)-PEG	curcumin (anti-cancer)	--	KBM-5, Jurkat, DU145, MDA-MB-231, HCT116,SEG-1 *In vivo*	nanoprecipitation	--	(Anand, *et al.*, 2010)
polylactide-*co*-glycolide–PEG–folate	docetaxel (anti-cancer)	folate	SKOV3	emulsification/solvent diffusion method	--	(Esmaeili, *et al.*, 2008)
poly(D,L-lactic-*co*-glycolic acid)-*block*-PEG	docetaxel (anti-cancer)	PSMA aptamer	LNCaP	nanoprecipitation	--	(Farokhzad, *et al.*, 2006)

Table 1.1- cont.

Polymer	Therapeutic agent	Ligand	Cell line	Drug binding	Stimuli	References
glycol chitosan-5β-cholanic acid	docetaxel (anti-cancer)	--	A549 *In vivo*	dialysis method	--	(Hwang, *et al.*, 2008)
poly(l-histidine)-*b*-PEG-folate (75 wt.%) and poly(L-lactide)-b-PEG-folate (25 wt.%)	doxorubicin (anti-cancer)	folate	MCF-7	dialysis method	pH	(Lee, *et al.*, 2005)
chitosan-poly(acrylic acid)	doxorubicin (anti-cancer)	--	HepG2 *In vivo*	direct dissolution	--	(Hu, *et al.*, 2007)
poly(ε-caprolactone)-PEG-poly(ε-caprolactone)	honokiol (anti-inflammation)	--	A549	direct dissolution	--	(Wei, *et al.*, 2009)
ethylcellulose methylcellulose	nimesulide (nonsteroid anti-inflammation)	--	fresh human blood	desolvation method	--	(Ravikumara, *et al.*, 2009)
poly(ethylene oxide)-modified poly(ε-caprolactone)	tamoxifen	--	MDA-MB-231 *In vivo*	solvent displacement	--	(Shenoy, *et al.*, 2005)
PEG-polycyanoacrylate	paclitaxel (anti-cancer)	transferrin	*In vivo*	solvent evaporation	--	(Xu, *et al.*, 2005)
poly (lactide-co-glycolide fumarate)/poly(lactide-co-ethylene oxide fumarate) poly (lactide-fumarate)/ poly(lactide-co-ethylene oxide fumarate)	paclitaxel (anti-cancer)	--	HCT116 *In vivo*	dialysis method	--	(He, *et al.*, 2008)
PEG750-block-poly(ε-caprolactone-co-trimethylenecarbonate)	paclitaxel (anti-cancer)	--	HeLa *In vivo*	solvent evaporation	--	(Danhier, *et al.*, 2009b)

Table 1.1- cont.

Polymer	Therapeutic agent	Ligand	Cell line	Drug binding	Stimuli	References
poly (lactide-co-glycolide)/ poly(ε-caprolactone)-PEG	paclitaxel (anti-cancer)	--	HeLa	simple emulsion or nanoprecipitation method	--	(Danhier, *et al.*, 2009a)
linoleic acid/poly(β-malic acid) Chitosan	paclitaxel (anti-cancer)	--	*In vivo*	sonication and dialysis method	--	(Zhao, *et al.*, 2009)
poly(β-amino ester)-graft-PEG	paclitaxel, camptothecin (anti-cancer)	--	SKOV-3	solvent displacement or dialysis method	pH	(Shen, *et al.*, 2009)
glycol chitosan-5β-cholanic acid	protophorphyrin IX (photosensitizer, photodynamic therapy)	--	SCC7 *In vivo* *Ex vivo*	dialysis method	--	(Lee, *et al.*, 2009)
poly(β-benzyl-l-aspartate)-*block*-poly(vinylpyrrolidone)	prednisone (anti-inflammation)	--	SW-1990	dialysis method	pH	(Wang, *et al.*, 2009a)
poly (10-undecenoic acid-b-N-isopropylacrylamide)	prednisone (anti-inflammation)	--	ECV304	dialysis method	pH, temperature	(Wei, *et al.*, 2006)
cellulose-*g*- poly(l-lactide)	prednisone (anti-inflammation)	--	3T3	dialysis method	--	(Dong, *et al.*, 2008)
galactosylated polycaprolactone-g-dextran	prednisone (anti-inflammation)	galactose	HepG2, 3T3 *In vivo*	dialysis method	--	(Wu, *et al.*, 2009)
poly(ethylene oxide)-modified poly(ε-caprolactone)	saquinavir (HIV-protease inhibitor)	--	THP-1	solvent displacement	--	(Shah, *et al.*, 2006)
water soluble chitosan	thymol (anti-microbial)	--	*Staphylococcus aureus* *Bacillus subtilis* *Escherichia coli*	sonication method	--	(Hu, *et al.*, 2009)

Several polymers have been exploited for the formulation of nanoparticulate carrier systems. PLA, PGA and PLGA have been extensively employed because of their biocompatibility, biodegradability and versatile degradation kinetics. For instance, haloperidol-loaded PLGA/PLA particles were produced by sonication or homogenization. The three most relevant properties regarding the release behavior were identified: polymer hydrophobicity, surface coating and particle size. The hydrophobicity of the polymer contributes to a reduction of the initial burst, extending the period of release. For example, the percentage of drug released after 1 and 35 days is respectively 46 and 70% for 220 nm PLA particles, as compared to 70 and 90% for PLGA particles with the same size. Coating the particle surface with chitosan considerably reduces the initial burst. For example, the initial burst registered at 1 day, using 220 nm PLGA particles, is reduced from 70 to 36% by surface coating with chitosan. Increasing the size of the particles also reduces both the initial burst and the rate of release. For example, increasing the size from 220 to 450 nm reduces the initial burst from 48 to 28%, a steady release of drug being observed over a 10 day time period in the later case, as compared to four days for the smaller particles (Budhian*, et al.*, 2008).

PEG has been extensively used to modulate the biodegradation, release profile, bloodstream clearance and biodistribution. For instance, nanoparticles engineered by blending PLA/PLGA homopolymers and PEG have been used to encapsulate betamethasone disodium 21-phosphate (BP). The drug release profile and the vascular circulation time-frame could be controlled by varying the composition/molecular weight of the polymer. The rate of *in vitro* BP release correlated inversely with the nanoparticles size and increased using PLGA instead of PLA homopolymers. Furthermore, higher PEG content reduces the uptake of nanoparticles by dendritic cells and accordingly improves the blood circulation time. Analysis of the BP organ biodistribution revealed a lower liver concentration when using blended nanoparticles instead of PLA nanoparticles (Ishihara*, et al.*, 2009). The *in vitro* degradation of the PLGA–mPEG nanoparticles increases with the proportion of mPEG in the copolymer chains. As expected, the hydrophilicity of PLGA–PEG copolymers, as evaluated by water uptake or contact angle measurements, was found to increase with an increase in PEG content. The higher degradation rate of the nanoparticles with high mPEG content may be attributed to the improved hydrophilicity, which apparently overrides the decreased content of cleavable ester bonds (Avgoustakis*, et al.*, 2002).

1.3.2 Protein, peptide and oligosaccharide delivery

The oral route is the most convenient and comfortable mean for drug administration. However, the poor bioavailability, mainly due to the low mucosal permeability and lack of stability in the gastrointestinal (GI) environment, resulting in compound degradation prior to absorption, hinders a generalized use for proteins and peptides administration. One possible way to improve the GI uptake of proteins and peptides is the encapsulation in micro/nanoparticles that, while protecting from degradation in the GI tract, facilitate the transportation into the systemic circulation. Polymeric nanoparticles meet these attributes (Des Rieux*, et al.*, 2006, Shu*, et al.*, 2010).

The rather large number of therapeutic proteins currently reaching the market or under clinical evaluation draws the urgent need for new delivery systems, using different routes of administration, which allow for improved stability – a main concern regarding therapeutic proteins – as well as controlled and targeted release. Cytokines emerge as a powerful tool for immunotherapy and vaccination purposes. Simultaneously, growth factors offer new opportunities for wound and tissue regeneration. Currently, the more effective approach to guarantee appropriate stability is protein pegylation. Other tools with more versatile properties are required. Colloidal polymeric carriers have arisen as a promising alternative for improving the transport of macromolecules:

- proteins such as insulin (Damge*, et al.*, 2007, Lin*, et al.*, 2007b, Mi*, et al.*, 2008, Qian*, et al.*, 2006, Sonaje*, et al.*, 2009);
- cytokines (Hasegawa*, et al.*, 2009, Shimizu*, et al.*, 2008) and growth factors (Bessa*, et al.*, 2009);
- peptides, e.g. RGD (Park*, et al.*, 2004), cyclosporin A (Campos*, et al.*, 2001, El-Shabouri, 2002), elcatonin (Prego*, et al.*, 2006, Yamamoto*, et al.*, 2005), vasoactive intestinal peptide (Gao*, et al.*, 2007), anti-cancer glycoprotein lectin A-chain (Lee*, et al.*, 2008) and a caspase inhibitor peptide (Aktas*, et al.*, 2005)
- oligossacharides, such as heparin (Bae*, et al.*, 2009, Chen*, et al.*, 2009, Oyarzun-Ampuero*, et al.*, 2009).

These recent reports on the development of new protein delivery systems are discussed below.

The cationic nature of chitosan makes it an interesting polymer for the association with and delivery of labile negatively charged macromolecules. Several studies addressed the nasal delivery of insulin with chitosan nanoparticles (Wang*, et al.*, 2009b, Zhang*, et al.*, 2008). The potential of protonated chitosan has been enforced by the recognition of its

ability to trigger the opening of tight junctions, thereby facilitating the transport of macromolecules through the epithelium. Indeed, it has been demonstrated that nanoparticles can enhance the oral bioavailability of encapsulated therapeutic proteins. For this purpose, a nanoparticulate system composed of trimethyl chitosan (TMC) and cysteine (Cys), attempting to combine the mucoadhesion and permeation enhancing effects, was tested. When reaching the small intestine, the positively charged nanoparticles - which interact electrostatically with the mucous layer - induce transient loosening of the tight junctions. The free thiol groups on TMC-Cys allow the formation of disulfide bonds with the cysteine-rich mucin. Therefore, a closer and prolonged action on the tight junctions favors both the paracellular transport of the insulin and nanoparticle internalization by enterocytes. Oral administration of insulin-loaded TMC-Cys nanoparticles led to notable hypoglycemic effects, which lasted until eight hours post-administration, with a maximum blood glucose depression of 35% (Yin*, et al.*, 2009).

In cytokine immunotherapy, a suitable delivery system that ensures slow-release of cytokines is required, the short *in vivo* half-life of these molecules ruins its therapeutic efficacy, while causing severe systemic toxic effects. Recombinant murine IL-12 (rmIL-12) was successfully incorporated into cholesterol-bearing pullulan (CHP). The subcutaneous injection of the CHP/rmIL-12 complex led to a prolonged elevation of IL-12 concentration in the serum. Repetitive administrations of the complex induced drastic growth retardation of reestablished subcutaneous fibrosarcoma, without causing toxicity (Shimizu*, et al.*, 2008).

Bone morphogenetic proteins (BMPs) are cytokines with a strong ability to promote new bone formation. Elastin-like nanoparticles, created by thermoresponsive self-assembly, were developed for the combined release of bone morphogenetic protein-2 (BMP-2) and bone morphogenetic protein-14 (BMP-14). These BMPs could be encapsulated efficiently into the elastin-like particles and delivered in a sustained way for 14 days. The activity of the growth factors was retained and increased bioactivity on C2C12 cells was observed following the combined release of BMP-2 and BMP-14 (Bessa*, et al.*, 2009).

The development of peptides and proteins acting on the central nervous system is drastically hindered by the blood-brain barrier (BBB). The surface engineering of nanoparticles with lectins opened a novel pathway for the delivery of drug-loaded biodegradable nanoparticles into the brain, following intranasal administration. The neuroprotective Vasoactive Intestinal Peptide (VIP) was efficiently incorporated into PEG-

PLA nanoparticles surface-modified with wheat germ agglutinin. This formulation allows a more effective delivery, as compared with the intranasal application of the soluble peptide. This is partially attributed to the higher affinity of the wheat germ agglutinin-conjugated nanoparticles to the olfactory mucosa, rather than to the respiratory one (Gao*, et al.*, 2007). The peptide Z-DEVD-FMK, a caspase inhibitor, reduces vulnerability of the neuronal cells. The clinical application is hindered by its inability to cross the BBB and diffuse into the brain tissue. Thus, chitosan-PEG nanospheres bearing the OX26 monoclonal antibody (affinity for the transferrin receptor) have been designed, which trigger the receptor-mediated transport across the BBB. An important amount of nanoparticles were located in the brain, outside of the intravascular compartment. Hence, OX26 functionalized chitosan-PEG nanoparticles are promising carriers for the transport of the anti-caspase peptide into the brain (Aktas*, et al.*, 2005).

The peptide Arg–Gly–Asp (RGD) draws much attention for tumor therapy applications, because it specifically binds $\alpha_v\beta_3$ integrins, expressed by angiogenic endothelial cells. Attempting to overcome the short half-lives of several systemic anti-angiogenic peptides, a carrier for the RGD peptide was produced, using self-assembled nanoparticles of hydrophobically modified glycol chitosan (HGC). A high RGD loading efficiency was achieved (over 85%), and the system showed prolonged and sustained release for about 1 week. The RGD loaded-HGC nanoparticles displayed anti-angiogenic activity, markedly suppressing bFGF (inducer of angiogenesis) as well as preventing microvessel formation. Due to the sustained RGD peptide delivery, RGD-HGC nanoparticles significantly decreased tumor growth and microvessel density, improving the effect obtained injecting the free RGD peptide, either intravenously or intratumorally (Kim*, et al.*, 2008a).

Limitations in the management of extraocular diseases include the inability to provide long-term extraocular drug delivery without compromising intraocular structures. Since the cornea has negative charge, mucoadhesive polymers can interact with the extraocular structures, increasing the concentration and residence time of immunosuppressive peptide cyclosporin A (CyA). The hydrophobic peptide, CyA, was associated to chitosan nanoparticles. *In vivo* experiments showed that, following topical instillation of CyA-loaded chitosan nanoparticles to rabbits, it was possible to achieve therapeutic concentrations in external ocular tissues (i.e., cornea and conjunctiva) during at least 48 hours, while maintaining negligible or undetectable CyA levels in inner ocular structures (i.e., iris/ciliary body and aqueous humor), blood and plasma (Campos and Sa, 2001).

Pulmonary drug delivery for both local and systemic action has many advantages over other delivery routes. The lungs offer a large surface area, a rather thin absorption barrier, low enzymatic metabolic activity and slow mucociliary clearance. Therefore, PLGA nanospheres, surface-modified with chitosan, were developed and used for pulmonary delivery of elcatonin, a calcitocin derivative (formulated for the management of several bone-related diseases). The coated nanospheres were eliminated from the lungs at slower rate. Loaded elcatonin reduced blood calcium levels to 80%, exhibiting a prolonged pharmacological action, for over 24 hours. The results showed that the nanospheres adhered to the bronchial mucus and lung tissue, allowing the sustained drug release at the adherence site. Additionally, flexible chitosan molecules on surface of the nanospheres enhanced the drug absorption, maybe by opening the intercellular tight junctions (Yamamoto*, et al.*, 2005).

The macromolecular drug heparin, a sulfated natural glycosaminoglycan, is vulgarly used as an injectable anticoagulant (Chen*, et al.*, 2009). Recently, heparin has been loaded into nanoparticles of chitosan and hyaluronic acid, developed for anti-asthmatic therapy applications. The nanosystems were stable in phosphate buffered saline pH 7.4 for at least 24 hours, and released 10.8% of unfractionated heparin within 12 hours of incubation. Fluorescent heparin-loaded nanoparticles were effectively internalized by rat mast cells. *Ex vivo* experiments, conducted to evaluate the capacity of heparin to prevent histamine release in rat mast cells, indicated that the free or encapsulated drug exhibited the same dose–response behavior (Oyarzun-Ampuero*, et al.*, 2009). Intracellular delivery of heparin by chitosan-g-PEG/heparin polyelectrolyte complexes has also been used to trigger caspase activation and consequently promote apoptotic death of cancer cells (Bae*, et al.*, 2009).

1.3.3 Vaccine delivery

The recent developments in nanotechnology increased considerably the interest in nano-particulate systems as a platform for the delivery of antigens. The key challenges are the induction of a potent and broad (both humoral and cellular) antigen-specific immune response, capable of protecting from infection (sterilizing vaccination) and/or disease (therapeutic vaccination) and finally, to develop effective immunity after a single injection of the vaccine. Particulate delivery systems mimic pathogens that are commonly recognized, phagocytosed, and processed by professional antigen-presenting cells (APCs). APCs, such as dendritic cells and macrophages, represent the sentinels of the

immune system and orchestrate antigen-specific T cell-mediated immune responses. Activated APCs migrate to regional lymph nodes where they present the antigen to T cells, thereby triggering cellular and humoral immunity. Most organisms are detected and destroyed within hours by defense mechanisms, which are not antigen-specific and do not require any prolonged period of induction. These are the mechanisms of innate immunity. Only when the infectious agent is capable of breaking this early line of defense, an adaptive immune response will develop. This includes generation of antigen-specific effector cells that specifically target the pathogen, secretion of antibodies (B cells), direct cytotoxic activity (T cells), or secretion of immunological mediators and effector molecules such as cytokines and chemokines. Although most of these effector cells will die within 10–14 days after infection, some cells will survive, as highly reactive plasma cells (B cells) or memory cells (B and T cells), and prevent subsequent infection by the same microorganism. Along with long-lasting antibodies against a specific pathogen, the induction of memory cells is the final goal of preventive vaccination.

Immunity against an infectious agent by vaccination can be achieved in various ways, normally including several components. Firstly, the antigen itself can be a synthetically produced peptide representing an epitope of a pathogen protein. It can also be the full-length protein carrying several epitopes that are recognizable by B and T cells. Such full-length proteins can be secreted from the pathogen or produced synthetically or recombinantly. Vaccine development has also focused on experimental vaccines where the gene encoding a particular protein is fused into a DNA or RNA plasmid. Secondly, the formulation or delivery system varies considerably from one vaccine to another. DNA and some protein vaccines can be administered in solution without adjuvant enhancement of the immune response. Today, still many of the most potent vaccines are given as a live attenuated or killed form of the particulate microorganism. A unique property, especially of live vaccines, is that they often induce strong T cell responses. This property is very much missed by protein or peptide vaccines administered with those adjuvants in general use today, e.g., aluminum salts. Thus, there is an urgent need for the development of potent and safe antigen-delivery systems. The development of nano-particulate vaccines is also motivated by safety concerns, e.g., to avoid the risk of infection induced by live attenuated vaccines and to suppress the excessive inflammation that is frequently caused by the use of Freund's adjuvant or aluminum salts adjuvant.

Cancer vaccines are a promising approach for anti-cancer therapy, as fewer side effects are induced than with other therapies and, more importantly, there is an opportunity for developing long-term immunity (Rosenberg, 2001). In contrast to general

medicines, which are directly targeted to specific molecules, cancer vaccines initiate a cascade of antigen specific immune responses against antigen-expressing tumor cells. Activating the immune system to trigger a specific response sufficient for the eradication of tumor cells, however, is a major challenge in the development of cancer immunotherapy.

A possible key for the successful development of new generation of vaccines may lie in the use of targeted delivery systems (Table 1.2). Nanoparticulate systems are particularly well suited for the delivery of antigens specifically to DCs, inducing the subsequent activation of T cell immunity, given its ability to permeate the lymphatic draining system and reach DCs in the lymph nodes. However, antigen delivery to - and activation of - DCs is a complex problem, involving antigen transport to DC-rich areas, DC binding and eventually antigen uptake, and antigen processing and presentation. Before an antigen can be processed and presented by DCs, the biomaterial vehicle itself must be internalized by DCs. Immature DCs internalize exogenous solutes, particles, and necrotic or apoptotic cells through macropinocytosis, receptor-mediated endocytosis and phagocytosis (Sallusto*, et al.*, 1995). Several studies confirmed that DCs can internalize polymeric nanoparticles (Elamanchili*, et al.*, 2004), the internalization mechanism being partially controlled by altering the properties of the biomaterial vehicle, namely the size (Reddy*, et al.*, 2006). Macropinocytosis is used to internalize extracellular fluid and smaller solutes such as macromolecules (Sallusto*, et al.*, 1995) and particularly small nanoparticles (< 50 nm), whereas phagocytosis occurs when larger nanoparticles (> 500 nm) are taken up (Lutsiak*, et al.*, 2002, Thiele*, et al.*, 2003). DCs also use surface receptors to endocytose ligands with a terminal sugar such as mannose (Avrameas*, et al.*, 1996). Thus, both the physicochemical and biochemical character of biomaterial vehicles can be adjusted to tailor DC uptake.

Following internalization, the biomaterial vehicle must then release the antigen intracellularly, in a manner that will enable processing by MHC class I, class II, or both (cross-presentation) pathways. The delivery of exogenous antigen inducing cellular immunity through the MHC class I pathway can be a challenging problem, as internalized particles are initially within endosomes but are trafficked rapidly to lysosomes, where they are degraded enzymatically, preventing the antigen from being processed and presented. To avoid lysosomal trafficking, smart polymers have been designed. These polymers are broken down inside the endosomes, due to the presence of acid-degradable acetal bonds, triggering the disruption of the endosomes in a pH-dependent fashion. The process occurs as follows: at pH 7.4 the polymers are PEGylated

("masked"); however, after endocytosis the acid labile linker is hydrolyzed and the polymer backbone becomes de-PEGylated ("umasked") and membrane-disruptive, causing endosomal disruption. The PEGs may be conjugated to the backbone via both acid-degradable linkages and disulfide bonds. These polymers release oligonucleotides and peptides into the cytoplasm as the endosome is acidified, avoiding the lysosomal fusion; releasing antigen into the cytoplasmic compartment enables processing by MHC class I instead of the MHC class II pathway (Murthy*, et al.*, 2003). This strategy exemplifies how smart biomaterials may be engineered as to overcome biological barriers and control the intracellular biodistribution.

Targeting lymph-node DCs, rather than peripheral ones, in the skin for example, offers many theoretical advantages (Randolph*, et al.*, 2005). The avoidance of premature antigen presentation, because DCs in lymph nodes are already at the site of antigen presentation, is one potential benefit. For successfully targeting lymph-node-resident DCs, it is crucial to engineer biomaterial vehicles that can be readily taken up into lymphatic vessels after subcutaneous or intradermal injection, being then retained in draining lymph nodes. It has been well-established that particle size is among the most crucial factors for lymphatic uptake from the interstitial space (Swartz, 2001).

As the mucosal route of administration (e.g., intranasal, oral) is considered a simple, safe, efficacious, non-invasive and less expensive method to deliver antigens, novel strategies for the achievement of safe and effective immunization strategies are under investigation regarding the routes of vaccination. Mucosal immunization is an attractive alternative to parenteral vaccination; using the appropriate delivery system it is possible to stimulate both mucosal and systemic immune responses (Sayin*, et al.*, 2008). Mucosal vaccination offers also several benefits over parenteral route, including ease of administration, reduced side effects, possibility of self-administration and, especially in developing countries, reduced risk of the unwanted spread of infectious agents via contaminated syringes.

Table 1.2. Polymeric nanoparticles for vaccine delivery

Polymer	Antigen	Remarks	Route	References
poly-l-lysine coated polystyrene particles	sOVA-C1 plasmid	Particles of different sizes may target different APCs.	intradermal	(Minigo, *et al.*, 2007)
poly-(ε-caprolactone) -poly(lactide-co-glycolide)	diphtheria toxoid	Correlations between polymer characteristic (e.g., hydrophobicity) and route of administration, indicate that such characteristics can have interesting implications in immune responses.	intranasal intramuscular	(Singh, *et al.*, 2006)
methoxyPEG–poly(lactide-co-glycolide)	recombinant hepatitis B surface antigen (HBsAg)	Delivery of HBsAg encapsulated within a nanoparticle is a superior way for generating faster immune responses, as compared to the non-encapsulated counterpart.	intraperitoneal	(Bharali, *et al.*, 2008)
poly lactic acid-PEG	HBsAg	Different compositions of PLA and PEG polymers were synthesized to stabilize the antigen. A comparison of their efficacy in the generation of effective immune responses is shown.	nasal	(Jain, *et al.*, 2009)
poly(γ-glutamic acid)-graft-L-phenylalanine	japanese encephalitis (JE) vaccine	A single dose of JE vaccine with nanoparticles enhanced the neutralizing antibody titer.	intraperitoneal	(Okamoto, *et al.*, 2008)
poly(γ-glutamic acid)-graft-l-phenylalanine	influenza hemagglutinin (HÁ) vaccine	Subcutaneous immunization with a mixture of HA vaccine and nanoparticles induced higher mononuclear cell proliferation and production of IFN-γ, IL-4, and IL-6 upon HA restimulation.	subcutaneous	(Okamoto, *et al.*, 2007)
poly (d,l-lactide-co-glycolide)–polyethyleneimine	DNA encoding Mycobacterium tuberculosis latency antigen Rv1733c	The polyplexes were able to mature human dendritic cells and stimulated the secretion of cytokines, comparable to levels observed after lipopolysaccharide stimulation.	intramuscular endotracheal	(Bivas-Benita, *et al.*, 2009)
hydrophobically modified poly(γ-glutamic acid)	gp120 (human immunodeficiency virus -1)	The protein-encapsulated nanoparticles induced cytotoxic T lymphocyte. Efficient uptake by immature DCs and induction of DCs maturation was observed.	intranasal	(Akagia, *et al.*, 2007)
chitosan	DNA vaccine encoding mite dust allergen Der p 2	Chitosan-DNA nanoparticles can generate a higher level expression of gene *in vivo*, therefore can preferentially activate specific Th1 immune responses thus preventing subsequent sensitization of Th2 cell-regulated specific IgE responses.	oral	(Li, *et al.*, 2009b)

Table 1.2- cont.

Polymer	Antigen	Remarks	Route	References
chitosan	plasmid DNA encoding surface protein of Hepatitis B virus (pRc/CMV-HBs(S))	Administration of nanoparticles resulted in serum anti-HBsAg titre and induced sIgA titre in mucosal secretions. Chitosan nanoparticles were able to induce humoral mucosal and cellular immune responses.	nasal	(Khatri, *et al*., 2008)
chitosan	DNA plasmids expressing different *M. tuberculosis* epitopes	Chitosan nanoparticles protect DNA from degradation by nucleases, induce dendritic cells maturation and increased IFN-γ secretion from T cells.	pulmonary	(Bivas-Benita, *et al*., 2004)
chitosan	pcDNA3-VP1, encoding VP1, major structural protein of coxsackievirus (CVB3)	Nasal administrated chitosan–DNA produced higher levels of serum IgG and mucosal secretory IgA. Strong cytotoxic T lymphocyte activities helped to effectively eliminate CVB3 viruses.	intranasal	(Xu, *et al*., 2004)
low molecular weight chitosan (LMWC)	plasmid DNA encoding human cholesteryl ester transfer protein C-terminal fragment	LMWC had lower binding affinity to DNA, but mediated higher transfection efficiency. Polyplexes could elicit significant systemic immune responses, modulate the plasma lipoprotein profile and attenuate the progression of atherosclerosis.	intranasal	(Yang, *et al*., 2009)
mono-N-carboxymethyl chitosan N-trimethyl chitosan	tetanus toxoid	Surface charge and particle size exert an important influence in the production of an enhanced immune response.	intranasal	(Sayin, *et al*., 2008)

1.3.4 Gene delivery

Nucleic acid-based biopharmaceuticals, such as pDNA, oligonucleotides (ODNs) and short interfering RNA (siRNA), are potential pioneering materials to cope with various incurable diseases. Cationic polymers condense DNA into nanosized polymer/DNA complexes (polyplexes), by a self-assembling process, consisting on the electrostatic interaction of the positively charged polymer with the negatively charged DNA. Polyplexes may interact with the negatively-charged cellular membrane, being internalized via endocytosis. In the intracellular environment, the polyplexes are normally located in endosomes that become acidified and finally fuse with lysosomes. In this case, DNA is prone to degradation by lysosomal enzymes. In order to transfer their DNA cargo successfully to the nucleus, polyplexes must escape from the endosome. After endosomal escape, polyplexes are located in the cytoplasm, ready to unpack DNA and deliver it to a suitable site near the nucleus or in the nucleus. Finally, after the DNA translocation into the nucleus, gene expression must occur. The low efficiency of polymer-mediated gene delivery may be due to the lack of mechanisms to overcome the physiological barriers. Cationic polymers need to have multiple functions to overcome these barriers, such as good DNA binding ability to condense DNA into polyplexes, high buffer capacity to induce endosomal escape and efficient intracellular vector unpacking to release DNA (Middaugh*, et al.*, 2003). Therefore, understanding of the correlations between polymeric functionalities and gene delivery properties is important for the rational design of efficient cationic polymeric vectors.

RNA may be advantageously used instead of DNA for gene delivery purposes. First, the delivery target is the cytosol, not the nucleus. Cytosol delivery is by far easier and more efficient than nucleus delivery. Quite recently, siRNA has emerged as a more powerful therapeutic genetic agent (Kim*, et al.*, 2006). High sequence specificity and relatively small dose requirement of siRNA make it even more attractive. The most challenging hurdles are serum instability during circulation in the bloodstream (Chapman, 2002), poor cellular uptake, and limitation in targeted delivery to specific tissues or cells. To address such problems, natural or synthetic polymeric delivery systems have been used. The natural polymers investigated for gene therapy include chitosan, collagen, gelatin and their modified derivatives (Dang*, et al.*, 2006) (Table 1.3). Among the synthetic polymers, poly(l-lysine) or polyethylenimine and their analogs have been widely used (Park*, et al.*, 2006) (Table 1.4).

Table 1.3.Natural-based polymers for gene delivery

Polymer	Therapeutic agent	Target	Remarks	References
chitosan	sense or antisense oligodeoxynucleotides (ODNs) against malarial topoisomerase II gene	--	Antisense-nanoparticles demonstrate a significant higher inhibition of human malaria parasite, as comparison with sense-nanoparticles and free ODNs. More easily dissociated complexes mediate a faster onset of action.	(Foger, *et al.*, 2006)
folate-N-trimethyl chitosan	pDNA	folate	Folate conjugation increased intracellular uptake, transfection efficiency and induce endosomal escape.	(Zheng, *et al.*, 2009)
folic acid-chitosan	pDNA (pVR1412)	folate	Nanoparticle with positive zeta potentials interact with the cell membrane allowing their endocytosis.	(Mansouri, *et al.*, 2006)
Galactosylated 6-amino-6-deoxychitosan	pDNA (pCMV-Luc)	galactose	The increase of transfection efficiency of Gal-6ACT was therefore likely due to improvements in intracellular trafficking and not due to the increase of cellular uptake.,	(Satoh, *et al.*, 2007)
chitosan/hyaluronic acid	pDNA(pEGFP-C1, pβ-gal)	hyaluronan	Polyplexes were able to provide high transfection without affecting cell viability, entering the corneal epithelial cells by CD44 receptor–mediated endocytic uptake.	(Fuente, *et al.*, 2008)
mannosylated chitosan	pDNA (pGL3-Luc)	mannose	Cellular uptake mediated by mannose recognition. Reduced toxicity and high transfection efficiency.	(Hashimoto, *et al.*, 2006)
chitosan –IL-1Ra folate- IL-1Ra-Chitosan	IL-1Ra plasmid DNA	folate	Folate-chitosan-DNA nanoparticles containing the IL-1 Ra gene prevent bone damage and inflammation in rat adjuvant-induced arthritis model that overexpress folate receptors.	(Fernandes, *et al.*, 2008)
PEG-Chitosan	pDNA (pRE-luciferase; pREP4;pCMV-luciferase)	transferrin KNOB protein	The transfection efficiency was much impressive with KNOB (130-fold improvement), in HeLa cells. Chitosan exhibited limited buffering capacity. The clearance of the PEGylated nanoparticles was slightly slower than that of the unmodified nanoparticles.	(Mao, *et al.*, 2001)
chitosan	plasmid pGL3-Luc	--	Polyplexes are endocytosed and possibly released from endosomes due to swelling of both lysosomes and polyplexes, causing the endosome rupture.	(Ishii, *et al.*, 2001)

Table 1.3- cont.

Polymer	Therapeutic agent	Target	Remarks	References
chitosan	pDNA (pAAV-tetO-CMV-mEpo and pCMVβ)	--	Oral gene therapy was efficient in delivering genes to enterocytes.	(Chen, *et al*., 2004)
thiolated Chitosan	pDNA (pEGFP-N2)	--	Improved gene delivery *in vitro* as well as *in vivo*. The extended pDNA release and subsequent gene expression were achieved by oxidation of introduced thiol groups to crosslink the thiolated chitosan.	(Lee, *et al*., 2007)
quaternized (trimethylated) chitosan oligomer	pDNA (pEGFcp1-GFP)	--	Transfection efficiency decreases increasing the degree of quaternization. The polymer effectively transfers the GFP gene into cells both in vitro and *in vivo*.	(Zheng, *et al*., 2007)
6-N,N,N-trimethyltriazole chitosan	pDNA (EGFP-N1)	--	The presence of the trimethyltriazole group led to significantly increased cellular uptake, which resulted in higher transfection efficiency in HEK 293 and MDA-MB-468 cells.	(Gao, *et al*., 2009)
methoxy PEG–PEI–chitosan	pDNA (pVRfat-1)	--	The mPEG increased the slow-releasing ability and water solubility, while PEI improved the transfection efficiency.	(Xu, *et al*., 2009b)
chitosan/ poly(γ-glutamic acid) (γ-PGA)	pDNAs (pEGFP-N2, pGL4.13 and pEGFP-N2)	--	The incorporation of γ-PGA in the chitosan nanoparticles facilitates the dissociation of chitosan and DNA, increasing transfection efficiency. Trypsin-cleavable proteins in cellular membrane affect internalization of polyplexes.	(Peng, *et al*., 2009)
methylated collagen	pDNA (pRELuc)	--	Methylated collagen improved DNA binding ability and the stability of the complexes at physiological conditions, as compared with unmodified native collagen.	(Wang, *et al*., 2004)
cationized gelatin	plasmid DNA of transforming growth factor-βR (TGF-*β*R) siRNA expression vector	--	The injection of polyplexes significantly decreased the level of TGF-*β*R and α-smooth muscle actin over-expression, the collagen content of mice kidney, and the fibrotic area of renal cortex, in contrast to free plasmid DNA injection.	(Kushibiki, *et al*., 2005)
PEG–modified thiolated gelatin	pDNA (EGFP-N1)	--	Nanoparticles released encapsulated plasmid DNA in response to varying concentrations of glutathione.	(Kommareddy, *et al*., 2007)

Table 1.3- cont.

Polymer	Therapeutic agent	Target	Remarks	References
chitosan	sense or antisense oligodeoxynucleotides (ODNs) against malarial topoisomerase II gene	--	Antisense-nanoparticles demonstrate a significant higher inhibition of human malaria parasite, as comparison with sense-nanoparticles and free ODNs. More easily dissociated complexes mediate a faster onset of action.	(Foger*, et al.*, 2006)
folate-N-trimethyl chitosan	pDNA	folate	Folate conjugation increased intracellular uptake, transfection efficiency and induce endosomal escape.	(Zheng*, et al.*, 2009)
folic acid-chitosan	pDNA (pVR1412)	folate	Nanoparticle with positive zeta potentials interact with the cell membrane allowing their endocytosis.	(Mansouri*, et al.*, 2006)
Galactosylated 6-amino-6-deoxychitosan	pDNA (pCMV-Luc)	galactose	The increase of transfection efficiency of Gal-6ACT was therefore likely due to improvements in intracellular trafficking and not due to the increase of cellular uptake.,	(Satoh*, et al.*, 2007)
chitosan/hyaluronic acid	pDNA(pEGFP-C1, pβ-gal)	hyaluronan	Polyplexes were able to provide high transfection without affecting cell viability, entering the corneal epithelial cells by CD44 receptor–mediated endocytic uptake.	(Fuente*, et al.*, 2008)
mannosylated chitosan	pDNA (pGL3-Luc)	mannose	Cellular uptake mediated by mannose recognition. Reduced toxicity and high transfection efficiency.	(Hashimoto*, et al.*, 2006)
chitosan –IL-1Ra folate- IL-1Ra-Chitosan	IL-1Ra plasmid DNA	folate	Folate-chitosan-DNA nanoparticles containing the IL-1 Ra gene prevent bone damage and inflammation in rat adjuvant-induced arthritis model that overexpress folate receptors.	(Fernandes*, et al.*, 2008)
PEG-Chitosan	pDNA (pRE-luciferase; pREP4;pCMV-luciferase)	transferrin KNOB protein	The transfection efficiency was much impressive with KNOB (130-fold improvement), in HeLa cells. Chitosan exhibited limited buffering capacity. The clearance of the PEGylated nanoparticles was slightly slower than that of the unmodified nanoparticles.	(Mao*, et al.*, 2001)
chitosan	plasmid pGL3-Luc	--	Polyplexes are endocytosed and possibly released from endosomes due to swelling of both lysosomes and polyplexes, causing the endosome rupture.	(Ishii*, et al.*, 2001)

Table 1.4. Polyethylenimine (PEI) and poly(l-lysine) (PLL)-based polymers for gene delivery

Polymer	Therapeutic agent	Target	Remarks	References
PEG-PEI (NanoGel™)	antisense oligonucleotide (ODN) targeting the mdr1 gene	transferrin insulin	Transport efficacy across the blood-brain barrier is increased by modification with transferrin or insulin. Improvement of ODN accumulation in the brain (15 fold).	(Vinogradov, *et al.*, 2004)
lactoferrin-PEI	pDNA	lactoferrin	Selectivity for bronchial epithelial cells. Lower cellular toxicity of polyplexes and higher transfection efficiency (5-fold higher), as compared with PEI/pDNA complexes.	(Elfinger, *et al.*, 2007)
RGD-PEG-PEI	siRNA inhibiting VEGF receptor-2	RGD	Selective tumor uptake, siRNA sequence-specific inhibition of protein expression within the tumor and inhibition of both tumor angiogenesis and growth rate.	(Schiffelers, *et al.*, 2004)
PEI-g-PEG-RGD	pDNA (pCMV-sFlt-1)	RGD	Efficient inhibition on proliferation of endothelial cells that expressed sFlt-1 predominantly bound to exogenous VEGF and blocked the binding of VEGF to the full-length Flt-1 receptor.	(Kim, *et al.*, 2005a)
siRNA-PEG-LHRH/PEI	siRNA (VEGF-vascular endothelial growth factor)	luteinizing hormone- releasing hormone (LHRH)	Enhancement of cellular uptake, as compared to those without LHRH, resulting in increased VEGF gene silencing efficiency via receptor-mediated endocytosis.	(Kim, *et al.*, 2008b)
EGF-PEG-PEI	pDNA (pCMVLuc)	epidermal growth factor (EGF) peptides	EGF-containing polyplexes were 10- to 100-fold more efficient than polyplexes without EGF.	(Blessing, *et al.*, 2001)
PEI	pDNA	Peptide (NL4-10K)	Polyplexes displayed no toxicity in neuronal cells. Enhancement of gene expression (up to 1000-fold) and transfection efficiency (59-fold higher), in dorsal root ganglia, compared to nontargeting polyplexes.	(Zenga, *et al.*, 2007)
PEI-g-Clenbuterol	pDNA (pCMVLuc)	β_2-adrenoceptor (clenbuterol)	Specific cellular uptake into alveolar (transfection efficiency 14-fold higher than for unmodified PEI) but not bronchial epithelial cells.	(Elfinger, *et al.*, 2009)
folate–PEG–PEI	pDNA (pCMV-Luc or pcDNA/rev-caspase-3)	folate	Higher transfection efficiency than other commercially available transfection agents.	(Chul Cho, *et al.*, 2005)

Table 1.4- cont.

Polymer	Therapeutic agent	Target	Remarks	References
PEI-PEG-Fab'	pDNA (pCMVLuc)	anti- glutamic acid decarboxylase (GAD)	Selectivity toward the islet cells. High transfection efficiency in GAD-expressing mouse insulinoma cells.	(Jeong, *et al.*, 2005)
HerPEI	pDNA(pcDNA3-CMV-Luc)	anti-HER2	The HerPEI polyplexes showed significantly greater transfection activity (up to 20-folds) than nonderivatized PEI-based polyplexes in the HER2 overexpressing breast cancer cells.	(Chiu, *et al.*, 2004)
mannose-PEI	pDNA	mannose	Dendritic cells transfected with polyplexes containing adenovirus particles are effective in activating T cells of T cell receptor transgenic mice in an antigen-specific fashion.	(Cotten, 1999)
methoxypolyethylen eglycol-PEI-cholesterol	pDNA (pmIL-12)	--	Inhibition of tumor growth enhanced when combined with specific chemotherapeutic agents.	(Fewell, *et al.*, 2005)
dextran-PEI	pDNA	--	Stability of the complex in the presence of BSA. The transfection efficiency depended on the molecular weight of dextran and the grafting degree.	(Tseng, *et al.*, 2003)
acid-labile PEI	pDNA (pCMV-Luc)	--	The acid-labile PEI was much less toxic and showed comparable transfection efficiency to that of PEI25K. Polyplexes may be rapidly degraded in acidic endosome.	(Kim, *et al.*, 2005b)
disulfide-crosslinked low molecular weight linear PEI-sodium hyaluronate	pDNA (pBR322, pEGFP-C1)	--	Polyplexes achieved significantly higher transfection efficiency than other polymer systems, especially in the presence of serum.	(Xu, *et al.*, 2009a)
galactosylated PLL	pDNA (pCAT)	galactose	Hepatoma cell line revealed high gene expression. After intravenous injection, polyplexes were rapidly eliminated from the circulation and preferentially taken up by the liver's parenchymal cells.	(Hashida, *et al.*, 1998)
Lactosylated PEG-siRNA/PLL	RNAi	lactose	pH-responsive and targetable polyplexes exhibited significant gene silencing human hepatoma cells.	(Oishi, *et al.*, 2005)

Table 1.4- cont.

Polymer	Therapeutic agent	Target	Remarks	References
AWBP-PEG-PLL	pDNA (pMNK)	Artery wall binding peptide (AWBP)	High transfection efficiency in bovine aorta endothelial cells and smooth muscle cells.	(Nah, *et al*., 2002)
Antibody-PLL	pDNA(pSV-b-galactosidase)	Anti JL1	Polyplexes internalization into Molt 4 cells and human leukemia T cells. Higher *in vitro* transfection efficiency than polyplexes without targeting ligand.	(Suh, *et al*., 2001)
RGD-PEG-*block*-PLL	pDNA	RGD	Synergistic effect of cyclic RGD peptide and disulfide cross-links toexert the smooth release of pDNA in the intracellular environment via reductive cleavage. Enhanced transfection efficiency against HeLa cells, due to a change in their intracellular trafficking route.	(Oba, *et al*., 2008)

Other synthetic alternative nano-carriers have been synthesized, engineered with linkages envisaging physiological degradation (Table 1.5). Specific targeting moieties may be conjugated to confer tissue specificity. Chitosan has emerged as an alternative non viral gene delivery system. The transfection efficiency of chitosan/DNA complexes is dependent on several factors: chitosan degree of acetylation and molecular weight (Huang*, et al.*, 2005, Sato*, et al.*, 2001, Wang*, et al.*, 2007b), amine/phosphate ratio of chitosan/DNA complexes (Kim*, et al.*, 2004, Weecharangsan*, et al.*, 2008), serum concentration, pH (Sato, *et al.*, 2001) and cell type (Bhattarai*, et al.*, 2008, Corsi*, et al.*, 2003). Chitosan derivatives (glycol, o-carboxymethyl, trimethylated, thiolated and 6-N,N,N-trimethyltriazole chitosan) including hydrophobic modifications (deoxycholic acid, 5β-cholanic acid, N-acylated chitosan) have been used to overcome the limited chitosan solubility and improve transfection efficiency. Concerning biodegradation, chitosan is degraded into oligomers by lysozyme, and then further degraded by N-acetyl-glucosaminidase, in animal cells. Both of these enzymes are present in the endosomal/lysosomal vesicles, thus the degradation and release of pDNA will start immediately after endocytosis of the chitosan polyplexes. Additionally, lysozyme is present at inflammation sites, which allow specific release. The chitosan cytotoxicity is lower than that of polyethylenimine, supporting the suggestion that chitosan may be a nontoxic alternative to polyethylenimine (Koping-Hoggard*, et al.*, 2001).

Table 1.5. Other synthetic polymers for gene delivery

Polymer	Therapeutic agent	Remarks	References
poly(imidazole/ 2-dimethylaminoethylamino) phosphazene	pDNA	Imidazole effect on cytotoxicity and transfection efficiency. Evaluation of half-lives under neutral and acidic conditions.	(Yang*, et al.*, 2008)
poly[α-(4-aminobutyl)-L-glycolic acid] (PAGA)	pDNA(pCAGGS-Il10, pCAGGS-Il4)	Combined administration of mouse *Il4* and *Il10* plasmids prevents the development of autoimmune diabetes in nonobese diabetic mice.	(Ko*, et al.*, 2001)
poly(4-hydroxy-L-proline ester)	pDNA(CMV-*β*Gal)	The minimum viability of cells incubated with poly(4-hydroxy-L-proline ester) was 85%, which is excellent when compared to the cases of polylysine (20%) and polyethylenimine (2%).	(Putnam*, et al.*, 1999)
poly(amido amine)s containing multiple disulfide linkages	pDNA	Buffer capacity of poly(amido amine)s in the pH range 7.4-5.1. High transfection efficiency and gene expression, in the presence of serum.	(Lin*, et al.*, 2007a)
cationic amphoteric polyamidoamine	pDNA (pEGFP)	Evaluation of toxicity and hemolytic activity in the pH range 4.0-7.4. Circulation time and organ accumulation assessment. Study of complex stability and transfection efficiency	(Ferruti*, et al.*, 2007)
three blocks of amino acids Ac-(AF)6-H5-K15-NH2 (FA32)	doxorubicin, pCMV-luciferase, pCMV-p53	Co-delivery of drug and gene using nanoparticles was demonstrated via confocal imaging, luciferase expression in the presence of doxorubicin, and synergy in cytotoxic effect towards HepG2 cells.	(Wiradharma*, et al.*, 2009)
N,N-diethylethylenediamine-polyurethane	pDNA (pCMV-*β*gal)	Cytotoxicity was substantially lower and transfection efficiency comparable to the well-known gene carrier poly(2-dimethylaminoethyl methacrylate	(Yang*, et al.*, 2004)

Polyethylenimine (PEI), often considered the gold standard of gene transfection, is one of the most prominent examples of cationic polymers capable of gene transfection. The transfection efficiency of PEI has been related to the buffering effect exerted by the amines, with different pKa values, over a wide range of pH. This buffering ability gives PEI an opportunity to escape the endosome (proton sponge effect) (Boussif*, et al.*, 1995). PEI, as poly-L-lysine (PLL), often show a relatively high cytotoxicity and, depending on the ionic strength, a tendency to aggregate and precipitate (Pasumarthy*, et al.*, 2001). The conjugation with PEG prevents the inter-particular aggregation of the complexes, increasing their stability (Choi*, et al.*, 1998, Petersen*, et al.*, 2002).

The non-degradability of non-viral carriers may represent a major limitation, since it implies they are not removed by physiological clearance systems and, therefore, can possibly accumulate within cells or tissues, eliciting further cytotoxicity. The backbone linkages of most polymeric gene carriers consist of a –C–C– bond or amide bond, which are not degraded in physiological solutions. Additionally, the biodegradation of the polymer may provide an extra tool to release the plasmid DNA into the cytosol. In an effort to develop alternative non-toxic and effective nano-carriers modified polymers, with functional groups labile under physiological conditions (ester, phosphorus or disulfide bonds), were produced. The use of the disulfide bond as bioreducible linker has received much attention in recent years (Lin*, et al.*, 2006, Oupicky*, et al.*, 2002). The disulfide bond can be cleaved intracellularly by reducing enzymes such as glutathione reductase and sulfhydryl components like glutathione. Since the concentration of these reducing species is much higher in the cytoplasm than in plasma (intracellular versus extracellular glutathione concentration 0.5–10 mM versus 2–20 μM) (Lin*, et al.*, 2008), the disulfide bond is relatively stable in the extracellular environment, but rapidly degradable inside the cells, due to the higher amounts of thiols. To achieve high efficiency of polymer-mediated gene delivery, endosomal escape is required. This mechanism can be improved with the addition of chloroquine or membrane-active peptide (Wolfert*, et al.*, 1998). An alternative method to promote endosomal lysis consists in engineering the carrier cationic polymers with histidine or imidazole groups. The transfection enhanced activity is assigned to the imidazole heterocycle, which displays a pKa around 6, thus possessing a buffering capacity at the endolysosomal pH (Yang*, et al.*, 2008).

Anti-angiogenic therapy has become an important route for cancer treatment. Among factors that regulate angiogenesis, the vascular endothelial growth factor (VEGF) appears to be the most critical regulator of tumor-induced angiogenesis, which is essential for the survival of rapidly proliferating cancer cells and sustained growth of

tumor. For this purpose, a PEG-conjugated VEGF-siRNA was complexed with polyethylenimine. Intravenous as well as intratumoral administration of these polyplexes significantly inhibited VEGF expression at the tumor tissue, suppressing tumor growth in an animal tumor model, without showing any detectable inflammatory responses in mice (Kim*, et al.*, 2008c).

Multidrug resistance remains a major barrier to the success of anticancer chemotherapy (Teicher, 2009). Overexpression of drug efflux transporters, such as P-glycoprotein, enables cancer cells to develop resistance to multiple anticancer drugs. A novel approach to overcome drug resistance consist in using the siRNA-mediated silencing the expression of the efflux transporter. Because P-glycoprotein plays an important role in the physiological regulation of endogenous and xenobiotic compounds, it is important to deliver the P-glycoprotein targeted siRNA (associated with anticancer drugs) specifically to tumor cells. Recent studies have shown that nanoparticles formulated with poly(D,L-lactide-co-glycolide) and polyethyleneimine result in sustained siRNA delivery and efficient gene silencing Nanoparticles were surface functionalized with biotin for active tumor targeting. *In vivo* studies, in a mouse model of drug-resistant tumor, demonstrated significantly greater tumor growth inhibition following treatment with biotin-functionalized nanoparticles encapsulating both paclitaxel and P-glycoprotein targeted siRNA. Remarkably, this effect was obtained using a paclitaxel dose ineffective in the absence of gene silencing (Patil*, et al.*, 2010). Recently, dual nanogels, for co-delivery of drug and gene, were synthesized and evaluated as carriers (Wang*, et al.*, 2007a, Wiradharma*, et al.*, 2009). Inhibition of ret/PTC1 oncogene, in the papillary thyroid carcinoma, has been achieved after administration of siRNA using chitosan-coated biodegradable poly(isobutylcyanoacrylate) nanoparticles. The nanoparticles protect the ret/PTC1 siRNA from *in vivo* degradation, leading to significant tumor growth inhibition after intratumoral administration, correlated to reduced ret/ PTC1 levels(Martimprey*, et al.*, 2008).

A novel approach for the control of inflammation in rheumatoid arthritis was reported. The strategy consisted in using chitosan/siRNA nanoparticle to silence the TNF-α expression in peritoneal macrophages. The nanoparticles, containing an unmodifed anti-TNF-α DsiRNA, mediated TNF-α knockdown (~66%) in primary peritoneal macrophages, *in vitro*. Histological analysis of joints revealed minimal cartilage destruction and inflammatory cell infiltration in anti-TNF-α-treated mice. Therefore, nanoparticle-mediated TNF-α knockdown in peritoneal macrophages may be a method to reduce local and systemic inflammation, and a novel strategy for arthritis treatment(Howard*, et al.*, 2009).

Other approach hypothesized that IL-1Ra (Interleukin-1 receptor antagonist) gene delivery can defend against inflammatory bone turnover, in rheumatoid arthritis patients. As compared to naked DNA and chitosan–DNA, folate–chitosan–DNA nanoparticles were less cytotoxic and enhanced IL-1Ra protein synthesis *in vitro*, offering a better protection against inflammation and abnormal bone metabolism in vivo (Fernandes, *et al.,* 2008).

Prevention of Respiratory Syncytial Virus (RSV) bronchiolitis, potentially reducing the later development of asthma associated with severe respiratory infections, was also evaluated using gene therapy. Plasmids expressing a short interfering RNA against the RSV-NS1gene (siNS1), were complexed with chitosan. Treatment of rats with siNS1, prior to RSV exposure, was effective in reducing virus titers in the lung, preventing the inflammation and airway hyperresponsiveness associated with the infection and asthma development (Kong*, et al.*, 2007). Similary, topical delivery of 5% imiquimod cream mixed with siRNA for natriuretic peptide receptor A (siNPRA) nanoparticles protected against asthma. In a mouse asthma model, the treatment with a imiquimod cream - containing siNPRA chitosan nanoparticles - significantly reduced the airway hyperresponsiveness, eosinophilia, lung histopathology and pro-inflammatory cytokines IL-4 and IL-5 in lung homogenates. By combining the treatment of imiquimod and siNPRA nanoparticles, a better protection against airway inflammation was achieved (Wang*, et al.*, 2008).

The feasibility of applying nanotechnology against *Plasmodium falciparum*, malarial parasites, was also investigated using antisense ODNs against malarial topoisomerase II gene, incorporated in chitosan nanoparticles. The *in vivo* use of nanoparticles against malaria is possible only if they are harmless to red blood cells. The erythrocyte membrane contains anionic glycoproteins, which can interact with protonated amino groups of chitosan. This process induces a curvature of the cell membrane, leading to rupture and hemoglobin release. In the presence of plasma, however, the membrane damage is reduced, an effect that might be explained by adsorption of negatively charged plasma proteins on the surface of charged particles; the plasma shielding effect suggests that chitosan nanoparticles indeed do not harm erythrocytes *in vivo*. Nanoparticles with negative surface charge exhibited a significantly stronger inhibitory effect (~87% inhibition) on the parasite growth in comparison to the positive ones (~74% inhibition) or free ODNs (~68% inhibition). This was the first study demonstrating the susceptibility of human malaria parasite to antisense nanoparticles (Foger, *et al*., 2006).

In conclusion, nanoparticulate systems are new tools that promise a revolution in the field of drug delivery. Nanodevices are suited to achieve the ideal of a controlled and

targeted release of bioactive molecules. Among the available nanosystems, self-assembled polymeric nanogels are particularly attractive, since they are easy to produce, affordable, and may effectively incorporate a variety of drugs, including biopharmaceuticals. Furthermore, they may be decorated with different kinds of molecules, improving the stability and target ability.

1.4 References

Akagia, T.; Wang, X.; Utob, T.; Baba, M.; Akashi, M. Protein direct delivery to dendritic cells using nanoparticles based on amphiphilic poly(amino acid) derivatives. *Biomaterials* **2007**, *28*, 3427-3436.

Aktas, Y.; Yemisci, M.; Andrieux, K.; Gursoy, R.N.; Alonso, M.J.; Fernandez-Megia, E.; Novoa-Carballal, R.; Quinoa, E.; Riguera, R.; Sargon, M.F.; Celik, H.H.; Demir, A.S.; Hincal, A.A.; Dalkara, T.; Capan, Y.; Couvreur, P. Development and brain delivery of chitosan-PEG nanoparticles functionalized with the monoclonal antibody OX26. *Bioconjugate Chemistry* **2005**, *16*, 1503-1511.

Anand, P.; Nair, H.B.; Sung, B.; Kunnumakkara, A.B.; Yadav, V.R.; Tekmal, R.R.; Aggarwal, B.B. Design of curcumin-loaded PLGA nanoparticles formulation with enhanced cellular uptake, and increased bioactivity in vitro and superior bioavailability in vivo. *Biochemical Pharmacology* **2010**, *79*, 330-338.

Arias, J.L.; Gallardo, V.; Ruiz, M.A.; Delgado, A.V. Ftorafur loading and controlled release from poly(ethyl-2-cyanoacrylate) and poly(butylcyanoacrylate) nanospheres. *International Journal of Pharmaceutics* **2007**, *337*, 282-290.

Avgoustakis, K.; Beletsi, A.; Panagi, Z.; Klepetsanis, P.; Karydas, A.G.; Ithakissios, D.S. PLGA-mPEG nanoparticles of cisplatin: in vitro nanoparticle degradation, in vitro drug release and in vivo drug residence in blood properties. *Journal of Controlled Release* **2002**, *79*, 123-135.

Avrameas, A.; McIlroy, D.; Hosmalin, A.; Autran, B.; Debre, P.; Monsigny, M.; Roche, A.C.; Midoux, P. Expression of a mannose/fucose membrane lectin on human dendritic cells. *European Journal of Immunology* **1996**, *26*, 394-400.

Bae, K.H.; Moon, C.W.; Lee, Y.; Park, T.G. Intracellular Delivery of Heparin Complexed with Chitosan-g-Poly(Ethylene Glycol) for Inducing Apoptosis. *Pharmaceutical Research* **2009**, *26*, 93-100.

Bessa, P.C.; Machado, R.; Dopler, D.; Banerjee, A.; Redl, H.; Griensven, M.V.; Reis, R.L.; Casal, M. Thermoresponsive self-assembled elastin-based nanoparticles for delivery of BMPs. *Journal of Controlled Release* **2010**, *142,* 312-318.

Bharali, D.J.; Pradhan, V.; Elkin, G.; Qi, W.; Hutson, A.; Mousa, S.A.; Thanavala, Y. Novel nanoparticles for the delivery of recombinant hepatitis B vaccine. *Nanomedicine* **2008**, *4*, 311-317.

Bhattarai, S.R.; K.C., R.B.; Aryal, S.; Bhattarai, N.; Kim, S.Y.; Yi, H.K.; Hwang, P.H.; Kim, H.Y. Hydrophobically modified chitosan/gold nanoparticles for DNA delivery *Journal of Nanoparticle Research* **2008**, *10*, 151-162.

Bivas-Benita, M.; Lin, M.Y.; Bal, S.M.; van Meijgaarden, K.E.; Franken, K.L.; Friggen, A.H.; Junginger, H.E.; Borchard, G.; Klein, M.R.; Ottenhoff, T.H. Pulmonary delivery of DNA encoding Mycobacterium tuberculosis latency antigen Rv1733c associated to PLGA-PEI nanoparticles enhances T cell responses in a DNA prime/protein boost vaccination regimen in mice. *Vaccine* **2009**, *27*, 4010-4017.

Bivas-Benita, M.; van Meijgaarden, K.E.; Franken, K.L.; Junginger, H.E.; Borchard, G.; Ottenhoff, T.H.; Geluk, A. Pulmonary delivery of chitosan-DNA nanoparticles enhances the immunogenicity of a DNA vaccine encoding HLA-A*0201-restricted T-cell epitopes of Mycobacterium tuberculosis. *Vaccine* **2004**, *22*, 1609-1615.

Blessing, T.; Kursa, M.; Holzhauser, R.; Kircheis, R.; Wagner, E. Different Strategies for Formation of PEGylated EGF-Conjugated PEI/DNA Complexes for Targeted Gene Delivery. *Bioconjugate Chemistry* **2001**, *12*, 529-537.

Boussif, O.; Lezoualc'h, F.; Zanta, M.A.; Mergny, M.D.; Scherman, D.; Demeneix, B.; Behr, J.P. A versatile vector for gene and oligonucleotide transfer into cells in culture and in vivo: polyethylenimine. *Proceedings of the National Academy of Sciences USA* **1995**, *92*, 7297-7301.

Brannon-Peppas, L.; Blanchette, J.O. Nanoparticle and targeted systems for cancer therapy. *Advanced Drug Delivery Reviews* **2004**, *56*, 1649-1659.

Budhian, A.; Siegel, S.J.; Winey, K.I. Controlling the in vitro release profiles for a system of haloperidol-loaded PLGA nanoparticles. *International Journal of Pharmaceutics* **2008**, *346*, 151-159.

Campos, A.M.D.; Sa, A. Chitosan nanoparticles: a new vehicle for the improvement of the delivery of drugs to the ocular surface. Application to cyclosporin A. *International Journal of Pharmaceutics* **2001**, *224*, 159-168.

Chapman, A.P. PEGylated antibodies and antibody fragments for improved therapy: a review. *Advanced Drug Delivery Reviews* **2002**, *54*, 531-545.

Chen, J.; Yang, W.; Li, G.; Qian, J.; Xue, J.; Fu, S.; Lu, D. Transfection of mEpo gene to intestinal epithelium in vivo mediated by oral delivery of chitosan-DNA nanoparticles. *World Journal of Gastroenterology* **2004**, *10*, 112-116.

Chen, M.; Wong, H.; Lin, K.; Chen, H.; Wey, S.; Sonaje, K.; Lin, Y.; Chu, C.; Sung, H. The characteristics, biodistribution and bioavailability of a chitosan-based nanoparticulate system for the oral delivery of heparin. *Biomaterials* **2009**, *30*, 6629-6637.

Chiu, S.; Ueno, N.T.; Lee, R.J. Tumor-targeted gene delivery via anti-HER2 antibody (trastuzumab, HerceptinR) conjugated polyethylenimine. *Journal of Controlled Release* **2004**, *97*, 357 - 369.

Choi, Y.H.; Liu, F.; Kim, J.-s.; Choi, Y.K.; Park, J.S.; Kim, S.W. Polyethylene glycol-grafted poly-L-lysine as polymeric gene carrier. *Journal of Controlled Release* **1998**, *54*, 39-48.

Chul Cho, K.; Hoon Jeong, J.; Jung Chung, H.; Joe, C.O.; Wan Kim, S.; Gwan Park, T. Folate receptor-mediated intracellular delivery of recombinant caspase-3 for inducing apoptosis. *Journal of Controlled Release* **2005**, *108*, 121-131.

Corsi, K.; Chellat, F.; Fernandes, J.C. Mesenchymal stem cells, MG63 and HEK293 transfection using chitosan-DNA nanoparticles. *Biomaterials* **2003**, *24*, 1255-1264.

Cotten, M. Mannose Polyethylenimine Conjugates for Targeted DNA Delivery into Dendritic Cells. *The Journal of Biological Chemistry* **1999**, *274*, 19087-19094.

Damge, C.; Maincent, P.; Ubrich, N. Oral delivery of insulin associated to polymeric nanoparticles in diabetic rats. *Journal of Controlled Release* **2007**, *117*, 163-170.

Dang, J.M.; Leong, K.W. Natural polymers for gene delivery and tissue engineering. *Advanced Drug Delivery Reviews* **2006**, *58*, 487-499.

Danhier, F.; Lecouturier, N.; Marchand-brynaert, J.; Feron, O. Paclitaxel-loaded PEGylated PLGA-based nanoparticles: In vitro and in vivo evaluation. *Journal of Controlled Release* **2009a**, *133*, 11-17.

Danhier, F.; Magotteaux, N.; Ucakar, B.; Lecouturier, N.; Brewster, M. Novel self-assembling PEG-p-(CL-co-TMC) polymeric micelles as safe and effective delivery system for Paclitaxel. *European Journal of Pharmaceutics and Biopharmaceutics* **2009b**, *73*, 230-238.

Des Rieux, A.; Fievez, V.; Garinot, M.; Schneider, Y.J.; Preat, V. Nanoparticles as potential oral delivery systems of proteins and vaccines: a mechanistic approach. *Journal of Controlled Release* **2006**, *116*, 1-27.

Dong, H.; Xu, Q.; Li, Y.; Mo, S.; Cai, S.; Liu, L. The synthesis of biodegradable graft copolymer cellulose-graft-poly(l-lactide) and the study of its controlled drug release. *Colloids and Surfaces B: Biointerfaces* **2008**, *66*, 26-33.

Dubernet, C.; Couvreur, P. Nanoparticles in cancer therapy and diagnosis. *Advanced Drug Delivery Reviews* **2002**, *54*, 631-651.

El-Shabouri, M.H. Positively charged nanoparticles for improving the oral bioavailability of cyclosporin-A. *International Journal of Pharmaceutics* **2002**, *249*, 101-108.

Elamanchili, P.; Diwan, M.; Cao, M.; Samuel, J. Characterization of poly(D , L -lactic-co-glycolic acid) based nanoparticulate system for enhanced delivery of antigens to dendritic cells. *Vaccine* **2004**, *22*, 2406-2412.

Elfinger, M.; Geiger, J.; Hasenpusch, G.; Uzgun, S.; Sieverling, N.; Aneja, M.K.; Maucksch, C.; Rudolph, C. Targeting of the β-adrenoceptor increases nonviral gene delivery to pulmonary epithelial cells in vitro and lungs in vivo. *Journal of Controlled Release* **2009**, *135*, 234-241.

Elfinger, M.; Mauckscha, C.; Rudolph, C. Characterization of lactoferrin as a targeting ligand for nonviral gene delivery to airway epithelial cells. *Biomaterials* **2007**, *28*, 3448-3455.

Esmaeili, F.; Ghahremani, M.H.; Ostad, S.N.; Atyabi, F.; Seyedabadi, M.; Malekshahi, M.R.; Amini, M.; Dinarvand, R. Folate-receptor-targeted delivery of docetaxel nanoparticles prepared by PLGA-PEG-folate conjugate. *Journal of Drug Targeting* **2008**, *16*, 415-423.

Farokhzad, O.C.; Cheng, J.; Teply, B.A.; Sheri, I.; Jon, S.; Kantoff, P.W.; Richie, J.P.; Langer, R. Targeted nanoparticle-aptamer bioconjugates for cancer chemotherapy in vivo. *Proceedings of the National Academy of Sciences USA* **2006**, *103*, 6315-6320.

Fernandes, J.C.; Wang, H.; Jreyssaty, C.; Benderdour, M.; Lavigne, P.; Qiu, X.; Winnik, F.M.; Zhang, X.; Dai, K.; Shi, Q. Bone-protective effects of nonviral gene therapy with folate-chitosan DNA nanoparticle containing interleukin-1 receptor antagonist gene in rats with adjuvant-induced arthritis. *Molecular Therapy* **2008**, *16*, 1243-1251.

Ferruti, P.; Franchini, J.; Bencini, M.; Ranucci, E.; Zara, G.P.; Serpe, L.; Primo, L.; Cavalli, R. Prevailingly cationic agmatine-based amphoteric polyamidoamine as a nontoxic, nonhemolytic, and "stealthlike" DNA complexing agent and transfection promoter. *Biomacromolecules* **2007**, *8*, 1498-1504.

Fewell, J.G.; Matar, M.; Slobodkin, G.; Han, S.O.; Rice, J.; Hovanes, B.; Lewis, D.H.; Anwer, K. Synthesis and application of a non-viral gene delivery system for immunogene therapy of cancer. *Journal of Controlled Release* **2005**, *109*, 288-298.

Foger, F.; Noonpakdee, W.; Loretz, B.; Joojuntr, S.; Salvenmoser, W.; Thaler, M.; Bernkop-Schnurch, A. Inhibition of malarial topoisomerase II in Plasmodium falciparum by antisense nanoparticles. *International Journal of Pharmaceutics* **2006**, *319*, 139-146.

Fuente, M.D.L.; Seij, B.n.; Alonso, M.J. Novel Hyaluronic Acid-Chitosan Nanoparticles for Ocular Gene Therapy. *Investigative Ophthalmology* **2008**, *49*, 2016-2024.

Gao, X.; Wu, B.; Zhang, Q.; Chen, J.; Zhu, J.; Zhang, W.; Rong, Z.; Chen, H.; Jiang, X. Brain delivery of vasoactive intestinal peptide enhanced with the nanoparticles conjugated with wheat germ agglutinin following intranasal administration. *Journal of Controlled Release* **2007**, *121*, 156-167.

Gao, Y.; Zhang, Z.; Chen, L.; Gu, W.; Li, Y. Synthesis of 6-N,N,N-trimethyltriazole chitosan via "click chemistry" and evaluation for gene delivery. *Biomacromolecules* **2009**, *10*, 2175-2182.

Gonçalves, C.; Martins, J.A.; Gama, F.M. Self-Assembled Nanoparticles of Dextrin Substituted with Hexadecanethiol. *Biomacromolecules* **2007**, *8*, 392-398.

Gonçalves, C.; Torrado, E.; Martins, T.; Pereira, P.; Pedrosa, J.; Gama, M. Dextrin nanoparticles: studies on the interaction with murine macrophages and blood clearance. *Colloids and Surfaces B: Biointerfaces* **2010**, *75*, 483-489.

Govender, T.; Riley, T.; Ehtezazi, T.; Garnett, M.C.; Stolnik, S.; Illum, L.; Davis, S.S. Defining the drug incorporation properties of PLA-PEG nanoparticles. *International Journal of Pharmaceutics* **2000**, *199*, 95-110.

Govender, T.; Stolnik, S.; Garnett, M.C.; Illum, L.; Davis, S.S. PLGA nanoparticles prepared by nanoprecipitation: drug loading and release studies of a water soluble drug. *Journal of Controlled Release* **1999**, *57*, 171-185.

Hans, M.L.; Lowman, A.M. Biodegradable nanoparticles for drug delivery and targeting. *Current Opinion in Solid State and Materials Science* **2002**, *6*, 319-327.

Hasegawa, U.; Sawada, S.-i.; Shimizu, T.; Kishida, T.; Otsuji, E.; Mazda, O.; Akiyoshi, K. Raspberry-like assembly of cross-linked nanogels for protein delivery. *Journal of Controlled Release* **2009**, *140*, 312-317.

Hashida, M.; Takemura, S.; Nishikawa, M.; Takakura, Y. Targeted delivery of plasmid DNA complexed with galactosylated poly(L-lysine). *Journal of Controlled Release* **1998**, *53*, 301-310.

Hashimoto, M.; Morimoto, M.; Saimoto, H.; Shigemasa, Y.; Yanagie, H.; Eriguchi, M.; Sato, T. Gene transfer by DNA/mannosylated chitosan complexes into mouse peritoneal macrophages. *Biotechnology Letters* **2006**, *28*, 815-821.

Hatakeyama, H.; Akita, H.; Ishida, E.; Hashimoto, K.; Kobayashi, H.; Aoki, T.; Yasuda, J.; Obata, K.; Kikuchi, H.; Ishida, T.; Kiwada, H.; Harashima, H. Tumor targeting of doxorubicin by anti-MT1-MMP antibody-modified PEG liposomes. *International Journal of Pharmaceutics* **2007**, *342*, 194-200.

He, X.; Mercado, A.E.; Xu, W.; Jabbari, E. Cytotoxicity of Paclitaxel in Biodegradable Self-Assembled Core-Shell Poly (Lactide-Co-Glycolide Ethylene Oxide Fumarate) Nanoparticles. *Pharmaceutical Research* **2008**, *25*, 1552-1562.

Hornig, S.; Bunjes, H.; Heinze, T. Preparation and characterization of nanoparticles based on dextran-drug conjugates. *Journal of Colloid and Interface Science* **2009**, *338*, 56-62.

Howard, K.A.; Paludan, S.R.; Behlke, M.A.; Besenbacher, F.; Deleuran, B.; Kjems, J. Chitosan/siRNA nanoparticle-mediated TNF-alpha knockdown in peritoneal macrophages for anti-inflammatory treatment in a murine arthritis model. *Molecular Therapy* **2009**, *17*, 162-168.

Hu, Y.; Ding, Y.; Ding, D.; Sun, M.; Zhang, L.; Jiang, X.; Yang, C. Hollow Chitosan/Poly(acrylic acid) Nanospheres as Drug Carriers. *Biomacromolecules* **2007**, *8*, 1069-1076.

Hu, Y.; Du, Y.; Wang, X.; Feng, T.; Science, E.; Key, H.P. Self-aggregation of water-soluble chitosan and solubilization of thymol as an antimicrobial agent. *Journal of Biomedical Materials Research Part A* **2009**, *90*, 874-881.

Huang, M.; Fong, C.W.; Khor, E.; Lim, L.Y. Transfection efficiency of chitosan vectors: effect of polymer molecular weight and degree of deacetylation. *Journal of Controlled Release* **2005**, *106*, 391-406.

Hwang, H.Y.; Kim, I.S.; Kwon, I.C.; Kim, Y.H. Tumor targetability and antitumor effect of docetaxel-loaded hydrophobically modified glycol chitosan nanoparticles. *Journal of Controlled Release* **2008**, *128*, 23-31.

Iinuma, H.; Maruyama, K.; Okinaga, K.; Sekine, T.; Ishida, O.; Ogiwara, N.; Johkura, K.; Yonemura, Y. Intracellular targeting therapy of cisplatin-encapsulated transferrin-polyethylene glycol liposome on peritoneal dissemination of gastric cancer. *International Journal Cancer* **2002**, *99*, 130 -137.

Ishihara, T.; Kubota, T.; Choi, T.; Takahashi, M.; Ayano, E.; Kanazawa, H.; Higaki, M. Polymeric nanoparticles encapsulating betamethasone phosphate with different release profiles and stealthiness. *International Journal of Pharmaceutics* **2009**, *375*, 148-154.

Ishii, T.; Okahata, Y.; Sato, T. Mechanism of cell transfection with plasmid/chitosan complexes. *Biochimica et Biophysica Acta* **2001**, *1514*, 51-64.

Jain, A.K.; Goyal, A.K.; Gupta, P.N.; Khatri, K.; Mishra, N.; Mehta, A.; Mangal, S.; Vyas, S.P. Synthesis, characterization and evaluation of novel triblock copolymer based nanoparticles for vaccine delivery against hepatitis B. *Journal of Controlled Release* **2009**, *136*, 161-169.

Jeong, J.H.; Lee, M.; Kim, W.J.; Yockman, J.W.; Park, T.G.; Kim, Y.H.; Kim, S.W. Anti-GAD antibody targeted non-viral gene delivery to islet beta cells. *Journal of Controlled Release* **2005**, *107*, 562 - 570.

Khatri, K.; Goyal, A.K.; Gupta, P.N.; Mishra, N.; Vyas, S.P. Plasmid DNA loaded chitosan nanoparticles for nasal mucosal immunization against hepatitis B. *International Journal of Pharmaceutics* **2008**, *354*, 235-241.

Kim, J.H.; Kim, Y.S.; Park, K.; Kang, E.; Lee, S.; Nam, H.Y.; Kim, K.; Park, J.H.; Chi, D.Y.; Park, R.W.; Kim, I.S.; Choi, K.; Chan Kwon, I. Self-assembled glycol chitosan nanoparticles for the sustained and prolonged delivery of antiangiogenic small peptide drugs in cancer therapy. *Biomaterials* **2008a**, *29*, 1920-1930.

Kim, S.H.; Jeong, J.H.; Lee, S.H.; Kim, S.W.; Park, T.G. LHRH Receptor-Mediated Delivery of siRNA Using Polyelectrolyte Complex Micelles Self-Assembled from siRNA-PEG-LHRH Conjugate and PEI. *Bioconjugate Chemistry* **2008b**, *19*, 2156-2162.

Kim, S.H.; Jeong, J.H.; Lee, S.H.; Kim, S.W.; Park, T.G. Local and systemic delivery of VEGF siRNA using polyelectrolyte complex micelles for effective treatment of cancer. *Journal of Controlled Release* **2008c**, *129*, 107-116.

Kim, S.H.; Mok, H.; Jeong, J.H.; Kim, S.W.; Park, T.G. Comparative Evaluation of Target-Specific GFP Gene Silencing Efficiencies for Antisense ODN, Synthetic siRNA, and siRNA Plasmid Complexed with PEI-PEG-FOL Conjugate. *Bioconjugate Chemistry* **2006**, *17*, 241-244.

Kim, S.Y.; Lee, Y.M. Taxol-loaded block copolymer nanospheres composed of methoxy poly(ethylene glycol) and poly(ε-caprolactone) as novel anticancer drug carriers. *Biomaterials* **2001**, *22*, 1697-1704.

Kim, T.H.; Park, I.K.; Nah, J.W.; Choi, Y.J.; Cho, C.S. Galactosylated chitosan/DNA nanoparticles prepared using water-soluble chitosan as a gene carrier. *Biomaterials* **2004**, *25*, 3783-3792.

Kim, W.J.; Yockman, J.W.; Lee, M.; Jeong, J.H.; Kim, Y.-h.; Kim, S.W. Soluble Flt-1 gene delivery using PEI-g-PEG-RGD conjugate for anti-angiogenesis. *Journal of Controlled Release* **2005a**, *106*, 224 - 234.

Kim, Y.H.; Park, J.H.; Lee, M.; Park, T.G.; Kim, S.W. Polyethylenimine with acid-labile linkages as a biodegradable gene carrier. *Journal of Controlled Release* **2005b**, *103*, 209-219.

Kirpotin, D.B.; Drummond, D.C.; Shao, Y.; Shalaby, M.R.; Hong, K.; Nielsen, U.B.; Marks, J.D.; Benz, C.C.; Park, J.W. Antibody Targeting of Long-Circulating Lipidic Nanoparticles Does Not Increase Tumor Localization but Does Increase Internalization in Animal Models. *Cancer Research* **2006**, *66*, 6732-6740.

Ko, K.S.; Lee, M.; Koh, J.J.; Kim, S.W. Combined Administration of Plasmids Encoding IL-4 and IL-10 Prevents the Development of Autoimmune Diabetes in Nonobese Diabetic Mice. *Molecular Therapy* **2001**, *4*, 313-316.

Kommareddy, S.; Amiji, M. Poly(ethylene glycol)-modified thiolated gelatin nanoparticles for glutathione-responsive intracellular DNA delivery. *Nanomedicine* **2007**, *3*, 32-42.

Kong, X.; Zhang, W.; Lockey, R.F.; Auais, A.; Piedimonte, G.; Mohapatra, S.S. Respiratory syncytial virus infection in Fischer 344 rats is attenuated by short interfering RNA against the RSV-NS1 gene. *Genetic Vaccines and Therapy* **2007**, *5*, 4-11.

Koping-Hoggard, M.; Tubulekas, I.; Guan, H.; Edwards, K.; Nilsson, M.; Varum, K.M.; Artursson, P. Chitosan as a nonviral gene delivery system. Structure-property relationships and characteristics compared with polyethylenimine in vitro and after lung administration in vivo. *Gene Therapy* **2001**, *8*, 1108-1121.

Kushibiki, T.; Nagata-nakajima, N.; Sugai, M.; Shimizu, A.; Tabata, Y. Delivery of plasmid DNA expressing small interference RNA for TGF-b type II receptor by cationized gelatin to prevent interstitial renal fibrosis. *Journal of Controlled Release* **2005**, *105*, 318 - 331.

Lee, A.L.Z.; Wang, Y.; Ye, W.; Yoon, H.S.; Chan, S.Y.; Yang, Y. Efficient intracellular delivery of functional proteins using cationic polymer core/shell nanoparticles. *Biomaterials* **2008**, *29*, 1224-1232.

Lee, D.; Zhang, W.; Shirley, S.A.; Kong, X.; Hellermann, G.R.; Lockey, R.F.; Mohapatra, S.S. Thiolated Chitosan/DNA Nanocomplexes Exhibit Enhanced and Sustained Gene Delivery. *Pharmaceutical Research* **2007**, *24*, 157-167.

Lee, E.S.; Na, K.; Bae, Y.H. Doxorubicin loaded pH-sensitive polymeric micelles for reversal of resistant MCF-7 tumor. *Journal of Controlled Release* **2005**, *103*, 405 - 418.

Lee, S.J.; Park, K.; Oh, Y.-k.; Kwon, S.-h.; Her, S.; Kim, I.-s.; Choi, K.; Lee, S.J.; Kim, H.; Lee, S.G.; Kim, K.; Kwon, I.C. Tumor specificity and therapeutic efficacy of photosensitizer-encapsulated glycol chitosan-based nanoparticles in tumor-bearing mice. *Biomaterials* **2009**, *30*, 2929-2939.

Li, F.; Wu, H.; Fan, L.; Zhang, H.; Zhang, H.; Chunhu, G. Study of dual responsive poly[(maleilated dextran)-graft-(N-isopropylacrylamide)] hydrogel nanoparticles: preparation, characterization and biological evaluation. *Polymer International* **2009a**, *58*, 1023-1033.

Li Fan, H.W., Hui Zhang, Fei Li, Tie-hong Yang, Chun-hu Gu and Qian Yang Novel Super pH-sensitive nanoparticles responsive to tumor extracellular pH. *Carbohydrate Polymers* **2008**, *73*, 390-400.

Li, G.; Liu, Z.; Liao, B.; Zhong, N. Induction of Th1-Type Immune Response by Chitosan Nanoparticles Containing Plasmid DNA Encoding House Dust Mite Allergen Der p 2 for Oral Vaccination in Mice. *Cellular & Molecular Immunology* **2009b**, *6*, 45-50.

Lin, C.; Engbersen, J.F.J. Effect of chemical functionalities in poly(amido amine)s for non-viral gene transfection. *Journal of Controlled Release* **2008**, *132*, 267-272.

Lin, C.; Zhong, Z.; Lok, M.C.; Jiang, X.; Hennink, W.E.; Feijen, J.; Engbersen, J.F.J. Linear poly(amido amine)s with secondary and tertiary amino groups and variable amounts of disulfide linkages: Synthesis and in vitro gene transfer properties. *Journal of Controlled Release* **2006**, *116*, 130 - 137.

Lin, C.; Zhong, Z.; Lok, M.C.; Jiang, X.; Hennink, W.E.; Feijen, J.; Engbersen, J.F.J. Novel Bioreducible Poly(amido amine)s for Highly Efficient Gene Delivery. *Bioconjugate Chemistry* **2007a**, *18*, 138-145.

Lin, Y. H.; Chen, C. T.; Liang, H. F.; Kulkarni, A.R.; Lee, P. W.; Chen, C. H.; Sung, H. W. Novel nanoparticles for oral insulin delivery via the paracellular pathway. *Nanotechnology* **2007b**, *18*, 1-11.

Lutsiak, M.E.; Robinson, D.R.; Coester, C.; Kwon, G.S.; Samuel, J. Analysis of poly(D,L-lactic-co-glycolic acid) nanosphere uptake by human dendritic cells and macrophages in vitro. *Pharmaceutical Research* **2002**, *19*, 1480-1487.

Luttmann, W.; Bratke, K.; Kupper, M.; Myrtek, D. *Immunology*. **2006**.

Mansouri, S.; Cuie, Y.; Winnik, F.; Qin, S.; Lavigne, P.; Benderdour, M.; Beaumont, E.; Fernandes, J.C. Characterization of folate-chitosan-DNA nanoparticles for gene therapy. *Biomaterials* **2006**, *27*, 2060-2065.

Mao, H.-q.; Roy, K.; Troung-le, V.L.; Janes, K.A.; Lin, K.Y.; Wang, Y.; August, J.T.; Leong, K.W. Chitosan-DNA nanoparticles as gene carriers: synthesis, characterization and transfection efficiency. *Journal of Controlled Release* **2001**, *70*, 399-421.

Martimprey, H.D.; Bertrand, J.-r.; Fusco, A.; Santoro, M.; Couvreur, P.; Vauthier, C.; Malvy, C. siRNA nanoformulation against the Ret/PTC1 junction oncogene is efficient in an in vivo model of papillary thyroid carcinoma. *Nucleic Acids Research* **2008**, *36*, 1-13.

Matsumura, Y.; Maeda, H. A New Concept for Macromolecular Therapeutics in Cancer Chemotherapy: Mechanism of Tumoritropic Accumulation of Proteins and the Antitumor Agent Smancs1. *Cancer Research* **1986**, *46*, 6387-6392.

Mehvar, R. Dextrans for targeted and sustained delivery of therapeutic and imaging agents. *Journal of Controlled Release* **2000**, *69*, 1-25.

Mi, F.; Wu, Y.; Lin, Y.; Sonaje, K.; Ho, Y.; Chen, C.; Juang, J.; Sung, H. Oral Delivery of Peptide Drugs Using Nanoparticles Self-Assembled by Poly(γ-glutamic acid) and a Chitosan Derivative Functionalized by Trimethylation. *Bioconjugate Chemistry* **2008**, *19*, 1248-1255.

Middaugh, C.R.; Wiethoff, C.M. Barriers to Nonviral Gene Delivery. *Journal of Pharmaceutical Sciences* **2003**, *92*, 203-217.

Minigo, G.; Scholzen, A.; Tang, C.K.; Hanley, J.C.; Kalkanidis, M.; Pietersz, G.A.; Apostolopoulos, V.; Plebanski, M. Poly-L-lysine-coated nanoparticles: a potent delivery system to enhance DNA vaccine efficacy. *Vaccine* **2007**, *25*, 1316-1327.

Mittal, G.; Sahana, D.K.; Bhardwaj, V.; Kumar, M.N.V.R. Estradiol loaded PLGA nanoparticles for oral administration: Effect of polymer molecular weight and copolymer composition on release behavior in vitro and in vivo. *Journal of Controlled Release* **2007**, *119*, 77 - 85.

Moghimi, S.M.; Hunter, A.C.; Murray, J.C. Long-circulating and target-specific nanoparticles: theory to practice. *Pharmacological Reviews* **2001**, *53*, 283-318.

Moghimi, S.M.; Hunter, A.C.; Murray, J.C. Nanomedicine: current status and future prospects. *The FASEB Journal* **2005**, *19*, 311-330.

Mu, L.; Feng, S.S. A novel controlled release formulation for the anticancer drug paclitaxel (Taxol): PLGA nanoparticles containing vitamin E TPGS. *Journal of Controlled Release* **2003**, *86*, 33-48.

Muller, R.H.; Jacobs, C.; Kayser, O. Nanosuspensions as particulate drug formulations in therapy. Rationale for development and what we can expect for the future. *Advanced Drug Delivery Reviews* **2001**, *47*, 3-19.

Murthy, N.; Campbell, J.; Fausto, N.; Hoffman, A.S.; Stayton, P.S. Bioinspired pH-Responsive Polymers for the Intracellular Delivery of Biomolecular Drugs. *Biochimica et Biophysica Acta* **2003**, *14*, 412-419.

Na, K.; Bum Lee, T.; Park, K.H.; Shin, E.K.; Lee, Y.B.; Choi, H.K. Self-assembled nanoparticles of hydrophobically-modified polysaccharide bearing vitamin H as a targeted anti-cancer drug delivery system. *European Journal of Pharmeutical Sciences* **2003a**, *18*, 165-173.

Na, K.; Lee, E.S.; Bae, Y.H. Adriamycin loaded pullulan acetate/sulfonamide conjugate nanoparticles responding to tumor pH: pH-dependent cell interaction, internalization and cytotoxicity in vitro. *Journal of Controlled Release* **2003b**, *87*, 3-13.

Nah, J.; Yu, L.; Han, S.; Ahn, C.; Kim, S.W. Artery wall binding peptide-poly(ethylene glycol)-grafted-poly(L-lysine)-based gene delivery to artery wall cells. *Journal of Controlled Release* **2002**, *78*, 273-284.

Nanjwade, B.K.; Bechra, H.M.; Derkar, G.K.; Manvi, F.V.; Nanjwade, V.K. Dendrimers: Emerging polymers for drug-delivery systems. *European Journal of Pharmaceutical Sciences* **2009**, *38*, 185-196.

Oba, M.; Aoyagi, K.; Miyata, K.; Matsumoto, Y.; Itaka, K.; Nishiyama, N.; Yamasaki, Y.; Koyama, H.; Kataoka, K. Polyplex Micelles with Cyclic RGD Peptide Ligands and Disulfide Cross-Links Directing to the Enhanced Transfection via Controlled Intracellular Trafficking. *Molecular Pharmaceutics* **2008**, *5*, 1080-1092.

Oishi, M.; Nagasaki, Y.; Itaka, K.; Nishiyama, N.; Kataoka, K. Lactosylated Poly(ethylene glycol)-siRNA Conjugate through Acid-Labile -Thiopropionate Linkage to Construct pH-Sensitive Polyion Complex Micelles Achieving Enhanced Gene Silencing in Hepatoma Cells. *Journal of the American Chemical Society* **2005**, *127*, 1624-1625.

Okamoto, S.; Yoshii, H.; Akagi, T.; Akashi, M.; Ishikawa, T.; Okuno, Y.; Takahashi, M.; Yamanishi, K.; Mori, Y. Influenza hemagglutinin vaccine with poly(γ-glutamic acid) nanoparticles enhances the protection against in uenza virus infection through both humoral and cell-mediated immunity. *Vaccine* **2007**, *25*, 8270-8278.

Okamoto, S.; Yoshii, H.; Ishikawa, T.; Akagi, T.; Akashi, M.; Takahashi, M.; Yamanishi, K.; Mori, Y. Single dose of inactivated Japanese encephalitis vaccine with poly(γ-glutamic acid) nanoparticles provides effective protection from Japanese encephalitis virus. *Vaccine* **2008**, *26*, 589-594.

Oupicky, D.; Parker, A.L.; Seymour, L.W. Laterally Stabilized Complexes of DNA with Linear Reducible Polycations: Strategy for Triggered Intracellular Activation of DNA Delivery Vectors. *Journal of the American Chemical Society* **2002**, *124*, 8-9.

Owens, D.E.; Peppas, N.A. Opsonization, biodistribution, and pharmacokinetics of polymeric nanoparticles. *International Journal of Pharmaceutics* **2006**, *307*, 93-102.

Oyarzun-Ampuero, F.A.; Brea, J.; Loza, M.I.; Torres, D.; Alonso, M.J. Chitosan-hyaluronic acid nanoparticles loaded with heparin for the treatment of asthma. *International Journal of Pharmaceutics* **2009**, *381*, 122-129.

Panyam, J.; Labhasetwar, V. Biodegradable nanoparticles for drug and gene delivery to cells and tissue. *Advanced Drug Delivery Reviews* **2003a**, *55*, 329-347.

Panyam, J.; Sahoo, S.K.; Prabha, S.; Bargar, T.; Labhasetwar, V. Fluorescence and electron microscopy probes for cellular and tissue uptake of poly(D,L-lactide-co-glycolide) nanoparticles. *International Journal of Pharmaceutics* **2003b**, *262*, 1-11.

Panyam, J.; Williams, D.; Dash, A.; Leslie-pelecky, D.; Labhasetwar, V. Solid-State Solubility Influences Encapsulation and Release of Hydrophobic Drugs from PLGA/PLA Nanoparticles. *Journal of Pharmaceutical Sciences* **2004**, *93*, 1804-1814.

Park, J.H.; Kwon, S.; Nam, J.O.; Park, R.W.; Chung, H.; Seo, S.B.; Kim, I.S.; Kwon, I.C.; Jeong, S.Y. Self-assembled nanoparticles based on glycol chitosan bearing β-cholanic acid for RGD peptide delivery. *Journal of Controlled Release* **2004**, *95*, 579-588.

Park, T.G.; Jeong, J.H.; Kim, S.W. Current status of polymeric gene delivery systems. *Advanced Drug Delivery Reviews* **2006**, *58*, 467-486.

Pasumarthy, M.; Cooper, M.J. Biological Properties of Poly-L-lysine-DNA Complexes Generated by Cooperative Binding of the Polycation. *The Journal of Biological Chemistry* **2001**, *276*, 34379 -34387.

Patil, Y.B.; Swaminathan, S.K.; Sadhukha, T.; Panyam, J. The use of nanoparticle-mediated targeted gene silencing and drug delivery to overcome tumor drug resistance. *Biomaterials* **2010**, *31*, 358-365.

Patnaik, S.; Sharma, A.K.; Garg, B.S.; Gandhi, R.P.; Gupta, K.C. Photoregulation of drug release in azo-dextran nanogels. *International Journal of Pharmaceutics* **2007**, *342*, 184-193.

Peng, S.; Yang, M.; Su, C.; Chen, H.; Lee, P.; Wei, M.; Sung, H. Effects of incorporation of poly(g-glutamic acid) in chitosan/DNA complex nanoparticles on cellular uptake and transfection efficiency. *Biomaterials* **2009**, *30*, 1797-1808.

Peracchia, M.T.; Fattal, E.; Desmaele, D.; Besnard, M.; Noel, J.P.; Gomis, J.M.; Appel, M.; d'Angelo, J.; Couvreur, P. Stealth PEGylated polycyanoacrylate nanoparticles for intravenous administration and splenic targeting. *Journal of Controlled Release* **1999**, *60*, 121-128.

Petersen, H.; Fechner, P.M.; Martin, A.L.; Kunath, K.; Stolnik, S.; Roberts, C.J.; Fischer, D.; Davies, M.C.; Kissel, T.; Kingdom, U. Polyethylenimine-graft-Poly(ethylene glycol) Copolymers: Influence of Copolymer Block Structure on DNA Complexation and Biological Activities as Gene Delivery System. *Bioconjugate Chemistry* **2002**, *13*, 845-854.

Plard, J.P.; Bazile, D. Comparison of the safety profiles of PLA(50) and Me.PEG-PLA(50) nanoparticles after single dose intravenous administration to rat. *Colloids and Surfaces B: Biointerfaces* **1999**, *16*, 173-183.

Prego, C.; Torres, D.; Fernandez-Megia, E.; Novoa-Carballal, R.; Quinoa, E.; Alonso, M.J. Chitosan-PEG nanocapsules as new carriers for oral peptide delivery. Effect of chitosan pegylation degree. *Journal of Controlled Release* **2006**, *111*, 299-308.

Putnam, D.; Langer, R. Poly(4-hydroxy-L-proline ester): Low-temperature Polycondensation and Plasmid DNA Complexation. *Macromolecules* **1999**, *32*, 3658-3662.

Qian, F.; Cui, F.; Ding, J.; Tang, C.; Yin, C. Chitosan Graft Copolymer Nanoparticles for Oral Protein Drug Delivery: Preparation and Characterization. *Biomacromolecules* **2006**, *7*, 2722-2727.

Randolph, G.J.; Angeli, V.; Swartz, M.A. Dendritic-cell trafficking to lymph nodes through lymphatic vessels. *Nature Reviews Immunology* **2005**, *5*, 617-628.

Ravikumara, N.R.; Madhusudhan, B.; Nagaraj, T.S.; Hiremat, S.R.; Gargi, R. Preparation and Evaluation of Nimesulide-loaded Ethylcellulose and Methylcellulose Nanoparticles and Microparticles for Oral Delivery. *Journal of Biomaterials Applications* **2009**, *24*, 47-64.

Reddy, S.T.; Rehor, A.; Schmoekel, H.G.; Hubbell, J.A.; Swartz, M.A. In vivo targeting of dendritic cells in lymph nodes with poly(propylene sulfide) nanoparticles. *Journal of Controlled Release* **2006**, *112*, 26 - 34.

Rinaudo, M. Non-Covalent Interactions in Polysaccharide Systems. *Macromolecular Bioscience* **2006**, *6*, 590-610.

Rosenberg, S.A. Progress in human tumour immunology and immunotherapy. *Nature* **2001**, *2*, 380-384.

Roser, M.; Fischer, D.; Kissel, T. Surface-modified biodegradable albumin nano- and microspheres. II: effect of surface charges on in vitro phagocytosis and biodistribution in rats. *European Journal of Pharmaceutics and Biopharmaceutics* **1998**, *46*, 255-263.

Sallusto, F.; Cella, M.; Danieli, C.; Lanzavecchia, A. Dendritic Cells Use Macropinocytosis and the Mannose Receptor to Concentrate Macromolecules in the Major Histocompatibility Complex Class II Compartment: Downregulation by Cytokines and Bacterial Products. *The Journal of Experimental Medicine* **1995**, *182*, 389-400.

Sato, T.; Ishii, T.; Okahata, Y. In vitro gene delivery mediated by chitosan. Effect of pH, serum, and molecular mass of chitosan on the transfection efficiency. *Biomaterials* **2001**, *22*, 2075-2080.

Satoh, T.; Kakimoto, S.; Kano, H.; Nakatani, M.; Shinkai, S.; Nagasaki, T. In vitro gene delivery to HepG2 cells using galactosylated 6-amino-6-deoxychitosan as a DNA carrier. *Carbohydrate Research* **2007**, *342*, 1427-1433.

Sayin, B.; Somavarapu, S.; Li, X.W.; Thanou, M.; Sesardic, D.; Alpar, H.O.; Senel, S. Mono-N-carboxymethyl chitosan (MCC) and N-trimethyl chitosan (TMC) nanoparticles for non-invasive vaccine delivery. *International Journal of Pharmaceutics* **2008**, *363*, 139-148.

Schiffelers, R.M.; Ansari, A.; Xu, J.; Zhou, Q.; Tang, Q.; Storm, G.; Molema, G.; Lu, P.Y.; Scaria, P.V.; Woodle, M.C. Cancer siRNA therapy by tumor selective delivery with ligand-targeted sterically stabilized nanoparticle. *Nucleic Acids Research* **2004**, *32*, 1-10.

Shah, L.K.; Amiji, M.M. Intracellular delivery of saquinavir in biodegradable polymeric nanoparticles for HIV/AIDS. *Pharmaceutical Research* **2006**, *23*, 2638-2645.

Shen, Y.; Tang, H.; Zhan, Y.; Kirk, E.A.V.; Murdoch, W.J. Degradable Poly(β-amino ester) nanoparticles for cancer cytoplasmic drug delivery. *Nanomedicine: Nanotechnology, Biology, and Medicine* **2009**, *5*, 192-201.

Shenoy, D.B.; Amiji, M.M. Poly(ethylene oxide)-modified poly(ε-caprolactone) nanoparticles for targeted delivery of tamoxifen in breast cancer. *International Journal of Pharmaceutics* **2005**, *293*, 261-270.

Shimizu, T.; Kishida, T.; Hasegawa, U.; Ueda, Y.; Imanishi, J.; Yamagishi, H.; Akiyoshi, K.; Otsuji, E.; Mazda, O. Nanogel DDS enables sustained release of IL-12 for tumor immunotherapy. *Biochemical and Biophysical Research Communications* **2008**, *367*, 330-335.

Shrivastava, S.K.; Jain, D.; Shrivastava, P.K.; Piyush, T. Flurbiprofen- and Suprofen-Dextran Conjugates: Synthesis, Characterization and Biological Evaluation. *Tropical Journal of Pharmaceutical Research* **2009**, *8*, 221-229.

Shu, S.; Sun, C.; Zhang, X.; Wu, Z.; Wang, Z.; Li, C. Hollow and degradable polyelectrolyte nanocapsules for protein drug delivery. *Acta Biomaterialia* **2010**, *6*, 210-217.

Singh, J.; Pandit, S.; Bramwell, V.W.; Alpar, H.O. Diphtheria toxoid loaded poly-(ϵ-caprolactone) nanoparticles as mucosal vaccine delivery systems. *Methods* **2006**, *38*, 96-105.

Sonaje, K.; Lin, Y.H.; Juang, J.H.; Wey, S.P.; Chen, C.T.; Sung, H.W. In vivo evaluation of safety and efficacy of self-assembled nanoparticles for oral insulin delivery. *Biomaterials* **2009**, *30*, 2329-2339.

Soppimath, K.S.; Aminabhavi, T.M.; Kulkarni, A.R.; Rudzinski, W.E. Biodegradable polymeric nanoparticles as drug delivery devices. *Journal of Controlled Release* **2001**, *70*, 1-20.

Storm, G.; Belliot, S.; Daemen, T.; Lasic, D.D. Surface modification of nanoparticles to oppose uptake by the mononuclear phagocyte system. *Advanced Drug Delivery Reviews* **1995**, *17*, 31-48.

Suh, W.; Chung, J.K.; Park, S.H.; Kim, S.W. Anti-JL1 antibody-conjugated poly (L-lysine) for targeted gene delivery to leukemia T cells. *Journal of Controlled Release* **2001**, *72*, 171-178.

Sun, T.; Du, J.; Yan, L.; Mao, H.; Wang, J. Self-assembled biodegradable micellar nanoparticles of amphiphilic and cationic block copolymer for siRNA delivery. *Biomaterials* **2008**, *29*, 4348-4355.

Swartz, M.A. The physiology of the lymphatic system. *Advanced Drug Delivery Reviews* **2001**, *50*, 3-20.

Tan, Y.; Liu, C. Self-aggregated nanoparticles from linoleic acid modified carboxymethyl chitosan: Synthesis, characterization and application in vitro. *Colloids and Surfaces B: Biointerfaces* **2009**, *69*, 178-182.

Tarragó-Trani, M.T.; Storrie, B. Alternative routes for drug delivery to the cell interior: pathways to the golgi apparatus and endoplasmic reticulum. *Advanced Drug Delivery Reviews* **2007**, *59*, 782-797.

Teicher, B.A. Acute and chronic in vivo therapeutic resistance. *Biochemical Pharmacology* **2009**, *77*, 1665-1673.

Thiele, L.; Merkle, H.P.; Walter, E. Phagocytosis and phagosomal fate of surface-modified microparticles in dendritic cells and macrophages. *Pharmaceutical Research* **2003**, *20*, 221-228.

Tseng, W.-c.; Jong, C.-m. Improved Stability of Polycationic Vector by Dextran-Grafted Branched Polyethylenimine. *Biomacromolecules* **2003**, *4*, 1277-1284.

Vila, A.; Sanchez, A.; Tobio, M.; Calvo, P.; Alonso, M.J. Design of biodegradable particles for protein delivery. *Journal of Controlled Release* **2002**, *78*, 15-24.

Vinogradov, S.V.; Batrakova, E.V.; Kabanov, A.V. Nanogels for oligonucleotide delivery to the brain. *Bioconjugate Chemistry* **2004**, *15*, 50-60.

Wang, J.; Lee, I.L.; Lim, W.S.; Chia, S.M.; Yu, H.; Leong, K.W.; Mao, H.Q. Evaluation of collagen and methylated collagen as gene carriers. *International Journal of Pharmaceutics* **2004**, *279*, 115-126.

Wang, L.; Zeng, R.; Li, C.; Qiao, R. Self-assembled polypeptide-block-poly(vinylpyrrolidone) as prospective drug-delivery systems. *Colloids and Surfaces B: Biointerfaces* **2009a**, *74*, 284-292.

Wang, X.; Xu, W.; Mohapatra, S.; Kong, X.; Li, X.; Lockey, R.F.; Mohapatra, S.S. Prevention of airway inflammation with topical cream containing imiquimod and small interfering RNA for natriuretic peptide receptor. *Genetic Vaccines and Therapy* **2008**, *6*, 7-15.

Wang, X.; Zheng, C.; Wu, Z.; Teng, D.; Zhang, X.; Wang, Z.; Li, C. Chitosan-NAC nanoparticles as a vehicle for nasal absorption enhancement of insulin. *Journal of Biomedical Materials Research B Applied Biomaterials* **2009b**, *88*, 150-161.

Wang, Y.; Wang, L.; Goh, S.; Yang, Y. Synthesis and Characterization of Cationic Micelles Self-Assembled from a Biodegradable Copolymer for Gene Delivery. *Biomacromolecules* **2007a**, *8*, 1028-1037.

Wang, Y.S.; Liu, L.R.; Jiang, Q.; Zhang, Q.Q. Self-aggregated nanoparticles of cholesterol-modified chitosan conjugate as a novel carrier of epirubicin. *European Polymer Journal* **2007b**, *43*, 43-51.

Watson, P.; Jones, A.T.; Stephens, D.J. Intracellular trafficking pathways and drug delivery: fluorescence imaging of living and fixed cells. *Advanced Drug Delivery Reviews* **2005**, *57*, 43-61.

Weecharangsan, W.; Opanasopit, P.; Ngawhirunpat, T.; Apirakaramwong, A.; Rojanarata, T.; Ruktanonchai, U.; Lee, R.J. Evaluation of chitosan salts as non-viral gene vectors in CHO-K1 cells. *International Journal of Pharmaceutics* **2008**, *348*, 161-168.

Wei, H.; Zhang, X.Z.; Cheng, H.; Chen, W.Q.; Cheng, S.X.; Zhuo, R.X. Self-assembled thermo- and pH responsive micelles of poly(10-undecenoic acid-b-N-isopropylacrylamide) for drug delivery. *Journal of Controlled Release* **2006**, *116*, 266-274.

Wei, X.; Gong, C.; Shi, S.; Fu, S.; Men, K.; Zeng, S.; Zheng, X.; Gou, M.; Chen, L.; Qiu, L.; Qian, Z. Self-assembled honokiol-loaded micelles based on poly(ε-caprolactone)-poly(ethylene glycol)-poly(ε-caprolactone) copolymer. *International Journal of Pharmaceutics* **2009**, *369*, 170-175.

Wiradharma, N.; Tong, Y.W.; Yang, Y.-y. Self-assembled oligopeptide nanostructures for co-delivery of drug and gene with synergistic therapeutic effect. *Biomaterials* **2009**, *30*, 3100-3109.

Wolfert, M.; Seymour, L. Chloroquine and amphipathic peptide helices show synergistic transfection in vitro. *Gene Therapy* **1998**, *5*, 409-414.

Wu, D.Q.; Lu, B.; Chang, C.; Chen, C.S.; Wang, T.; Zhang, Y.Y.; Cheng, S.X.; Jiang, X.J.; Zhang, X.Z.; Zhuo, R.X. Galactosylated fluorescent labeled micelles as a liver targeting drug carrier. *Biomaterials* **2009**, *30*, 1363-1371.

Xu, P.; Kirk, E.A.V.; Murdoch, W.J.; Zhan, Y.; Isaak, D.D.; Radosz, M.; Shen, Y. Anticancer Efficacies of Cisplatin-Releasing pH-Responsive Nanoparticles. *Biomacromolecules* **2006**, *7*, 829-835.

Xu, P.; Quick, G.K.; Yeo, Y. Gene delivery through the use of a hyaluronate-associated intracellularly degradable crosslinked polyethyleneimine. *Biomaterials* **2009a**, *30*, 5834-5843.

Xu, W.; Shen, Y.; Jiang, Z.; Wang, Y.; Chu, Y.; Xiong, S. Intranasal delivery of chitosan-DNA vaccine generates mucosal SIgA and anti-CVB3 protection. *Vaccine* **2004**, *22*, 3603-3612.

Xu, Z.; Gu, W.; Huang, J.; Sui, H.; Zhou, Z.; Yang, Y.; Yan, Z.; Li, Y. In vitro and in vivo evaluation of actively targetable nanoparticles for paclitaxel delivery. *International Journal of Pharmaceutics* **2005**, *288*, 361-368.

Xu, Z.; Wan, X.; Zhang, W.; Wang, Z.; Peng, R.; Tao, F.; Cai, L.; Li, Y.; Jiang, Q.; Gao, R. Synthesis of biodegradable polycationic methoxy poly(ethylene glycol)–polyethylenimine–chitosan and its potential as gene carrier *Carbohydrate Polymers* **2009b**, *78*, 46-53.

Yamamoto, H.; Kuno, Y.; Sugimoto, S.; Takeuchi, H.; Kawashima, Y. Surface-modified PLGA nanosphere with chitosan improved pulmonary delivery of calcitonin by mucoadhesion and opening of the intercellular tight junctions. *Journal of Controlled Release* **2005**, *102*, 373 - 381.

Yang, T.; Chin, W.; Cherng, J. Synthesis of Novel Biodegradable Cationic Polymer: N,N-Diethylethylenediamine Polyurethane as a Gene Carrier. *Biomacromolecules* **2004**, *5*, 1926-1932.

Yang, X.; Yuan, X.; Cai, D.; Wang, S.; Zong, L. Low molecular weight chitosan in DNA vaccine delivery via mucosa. *International Journal of Pharmaceutics* **2009**, *375*, 123-132.

Yang, Y.; Xu, Z.; Jiang, J.; Gao, Y.; Gu, W.; Chen, L.; Tang, X.; Li, Y. Poly(imidazole/DMAEA)phosphazene/DNA self-assembled nanoparticles for gene delivery: synthesis and in vitro transfection. *Journal of Controlled Release* **2008**, *127*, 273-279.

Yin, L.; Ding, J.; He, C.; Cui, L.; Tang, C.; Yin, C. Drug permeability and mucoadhesion properties of thiolated trimethyl chitosan nanoparticles in oral insulin delivery. *Biomaterials* **2009**, *30*, 5691-5700.

Zambaux, M.F.; Bonneaux, F.; Gref, R.; Dellacherie, E.; Vigneron, C. Preparation and characterization of protein C-loaded PLA nanoparticles. *Journal of Controlled Release* **1999**, *60*, 179-188.

Zenga, J.; Wanga, X.; Wang, S. Self-assembled ternary complexes of plasmid DNA, low molecular weight polyethylenimine and targeting peptide for nonviral gene delivery into neurons. *Biomaterials* **2007**, *28*, 1443-1451.

Zhang, S. Emerging biological materials through molecular self-assembly. *Biotechnology Advances* **2002**, *20*, 321-339.

Zhang, X.; Zhang, H.; Wu, Z.; Wang, Z.; Niu, H.; Li, C. Nasal absorption enhancement of insulin using PEG-grafted chitosan nanoparticles. *European Journal of Pharmaceutics and Biopharmaceutics* **2008**, *68*, 526-534.

Zhao, Z.; He, M.; Yin, L.; Bao, J.; Shi, L.; Wang, B.; Tang, C.; Yin, C. Biodegradable Nanoparticles Based on Linoleic Acid and Poly(β-malic acid) Double Grafted Chitosan Derivatives as Carriers of Anticancer Drugs. *Biomacromolecules* **2009**, *10*, 565-572.

Zheng, F.; Shi, X.; Yang, G.; Gong, L.; Yuan, H.; Cui, Y.; Wang, Y.; Du, Y.; Li, Y. Chitosan nanoparticle as gene therapy vector via gastrointestinal mucosa administration: Results of an in vitro and in vivo study. *Life Sciences* **2007**, *80*, 388 - 396.

Zheng, Y.; Cai, Z.; Song, X.; Yu, B.; Bi, Y.; Chen, Q.; Zhao, D.; Xu, J.; Hou, S. Receptor mediated gene delivery by folate conjugated N-trimethyl chitosan in vitro. *International Journal of Pharmaceutics* **2009**, *382*, 262-269.

2. Self –assembled nanoparticles of dextrin substituted with hexadecanethiol

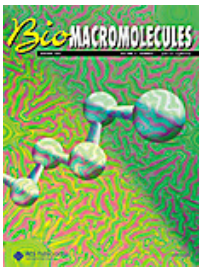

Adapted from **Biomacromolecules** (2007) 8, 392-398

The amphiphilic molecule dextrin-VA-SC_{16} ($dexC_{16}$) was synthesized and studied in this work. $DexC_{16}$ has a hydrophilic dextrin backbone with grafted acrylate groups (VA), substituted with hydrophobic 1-hexadecanethiol (C_{16}). A versatile synthetic method was developed allowing control of the dextrin degree of substitution with the hydrophobic chains (DS_{C16}, number of alkyl chains per 100 dextrin glucopyranoside residues). Materials with different DS_{C16} were prepared and characterized using ^{1}H NMR. $DexC_{16}$ self assembles in water through association of the hydrophobic alkyl chains, originating nanoparticles. The nanoparticles properties were studied by dynamic light scattering (DLS), fluorescence spectroscopy, and atomic force microscopy (AFM).

2.1 Introduction

Amphiphilic molecules, such as surfactants or lipids, spontaneously self-assemble in water, forming self-aggregates, such as micelles, bilayer membranes, tubes and vesicles. Amphiphilicity of biopolymers is one of the most important factors for their self-organization in water. Among the different types of amphiphilic polymers, water-soluble polymers with hydrophobic molecules grafted on side chains have received special attention. By self-assembling, the hydrophobic segments are segregated from the aqueous exterior to form an inner core surrounded by hydrophilic chains. Polymeric micelles or nanoparticles with a hydrophobic core and hydrophilic shell are thus prepared. This kind of structure is suitable for trapping hydrophobic substances, such as fluorescent probes (Akiyoshi, *et al.*, 1993), proteins (Akiyoshi, *et al.*, 1998), and hydrophobic pharmaceuticals (Liu, *et al.*, 2005). The size, density and colloidal stability of nanoparticles can be controlled by changing the degree of substitution of hydrophobes and its hydrophobicity (Akiyoshi*, et al.*, 1996). The association mechanism is mainly governed by the alkyl side chain concentration and length and is little influenced by the molecular weight of the polymer backbone (Petit-Agnely, *et al.*, 2000). However, with low molecular weight polymers, the hydrophobic aggregates are not connected via the polymer backbone (Petit-Agnely*, et al.*, 1999). The study of nanogels (hydrogel nanoparticles) has intensified during the past decade due to enormous potential applications in the development and implementation of new environmentally responsive materials, biomimetics, biosensors, artificial muscles and drug delivery systems (Lee*, et al.*, 2004). Solid nanoparticles made from biodegradable polymers have been widely investigated for long-term delivery of drugs (Hans, *et al.*, 2005). They can potentially provide benefits such as increased therapeutic effect, prolonged bioactivity, controlled release rate, and finally decreased administration frequency, thereby increasing patient compliance.

Nanostructures spontaneously form when the concentration of the polymer is higher than its critical micelle concentration (CMC). Self-assembly in water of a hydrophobically modified dextrin (dexC_{16}) was investigated in this work. The structural change upon dilution of the dexC_{16} self-aggregates in water was investigated by fluorescence in the presence of pyrene as the fluorescent probe. Pyrene shows interesting photophysical properties due to the long lifetime of its monomers. Pyrene is one of the few condensed aromatic hydrocarbons which show significant fine structure (vibronic bands) in its monomer fluorescence spectra in solution. The vibrational fine structure intensities

undergo significant perturbations on going from nonpolar solvents to polar solvents with high permanent dipoles. The five predominant peaks of pyrene are numbered I-V, and peak III shows maximum variations in intensity relative to peak I. The I_3/I_1 ratio will be used for determination of the CMC (Nizri*, et al.*, 2005). The CMC value depends mostly on the chemical structure of the amphiphilic polymer and the number of hydrophobic chains grafted on the polymer backbone. Other relevant properties of the nanoparticles, such as the size, stability, and shape, were also evaluated in this work.

2.2 Experimental section

2.2.1 Materials

Dextrin-VA was synthesized by transesterification of dextrin with vinyl acrylate (VA) as described by Ferreira *et al.* (Ferreira, *et al.*, 2002) for the transesterification of dextran with VA, with few modifications. The transesterification of dextran requires an enzyme (Proleather), but using dextrin as substrate the enzyme does not catalyse the transesterification. In this work, dextrin-VA with 20 acrylate groups per 100 dextrin glucopyranoside residues was used. Dimethyl sulfoxide (DMSO), triethylamine (TEA), and deuterium oxide (D_2O) were from Aldrich. Regenerated cellulose tubular membranes, with 3500 MWCO, were obtained from Membrane Filtration Products.

Pyrene (Py) was from Aldrich and was used after appropriate recrystallization. Distilled water was used for the preparation of aqueous solutions.

2.2.2 Synthesis of dexC_{16}

Dextrin-VA and 1-hexadecanethiol were dissolved in dimethyl sulfoxide (equivalent VA = 0.0413 M). Different molar percentages of 1-hexadecanethiol (10%, 20%, 40%, 60%, and 100% relative to VA) were added to the reaction mixture in order to obtain different degrees of substitution (DS). Triethylamine (1 mol equiv to VA) was added to the reaction mixture. The medium was stirred for 24 h, at 50 ºC. The mixture was dialysed for 48 h against water with frequent water change. After freezing, the mixture was lyophilized and stored.

2.2.3 Sample preparation

Lyophilized $dexC_{16}$ was dissolved in water under stirring at 50 ºC and then further sonicated for 20 min until a clear solution was obtained. The degree of solubility of $dexC_{16}$ depends on the degree of substitution. Increasing the degree of substitution reduces the solubility. In the range of DS_{C16} used, to prepare a 1.0 g/dL solution, 3 h of stirring is the maximum time required to dissolve $dexC_{16}$.

2.2.4 Dynamic light scattering

The size distribution was determined with a Malvern Zetasizer, MODEL NANO ZS (Malvern Instruments Limited, U.K.). A dispersion of nanoparticles in ultrapure water (1 mL) was analysed at 25 ºC in a polystyrene cell using a Helium-Neon laser - wavelength of 633 nm and a detector angle of 173º. The dispersion was filtered through a 0.45 μm pore.

2.2.5 ^{1}H NMR

Lyophilized $dexC_{16}$ was dispersed in deuterium oxide (1.0 g/dL). Solutions were transferred to 5 mm NMR tubes. 1D ^{1}H NMR measurements were performed with a Varian Unity Plus 300 spectrometer operating at 299.94 MHz. 1D ^{1}H NMR spectra were measured at 298 K with 80 scans, a spectral width of 4800 Hz, a relaxation delay of 1 s between scans, and an acquisition time of 3.75 s.

2.2.6 Fluorescence spectroscopy

Fluorescence measurements were performed on a Varian Cary Eclipse fluorescence spectrofluorometer using a quartz cell. The pyrene spectra were obtained using an excitation wavelength of 337 nm and recording the emission over the range 350-500 nm at a scan rate of 120 nm/min. The slit width was set at 20 nm for the excitation and 2.5 nm for the emission. The fluorescence intensity, for each vibronic peak, was measured at the maximum of each peak.

2.2.7 Atomic force microscopy

Tapping-mode imaging was carried out on a Nanoscope IIIa Multimode (Digital Instruments, Veeco) scanning probe microscope. A silicon tip doped with phosphorus, with a radius curvature of less than 10 nm (RTESP, VEECO), was used. This tip has a typical resonance frequency of 288-328 kHz and a typical force constant of 20-80 N/m. A scan rate of 1.4-1.8 Hz was sufficient to maintain a good signal-to-noise ratio. A drop of aqueous solution (0.01 g/dL) of dexC_{16} was placed on new-cleaved HOPG surface, thoroughly rinsed with water, and dried under a N_2 flux.

2.3 Results and discussion

2.3.1 Synthesis of the dextrin-VA-SC_{16}

The reaction between the thiol moiety and the acrylate group of dextrin-VA is a Michael addition with thiol acting as a nucleophile (Scheme 2.1).

Scheme 2.1. Synthesis of $DexC_{16}$.

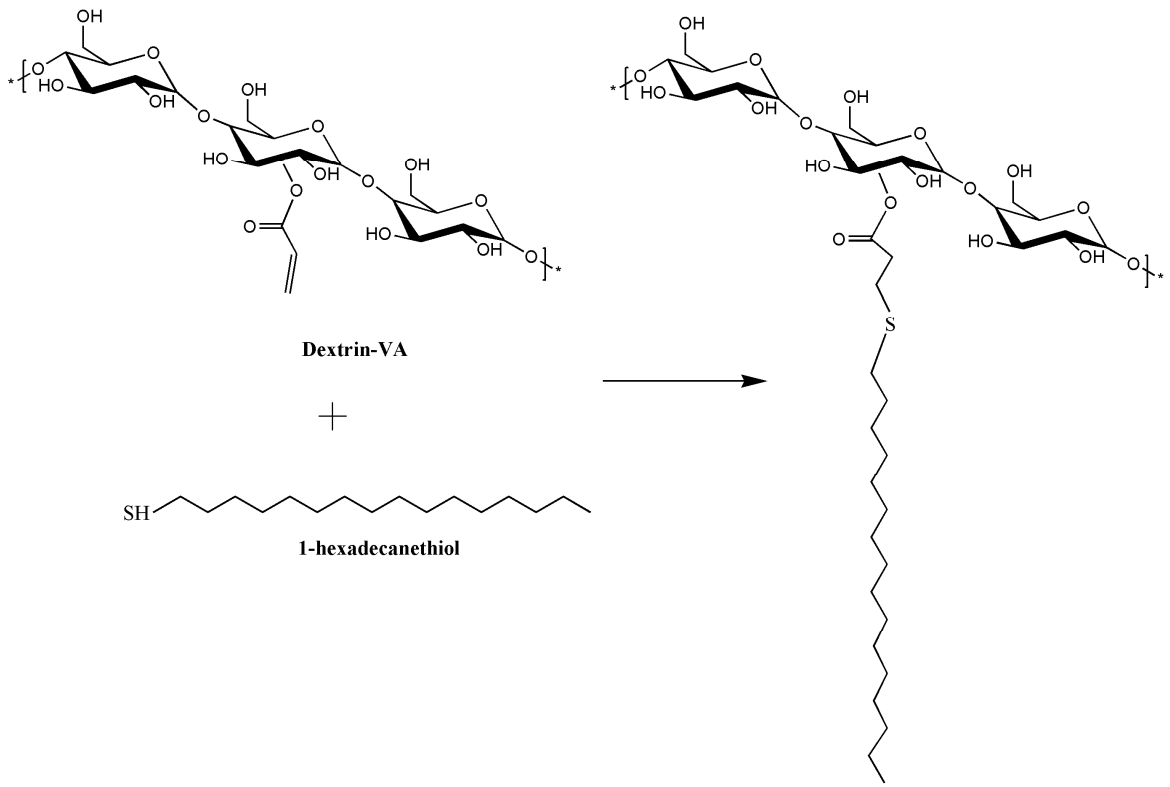

^{1}H NMR was used to analyse the structure of the reaction product. The signals between 5.8 and 3.0 ppm in the ^{1}H NMR spectrum of dextrin-VA are assigned to protons from the dextrin scaffold. The protons from the acrylate group, attached to the dextrin backbone are observed between 6.6 and 6.0 ppm (Ferreira, *et al.*, 2002), as shown in Figure 2.1. The presence of two different positional isomers in dextrin-VA was revealed by the ^{1}H-^{1}H COSY and ^{1}H-^{13}C HMQC spectra. The two positional isomers are located at positions 2 and 3 in the glucopyranosyl residues (data not shown) in the main dextrin backbone. For the sake of simplicity, only the 2-*O*-acryloyl regioisomer is represented in Scheme 2.1.

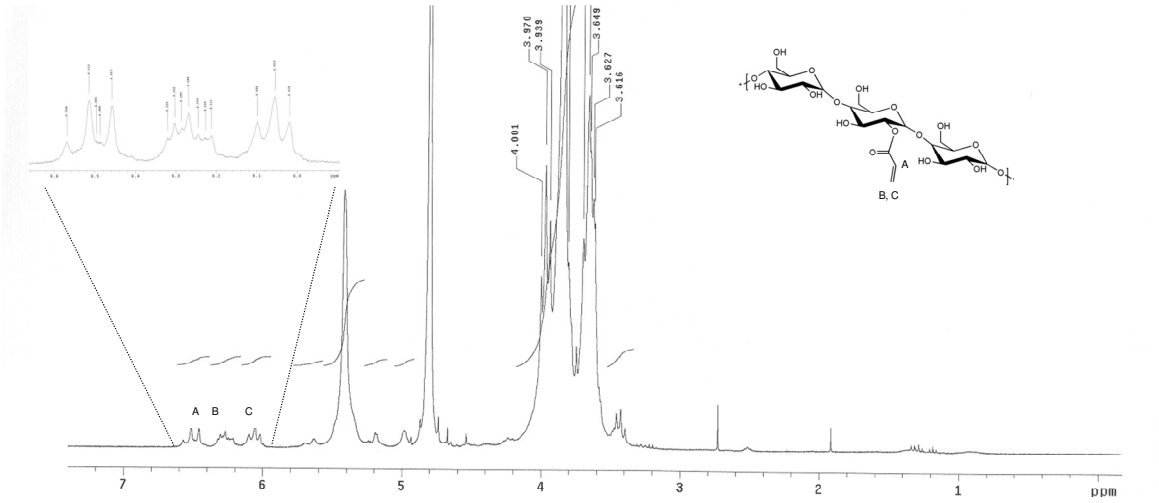

Figure 2.1 ^{1}H NMR spectra of dextrin-VA (DS_{VA} 20%) in D_2O at 25 ºC.

The reaction between the grafted acrylate and the thiol hexadecanethiol follows a mechanism of Michael addition. The intensity of the signals from protons of the unsaturated carbons of the acrylate groups decreases as the reaction progresses, and the signals should eventually disappear completely when all acrylate groups are grafted with thiol moieties. Simultaneously, a new signal assigned to the methylene protons should appear. Preliminary experiments were carried out without a base catalyst. Although it was possible to identify the signals corresponding to the grafted alkyl moiety, between 2.0 and 0.6 ppm, the acrylate protons are still detected. Using TEA as a catalyst, the signals from thiol moieties have higher intensity and the acrylate signals completely disappear, confirming the success of the synthesis (Figure 2.2). Therefore, a base catalyst must be used for a high reaction yield to be obtained.

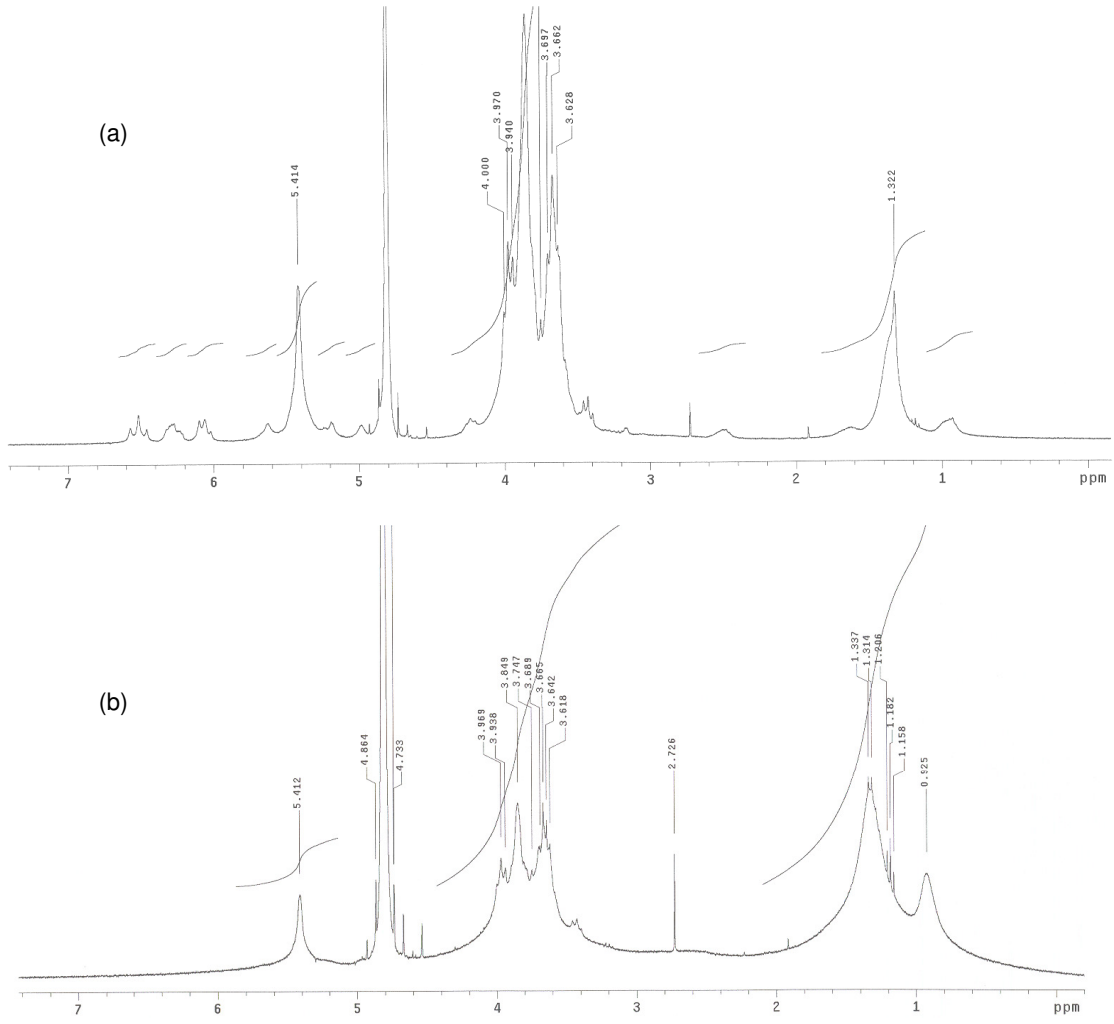

Figure 2.2. ^{1}H NMR spectra in D_2O of dextrin-VA reacted with hexadecanethiol (a) without or (b) with TEA.

In order to ascertain whether the thiol is covalently bound, $dexC_{16}$ was washed several times with *n*-hexane. As no differences were detected in the ^{1}H NMR analysis, it may be concluded that the alkyl chain is covalently bound to acrylate.

DLS was also used to check the possibility of self-polymerization of acrylic groups at 50 ºC. The size distribution of dextrin-VA in DMSO was evaluated before and after stirring at 50 ºC for 24 h. No differences were observed; therefore, the polymerization does not take place during the synthesis reaction.

2.3.2 Degree of substituion

The synthesis of $dexC_{16}$ with different degrees of substitution was accomplished by varying the molar ratio hexadecanethiol/VA in the reaction mixture. The ^1H NMR spectrum of $dexC_{16}$, in deuterated water, was used to determine the degree of substitution obtained (DS_{C16}, amount of alkyl chains per 100 dextrin glucopyranoside residues). DS_{C16} was calculated as a peak area ratio in the NMR spectra, according to Equation 2.1:

$$DS_{C16} = \frac{7 \times x}{37 \times y} \times 100 \qquad \text{(Equation 2.1)}$$

where *x* is the average integral corresponding to the protons from alkyl moieties (2.0 - 0.6 ppm) and *y* is the integral of all dextrin protons (3.0 - 5.8 ppm). Table 2.1 presents the DS values obtained for $dexC_{16}$ and the respective efficiency. The data presented in Table 2.1 correspond to the equilibrium position as it was verified by performing the assay with longer reaction times.

Table 2.1. Dextrin degree of substitution obtained using different hexadecanethiol/VA molar ratio

Theoretical DS [a] (%)	Obtained DS [b] (%)	Efficiency [c] (%)
10	2	20
20	4	20
40	14	35
60	23	38
100	59	59

[a] Calculated as the molar ratio of hexadecanethiol to acrylate groups (×100) in the reaction mixture. [b] Determined by ^1H NMR. The value shown is the calculated using equation 2.1, and multiplied by 5 to obtain the DS relatively to acrylate groups. [c] Calculated as the ratio of the obtained to the theoretical DS (×100).

These results demonstrate that the synthesis method is versatile, allowing production, in a simple two-step procedure, of materials with controlled amounts of grafted hydrophobes. Thus, fine tuning the properties of the materials is possible. Furthermore, different hydrophobic chemicals may be grafted (for instance thiocholesterol).

2.3.3 Formation of nanoparticles

The dissolution of $dexC_{16}$ in water is expected to give rise to micelle formation, owing to the amphiphilic nature of the molecule. The nanoparticles formation was accessed using both ^1H NMR and AFM.

Due to the limited mobility of the alkyl hydrophobic chains inside the nanoparticles, the shape and width of the ^1H NMR signals assigned to the alkyl chain protons (2.0 - 0.6 ppm) are dependent on the solvent ($D_2O/DMSO_d$) used to record the ^1H NMR spectra. The ^1H NMR signals assigned to the methyl (0.8 ppm) and methylene (1.1 ppm) groups are sharp in DMSO (Figure 2.3a), which is a good solvent for $dexC_{16}$. Progressive broadening at the base is noticeable as the percentage of water in D_2O/DMSO mixtures increases (Figure 2.3b). In pure D_2O extensive broadening is noticeable (Figure 2.3c). The shape of the ^1H NMR alkyl chain signals in deuterated water is characteristic of a superposition of peaks representing a collection of chemically identical species yet possessing various degrees of mobility (Hrkach, *et al.*, 1997). This result suggests that alkyl chains have different environments when dispersed in water. Some chains might be involved in hydrophobic microdomains (low mobility) with others remaining exposed to the hydrophilic solvent (high mobility). In DMSO, all hydrophobic chains are exposed to the solvent, having the same mobility.

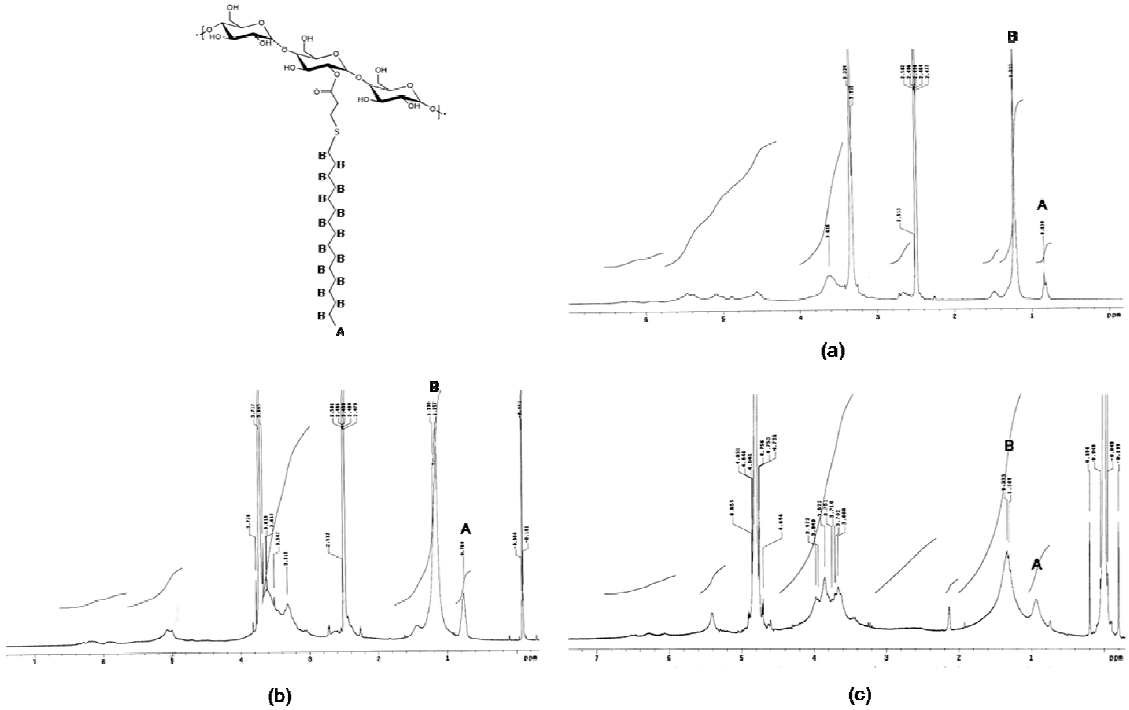

Figure 2.3. ^1H NMR spectra of $dexC_{16}$ (1.0 g/dL) in (a) DMSO-d_6, (b) 10% D2O in DMSO-d_6 and (c) D_2O.

In addition, self-assembled particles were observed using AFM. The AFM images (Figure 2.4) reveal spherical nanoparticles. The AFM results indicate that, for $dexC_{16}$ with DS_{C16} 7.0%, the mean diameter of nanoparticles is roughly 20 nm. In general, the nanoparticles appear to have a narrow size distribution.

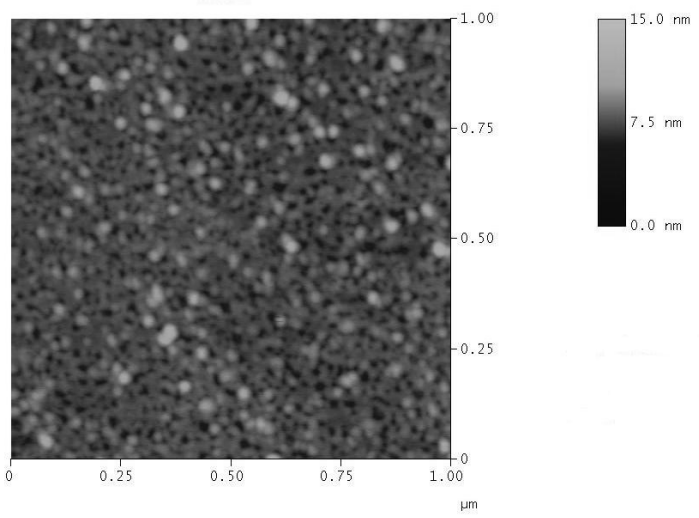

Figure 2.4. Tapping mode AFM image of $dexC_{16}$ (DS_{C16} 7.0%) nanoparticles adsorbed on HOPG (or graphite) from aqueous solution (0.01 g/dL).

2.3.4 Nanoparticles stability

To evaluate the stability of nanoparticles, the size was determined by DLS at 25 ºC up to 56 days (Figure 2.5).

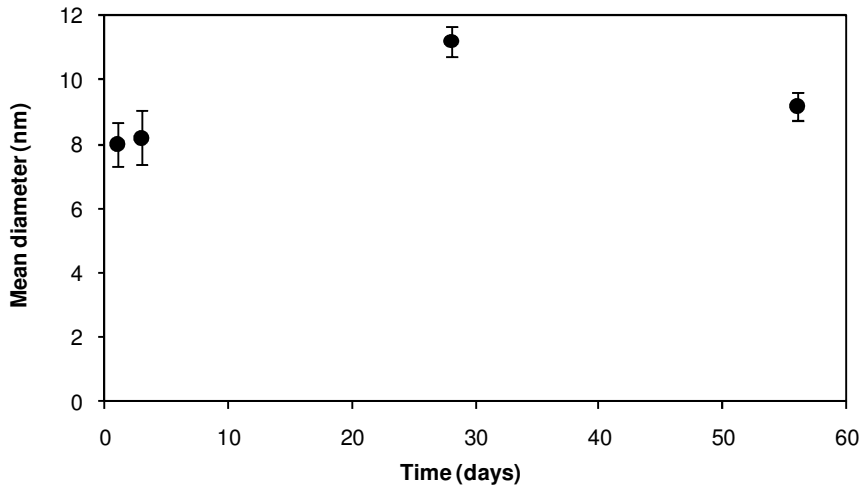

Figure 2.5. Colloidal stability of nanoparticles in water. The dexC_{16} (DS_{C16} 7.0%) solution (0.1 g/dL) was stored at 25ºC up to 56 days. The error bar is for standard deviation (n=5).

Nanoparticles conserved their size during this study, indicating the high colloidal stability of nanoparticles in the aqueous medium.

2.3.5 Size and size distribution

The dynamic light scattering (DLS) studies were done using a Nano-ZS (Malvern) instrument. Solutions with different concentrations of dexC_{16} (DS_{C16} 7.0%) were prepared by dilution of a 0.1 g/dL solution and analysed by DLS. The results are presented in Figure 2.6. DLS provides valuable information on the homogeneity of the dispersion. A single sharp peak in the DLS profile implies the existence of a single population of particles. The polydispersity index (PdI) is also helpful in the characterization of the size distribution. PdI-values close to 1 are indicative of heterogeneity.

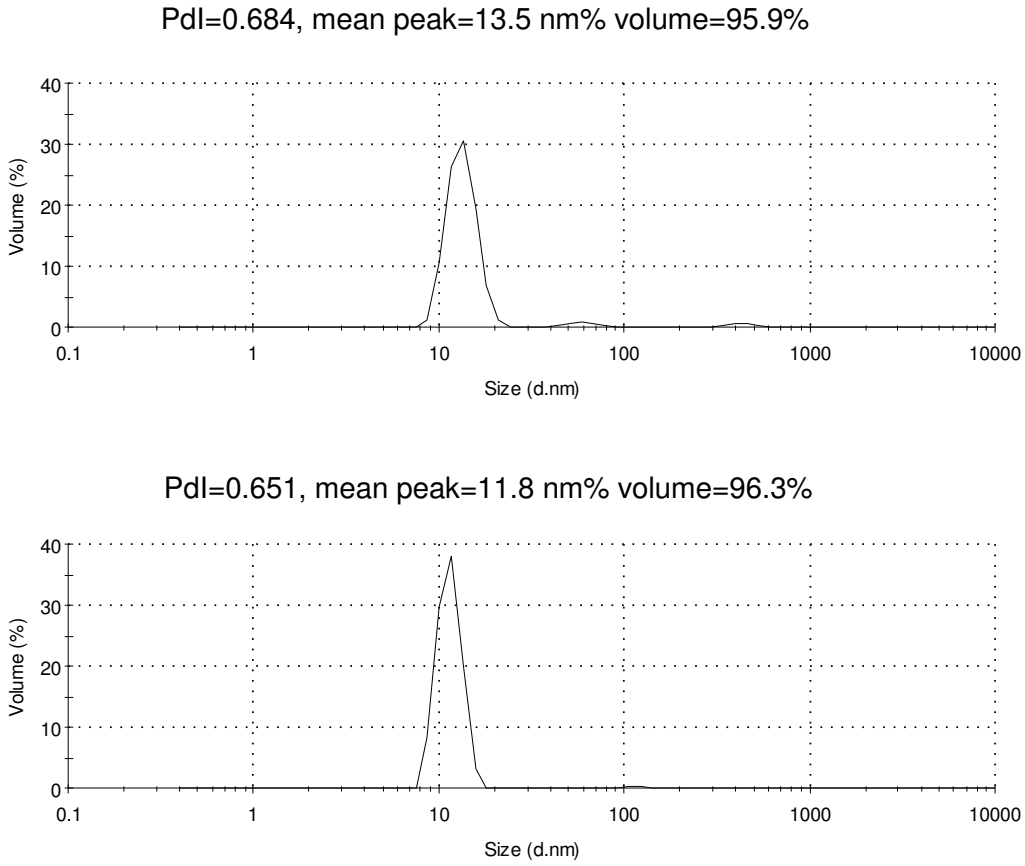

Figure 2.6. Size distribution of dexC_{16} (DS_{C16} 7.0%) aqueous dispersion (a) 0.01 and (b) 0.1 g/dL.

Figure 2.6 shows that the dilution of the sample has an effect on the particle size in the concentration range used. The hydrodynamic diameter of the predominant population of nanoparticles increases slightly with decreasing concentration. The DLS results are in good agreement with AFM results presented above. The small nanoparticles with a diameter of around 10-15 nm are the predominant population.

2.3.6 Critical micelle concentration

Pyrene may be used as a fluorescent probe to detect aggregate formation (Nichifor, *et al.*, 2004). The fluorescent properties of pyrene change when it is transferred from an aqueous environment to the hydrophobic microenvironment of the nanoparticles. Figure 2.7 presents the fluorescence spectra of pyrene in water (1×10^{-6} M) and in the presence of dexC_{16}. The CMC was determined from the change in the ratio of intensities of the third and first peak (I_3/I_1) in the emission spectra.

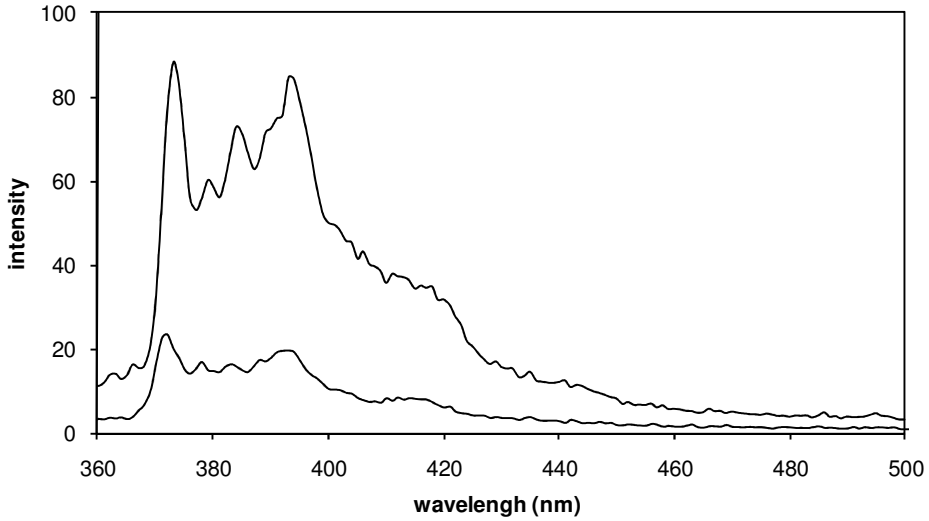

Figure 2.7. Emission spectra of (a) an aqueous solution of pyrene (1×10^{-6} M) and (b) an aqueous solution of pyrene (1×10^{-6} M) with dissolved dexC_{16} (DS_{C16} 7.0%) at a polymer concentration of 0.02 g/dL, λ_{ex} = 337 nm.

The pyrene concentration is in all experiments very low (1×10^{-6} M) to prevent excimer formation (detectable at ≈ 470 nm). The I_3/I_1 values, corresponding to samples with different polymer concentrations, were calculated and plotted in Figure 2.8.

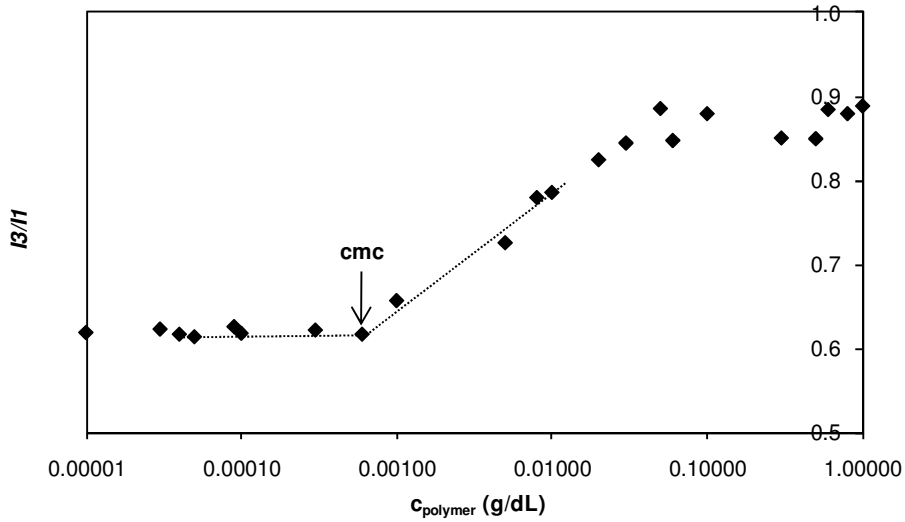

Figure 2.8. Fluorescence intensity ratio I_3/I_1 as a function of the dexC_{16} (DS_{C16} 7.0%) concentration.

At low polymer concentrations, I_3/I_1 is almost constant and equal to 0.62, i.e., pyrene experiences an aqueous environment. For higher polymer concentrations I_3/I_1 starts to increase, showing that pyrene senses a less polar environment due to its solubilization in the hydrophobic domains that are formed by self-assembly (for polymer concentration > 0.0008 g/dL), where it senses a less polar environment. The curve is sigmoidal, as observed for other amphiphilic polymers. The ratio I_3/I_1 eventually reaches a constant value as there are enough nanoparticles to solubilise all pyrene molecules. The variation in pyrene fluorescence is due to the partition between water and the hydrophobic microdomains, until equilibrium (or probe saturation) occurs.

The CMC determination from fluorescence data can be based on different assumptions, due to the relatively large concentration range over which the fluorophore response stretches. Different researchers have proposed the CMC as either the onset, the offset, or the midpoint of the increased fluorophore response ratio as a function of the polymer concentration (Nichifor, *et al.*, 2004). In this study, the polymer concentration corresponding to the onset of the variation was considered the CMC as it indicates the onset of the association event (Figure 2.8). This event can be an incipient association of side-chain hydrophobes (at least the very first association of two hydrophobes). The results on Figure 2.8 demonstrate that a phase transition occurs when the polymer concentration increases (CMC of about 0.0008 g/dL) owing to a structural reorganization of the dissolved molecules that leads to formation of hydrophobic domains. Dissolution of pyrene in these domains results in higher fluorescence intensity and I_3/I_1 values.

The variation in the particle sizes, as a function of the concentration, can also be studied by DLS. Figure 2.9 shows the particle size and the respective percent volume for dexC_{16} (DS_{C16} 7.0%) at polymer concentrations ranging between 0.0001 g/dL and 0.1 g/dL.

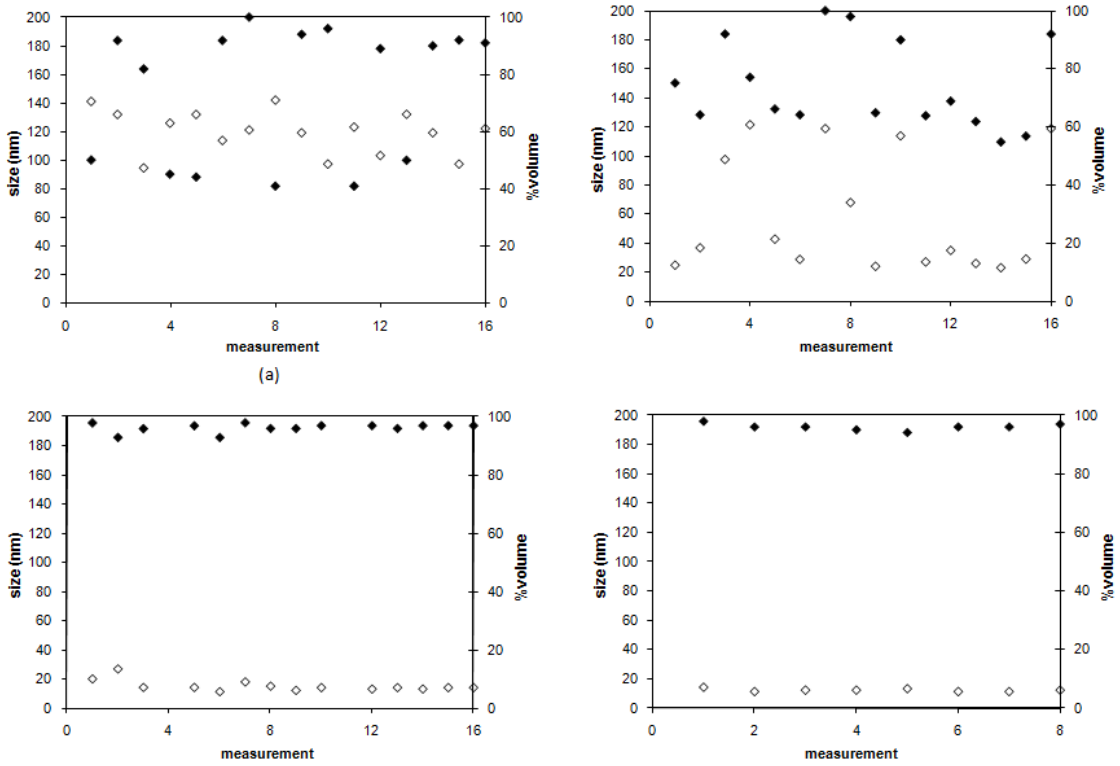

Figure 2.9. Size (◊) and the respective percent volume (♦) obtained in consecutive analysis for dexC_{16} (DS_{C16} 7.0%) at (a) 0.0001 g/dL, (b) 0.001 g/dL, (c) 0.01 g/dL and (d) 0.1 g/dL. While in experiments a, c and d a consistent measure of the particles size was possible, for the concentration used in experiment b, close to CMC, the size detected varies from one measurement to another, suggesting that the material is unstable and particles with different size are present in the mixture.

The particle size detected depends on the sample concentration, a dramatic reduction in size being detected as the concentration reaches CMC (as roughly estimated by DLS, and showing good agreement with the fluorescence experiments). The particles have a hydrodynamic diameter inferior to 20 nm for the higher concentrations (Figure 2.9c and d) and a hydrodynamic diameter of about 120 nm for the lower concentrations (Figure 2.9a). A transition is noticeable at about 0.001 g/dL (Figure 2.9b). Thus, it appears that the polymer is not very soluble, and probably aggregates are being detected in the DLS measurements for the low polymer concentration. In fact, dextrin – obtained from starch - is not very soluble, giving rise to colloidal dispersions in water. As the concentration increases, the hydrophobic domains give rise to formation of nanoparticles with a hydrophobic core (as shown in the fluorescence experiments). Apparently, nanoparticles

formation gives rise to a more compact structure induced by the hydrophobic force. The beginning of the association event seems to occur close to 0.001 g/dL, corresponding to the CMC, in good agreement with the fluorescence results.

2.4 Conclusions

In the present study we report the synthesis of a hydrophobized dextrin polymer, $dexC_{16}$. The synthesis method is versatile as it allows controlling the degree of substitution with hexadecanethiol and therefore fine-tuning the properties of the materials. $DexC_{16}$ self-aggregates in water, originating colloidally stable (over 2 months) nanoparticles with a narrow size distribution. A diameter of about 20 nm was determined by DLS and AFM. The CMC value, around 0.001g/dL, was determined using pyrene as a fluorescent probe and confirmed by DLS. The value determined is lower than that reported for the most common low molecular weight surfactants. The low CMC may be due to the low solubility of dextrin. Reaction of dextrin-VA with other (thiol) nucleophiles might open access to a variety of amphiphilic materials with tailored properties.

Acknowledgments. The authors acknowledge the contributions from Dr. Lino Ferreira for fruitful discutions and Drs. Margarida Bastos, Marieta Nichifor, and Paula Gameiro for revising the manuscript and contributions to the fluorescence analysis.

2.5 References

Akiyoshi, K.; Deguchi, S.; Moriguchi, N.; Yamaguchi, S.; Sunamoto, J. Self-aggregates of hydrophobized polysaccharides in water. Formation and characteristics of nanoparticles. *Macromolecules* **1993**, *26*, 3062-3068.

Akiyoshi, K.; Kobayashi, S.; Shichibe, S.; Mix, D.; Baudys, M.; Kim, S.W.; Sunamoto, J. Self-assembled hydrogel nanoparticle of cholesterol-bearing pullulan as a carrier of protein drugs: complexation and stabilization of insulin. *Journal of Controlled Release* **1998**, *54*, 313-320.

Akiyoshi, K.; Sunamoto, J. Supramolecular assembly of hydrophobized polysaccharides *Supramolecular Science* **1996**, *3*, 157-163.

Carvalho, J.; Gonçalves, C.; Gil, A.M.; Gama, F.M. Production and characterization of a new dextrin based hydrogel. *European Polymer Journal* **2007**, *43*, 3050-3059.

Ferreira, L.; Gil, M.H.; Dordick, J.S. Enzymatic synthesis of dextran-containing hydrogels. *Biomaterials* **2002**, *23*, 3957-3967.

Hans, M.; Shimoni, K.; Danino, D.; Siegel, S.J.; Lowman, A. Synthesis and characterization of mPEG-PLA prodrug micelles. *Biomacromolecules* **2005**, *6*, 2708-2717.

Hrkach, J.S.; Peracchia, M.T.; Domb, A.; Lotan, N.; Langer, R. Nanotechnology for biomaterials engineering: structural characterization of amphiphilic polymeric nanoparticles by ^{1}H NMR spectroscopy. *Biomaterials* **1997**, *18*, 27-30.

Lee, I.; Akiyoshi, K. Single molecular mechanics of a cholesterol-bearing pullulan nanogel at the hydrophobic interfaces. *Biomaterials* **2004**, *25*, 2911-2918.

Liu, C.G.; Chen, X.G.; Park, H.J. Self-assembled nanoparticles based on linoleic-acid modified chitosan: Stability and adsorption of trypsin. *Carbohydrate Polymers* **2005**, *62*, 293-298.

Nichifor, M.; Lopes, S.; Bastos, M.; Lopes, A. Self-aggregation of amphiphilic cationic polyelectrolytes based on polysaccharides. *Journal of Physical Chemistry B* **2004**, *108*, 16463-16472.

Nizri, G.; Magdassi, S. Solubilization of hydrophobic molecules in nanoparticles formed by polymer-surfactant interactions. *Journal of Colloid and Interface Science* **2005**, *291*, 169-174.

Petit-Agnely, F.; Iliopoulos, I. Aggregation Mechanism of Amphiphilic Associating Polymers Studied by 19F and 13C Nuclear Magnetic Resonance. *The Journal of Physical Chemistry B* **1999**, *103*, 4803-4808.

Petit-Agnely, F.; Iliopoulos, I.; Zana, R. Hydrophobically Modified Sodium Polyacrylates in Aqueous Solutions: Association Mechanism and Characterization of the Aggregates by Fluorescence Probing. *Langmuir* **2000**, *16*, 9921-9927.

3. Characterization of the self-assembly process of hydrophobically modified dextrin

Adapted from **European Polymer Journal** (2008) 44, 3529-3534

Hydrophobized dextrin, randomly substituted by long alkyl chain, forms stable hydrogel nanoparticles by self-assembling in water. Hydrophobic chains, distributed along the polymer backbone, promote the formation of hydrophobic microdomains within the nanoparticles. The influence of degree of substitution with hydrophobic chains (DS_{C16}) on nanoparticles size, colloidal stability, density, aggregation number and nanoparticle weight was studied. Size distribution was also evaluated at different pH, urea concentration and ionic strength conditions. As shown by dynamic light scattering and transmission electron microscopy, the particles are spherical having a diameter of about 20 nm. The more substituted polymer forms more densely packed hydrophobic microdomains, such that the colloidal stability (in water and PBS buffer) of nanoparticles is increased. The knowledge of the aggregate building process and the characteristics of the nanoparticles are crucial for the design of drug delivery systems.

3.1 Introduction

Self-assembled hydrogel nanoparticles have potential biomedical and pharmaceutical application due to their biomimetic properties, i.e., their resemblance to biological macromolecules. Amphiphilicity is one of the important factors for the molecular self-organization in water. Various amphiphilic polymers, such as block copolymers (Chen*, et al.*, 2006 a, b, Gaucher*, et al.*, 2005, Letchford*, et al.*, 2007, Liang*, et al.*, 2006) and hydrophobized polymers (Na*, et al.*, 2000, Roux*, et al.*, 2007), have been synthesized and studied. Water-soluble polymers hydrophobically modified with hydrophobes grafted to the side chains have special interest. The hydrophobic chains lead to a self-assembly of the polymer, in water, promoting the formation of microdomains within the hydrogel nanoparticles. The microdomains solubilise therapeutic agents, namely hydrophobic drugs. Therefore, they can be used as drug delivery systems.

The attention of the researchers has mainly focused on the preparation of drug-loaded polymeric nanoparticles by varying the polymer/drug ratio, and analysing the drug loading content, entrapment efficiency and drug release profiles. Less attention has been paid to the aggregate building process and to the characterisation of the aggregates. Such assemblies of amphiphilic macromolecules are of interest both for understanding of supramolecular assembly in nature and for designing new materials in biotechnology and medicine. The size, density and stability of the hydrogel nanoparticles may be controlled by changing the hydrophobic group, and also the degree of substitution (Akiyoshi*, et al.*, 1996, Nichifor*, et al.*, 2004). Akiyoshi and others developed a variety of nanogels made of hydrophobized polysaccharides such as pullulan, mannan and dextran (Akiyama*, et al.*, 2007, Akiyoshi*, et al.*, 1993, Kim*, et al.*, 2000).

In this work, dextrin derivatives were used for the preparation of self-assembled hydrogel nanoparticles, a new system reported in a previous work (Gonçalves*, et al.*, 2007). The hydrophobized polysaccharide form relatively monodisperse and colloidally stable nanoparticles (≈20 nm), in water, upon self-aggregation. The nanoparticles characteristics depend on the polymer concentration, degree of substitution with hydrophobic chains (C_{16}), ionic strength and additives. One of the most fundamental and important structural parameters of micellar aggregates is the aggregation number, the average number of hydrophobic molecules in a micelle unit (Turro*, et al.*, 1978, Vorobyova*, et al.*, 2001). The aim of the present work is to study the aggregate building process and the characteristics of the nanoparticles formed. This fundamental information

enables us to design a useful nanosized delivery system suitable for carrier of hydrophobic drugs.

3.2 Experimental section

3.2.1 Materials

Dextrin-VA-SC_{16} ($dexC_{16}$) was synthesized as described previously (Gonçalves*, et al.*, 2007). In this work, dextrin-VA with 20 acrylate groups per 100 dextrin glucopyranoside residues (DS_{VA} 20%) was used.

Pyrene (Py) and cetylpyridinium bromide (CPB) were obtained from Aldrich. Pyrene was used after recrystallization. Ultra-pure water (Milli Q) was used for the preparation of aqueous solutions.

3.2.2 Preparation of self-assembled nanoparticles

Lyophilized $dexC_{16}$ was dissolved in ultra-pure water under stirring, at 50 ºC, and then further sonicated for 20 min until a clear solution was obtained. The solution of self-assembled nanoparticles was then filtrated through a 0.20 μm filter and stored at room temperature.

3.2.3 Size distribution and zeta potential

The size distribution, zeta potential and nanoparticle weight were determined with a Malvern Zetasizer, NANO ZS (Malvern Instruments Limited, U.K.), using a He-Ne laser (wavelength of 633 nm) and a detector angle of 173º. Size distribution and zeta potential were determined by dynamic light scattering (DLS).

For size distribution measurements, a dispersion of nanoparticles in ultra-pure water or PBS buffer (1 mL) was analysed at 25 ºC in a polystyrene cell. The concentration of nanoparticles was adjusted by dilution with ultra-pure water of concentrated nanoparticle dispersion.

The DLS cumulants analysis provides the characterization of a sample through the mean value (z-avg) for the size, and a width parameter known as the polydispersity, or polydispersity index (PdI). The z-avg diameter is the mean hydrodynamic diameter, determined from the intensity of scattered light. The fundamental size distribution generated by DLS is an intensity distribution; this can be converted, using Mie theory, to a volume distribution. This volume distribution can also be further converted to a number distribution. In the present work, we will consider the z-avg as the best approach to the actual nanoparticles size.

For zeta potential measurements, the aqueous solutions of nanoparticles at different pH values were obtained by dissolving dexC_{16} with DS_{C16} 6.1% (0.1 g/dL) in phosphate-citrate buffer (pH 2.2-8.0). Each sample was analysed in a folded capillary cell. The zeta potential values were calculated using the Smoluchowski equation. Repeated measurements were performed (3 times) and the values reported are average values.

3.2.4 Static light scattering

Nanoparticle weight was determined by static light scattering (SLS). The intensity of scattered light produced by macromolecules is proportional to the product of the weight-average nanoparticle weight and the concentration of the macromolecule. For molecules that show no angular dependence in the light scattering (when molecules are not large enough to accommodate multiple photon scattering), the relationship between the intensity of scattered light and the molecular weight is given by the Rayleigh equation. In the present study the nanoparticle weight will be evaluated using the follow equation (Equation 3.1):

$$\frac{KC}{R_\theta} = \left(\frac{1}{NP_w} + 2A_2 C \right) \qquad \text{(Equation 3.1)}$$

NP_w is the weight-average nanoparticle weight, A_2 is the second virial coefficient and C is the sample concentration, K is an optical constant as defined below (Equation 3.2):

$$K = \frac{2\pi^2}{\lambda_o{}^4 N_A} \left(n_o \frac{dn}{dc} \right)^2 \qquad \text{(Equation 3.2)}$$

N_A, Avogadro`s constant; λ_0, laser wavelength; n_0, solvent refractive index; dn/dc, differencial refractive index increment.

R_θ is the Rayleigh ratio – the ratio of scattered light to incident light of the sample. The standard approach for weight measurements is to first measure the scattering intensity of the analyte used relative to that of a well described "standard" pure liquid with a known Rayleigh ratio. Toluene was used as standard. The refractive index increment (dn/dc) used in SLS measurements was measured in a differencial refractometer. For the present polymer dn/dc of 0.140 mL/g was obtained. In the plot of KC/R_θ versus C (known as Debye plot) the intercept is equivalent to $1/NP_w$ and the slope allows the calculation of the second virial coefficient A_2. The second virial coefficient is a property describing the interaction strength between the nanoparticles and the solvent. For samples where $A_2>0$, the nanoparticles are stable in solution. When $A_2 = 0$, the nanoparticle-solvent interaction is equivalent to the nanoparticle-nanoparticle interaction and the solvent is described as a theta solvent. When $A_2<0$, the nanoparticles are unstable, and aggregate.

A glass cell was used for nanoparticle weight measurements. All dispersions were filtered using disposable 0.20 μm filters. This filtration has a significant effect on the size distribution, reducing the polydispersity index. A larger PdI being observed when a 0.45 μm filter was used.

3.2.5 Transmission electron microscopy

For visualization by transmission electron miscroscopy (50 kV; Zeiss EM 902C), nanoparticles were adsorbed to glow-discharged carbon-coated collodion film on 400-mesh copper grids. Grids were washed with deionized water and stained with 0.75% uranyl acetate.

3.2.6 Fluorescence spectroscopy

Fluorescence measurements were performed on a VARIAN Cary Eclipse fluorescence spectrofluorometer using a quartz cell. Experiments were performed with Py as a fluorescent probe (1×10^{-6} M) and CPB as a quencher (0.01-0.1 mM). A stock solution of CPB (1 mM in methanol) was prepared, and aliquots of this solution were added to empty flasks in the amount required for the final CPB concentration. Methanol was evaporated and then a polymer solution with a 0.3 g/dL concentration, prepared in 1×10^{-6} M Py, was added to each flask. The mixtures were left to equilibrate under mild shaking for 24h. The pyrene spectra were obtained using an excitation wavelength of 337 nm, and recording

the emission over the range 350-500 nm, at a scan rate of 20 nm/min. The slit width was set at 20 nm for the excitation and 2.5 nm for the emission.

3.3 Results and discussion

3.3.1 Size of the dexC_{16} self-aggregates

Several samples of dexC_{16} were prepared, as reported previously, with DS_{C16} (C_{16} groups per 100 dextrin glucopyranoside residues) of 3.4, 4.8, 6.0, 8.8 and 10.0%. The size and size distribution of the self-assembled hydrogel nanoparticles in aqueous medium were measured by DLS. Figure 3.1 shows the particle size of the samples at different polymer concentrations. The concentration range is above critical micelle concentration (≈ 0.0008 g/dL) and below the solubility limit (≈ 1.0 g/dL) (Gonçalves*, et al.*, 2007).

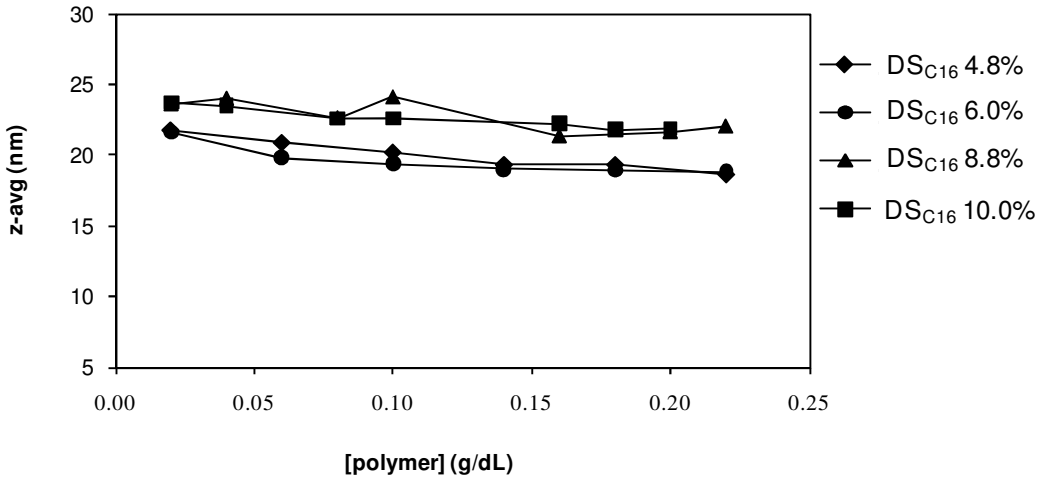

Figure 3.1. Mean hydrodynamic diameter (z-avg) analysis of self-assembled hydrogel nanoparticles with DS_{C16} 4.8, 6.0, 8.8 and 10.0%.

The mean hydrodynamic diameter obtained, for samples with DS_{C16} 4.8, 6.0, 8.8 and 10.0%, was 20.0 ± 1.2, 19.6 ± 1.1, 22.7 ± 1.1 and 22.6 ± 0.7 nm, respectively (± confidence interval at 95%), with corresponding average polydispersity index of 0.390,

0.354, 0,559 and 0.306. These results indicate that the particle size of the self-assembled hydrogel nanoparticles is only slightly influenced by the DS_{C16} or polymer concentration.

As can be seen in Figure 3.2, the size distribution of hydrophobized polysaccharide in water, upon self-aggregation, is relatively monodisperse. The intensity distribution is rather influenced by the presence of larger particles, while the volume distribution provides a better approach to characterize the more representative population.

			Diam.(nm)	% Intensity	Width (nm)
Z-Average (d.nm):	23.6	Peak 1:	21.8	73.9	10.3
PdI:	0.363	Peak 2:	164	26.1	80.5
Intercept:	0.919	Peak 3:	0.0	0.0	0.0

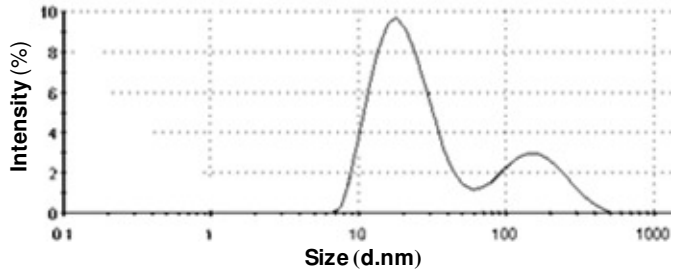

(a)

			Diam.(nm)	% Volume	Width (nm)
Z-Average (d.nm):	23.6	Peak 1:	13.9	100	7.8
PdI:	0.363	Peak 2:	0.0	0.0	0.0
Intercept:	0.919	Peak 3:	0.0	0.0	0.0

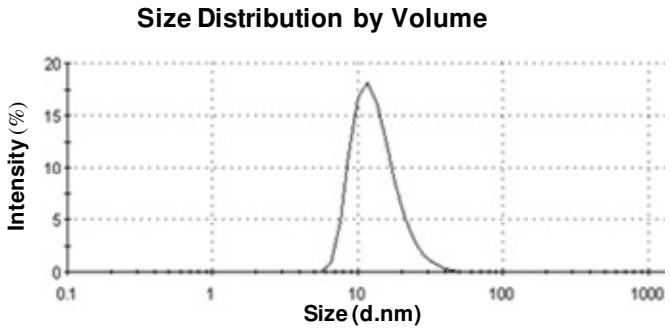

(b)

Figure 3.2. Size distribution in (a) intensity (%) and (b) volume (%), of aqueous dispersion 0.02 g/dL of $dexC_{16}$ with DS_{C16} 8.8%.

In addition, the self-assembled nanoparticles were observed using transmission electron microscopy (TEM). Figure 3.3 reveals spherical nanoparticles with a predominant population with diameters of about 20 nm for dexC_{16} with DS_{C16} 8.8%. The TEM results are in good agreement with DLS results presented above.

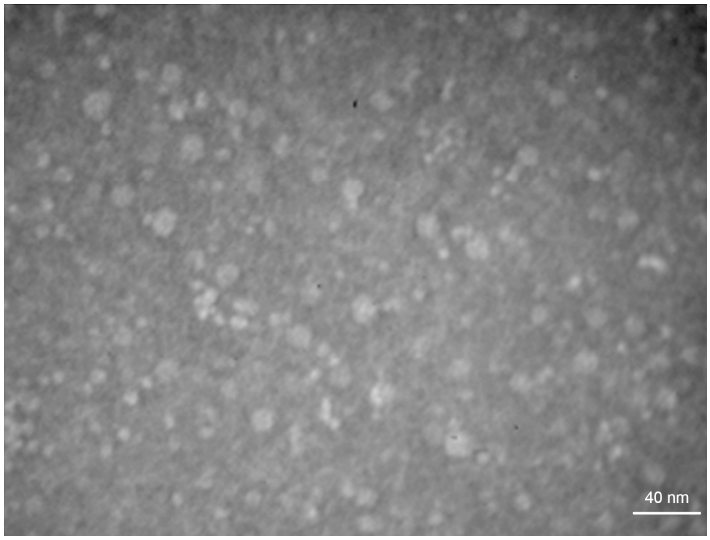

Figure 3.3. Transmission electron microscopy of negatively stained nanoparticles with DS_{C16} 8.8%.

3.3.2 Aggregation number

Fluorescence quenching is a common method for the measurement of the aggregation number. The method is based on the quenching of a probe´s emission using a specific quencher (Q). Both probe and quencher should have a high affinity for the nanoparticles. Considering a well-defined but unknown microdomains concentration [MD] and a concentration of quencher [Q], selected such that it resides exclusively in the nanoparticles, then Q will be distributed among the available nanoparticles. If a fluorescent molecule P, which is also entirely associated with nanoparticles, is now added to the system, P will partition between nanoparticles containing Q and the “empty” nanoparticles. A Poisson distribution of the P and Q among the nanoparticles may be assumed. If P is fluorescent only when it occupies an empty nanoparticle, then the measured ratio of fluorescence intensities (I/I_0), obtained in the presence (I) or absence (I_0) of Q, is related by the Equation 3.3:

$$\left(\frac{I}{I_0}\right) = \exp\left\{-\frac{[Q]}{[MD]}\right\} \Leftrightarrow \ln\left(\frac{I_0}{I}\right) = \frac{[Q]}{[MD]} \qquad \text{(Equation 3.3)}$$

In this work, CPB was used as the pyrene quencher. We used a low concentration of CPB (0.01-0.1 mM) to minimize a possible aggregation of this pyridinium surfactant (critical micelle concentration of CPB is about 0.6 mM). For the quenching experiments, the polymer concentration used was in the range where saturation with pyrene takes place, that is, where a constant value for the ratio I_3/I_1 is reached (Gonçalves, *et al.*, 2007).

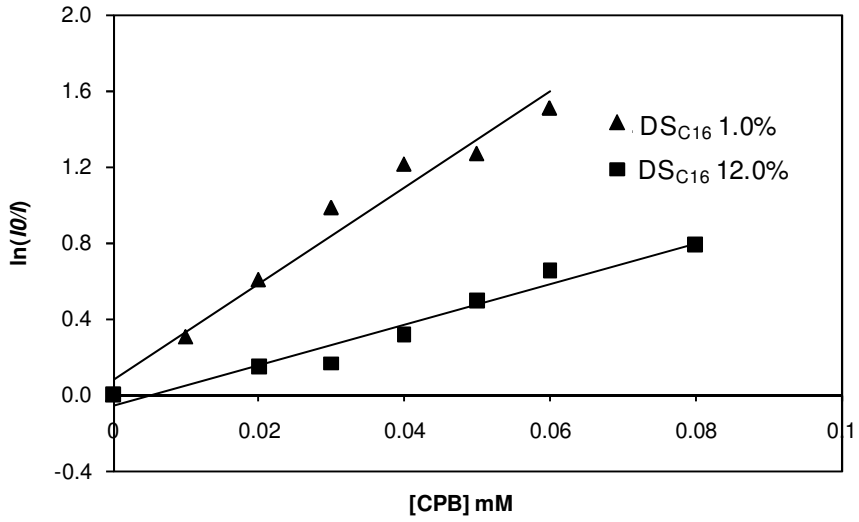

Figure 3.4. Variation of ln(I_0/I) as a function of CPB concentration, for different degree of substitution of the polymer.

The plots of ln(I_0/I) versus [Q] give straight lines (Figure 3.4) allowing the calculation of [MD] and then N_{agg}, according to Equation 3.4:

$$N_{agg} = \frac{c_H}{[MD]} \qquad \text{(Equation 3.4)}$$

where c_H is the hydrophobic groups concentration, in mM.

The fluorescence quenching study reveals that the hydrophobic microdomains (MD) have a number of alkyl chains that increases with DS_{C16}, from 4 to 18, in the range of the DS_{C16} values analysed (Figure 3.5).

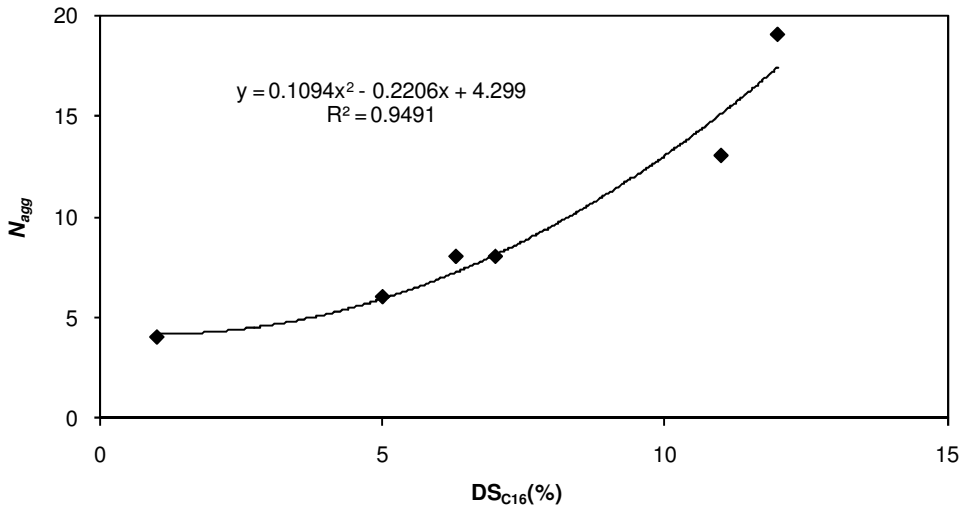

Figure 3.5. Aggregation number (N_{agg}) of the microdomains as a function of the degree of substitution, for a polymer concentration of 0.3 g/dL.

The more substituted polymer forms more densely packed hydrophobic microdomains, due to an increase in the number of alkyl chains. However, the nanoparticle diameter is not significantly influenced. The higher N_{agg} of the more substituted material (higher DS_{C16}) probably corresponds to nanoparticles with improved stability, due to the increased hydrophobic interaction on the microdomains. The stability of nanoparticles obtained with DS_{C16} 4.8 and 8.7% was evaluated up to 7 days. Aqueous dispersions (0.1 g/dL) were stored in the DLS polystyrene cell, at room temperature. The size distribution was constant, for DS_{C16} 8.7%, with low polydispersity index (< 0.5), up to 7 days. In the case of DS_{C16} 4.8% some aggregates are detected in the first day of the assay (≈ 500 nm), but the main peak was conserved. The stability was also evaluated for DS_{C16} 8.7% in PBS (0.1 g/dL). The sample was highly stable, since no aggregates were detected and the low polydispersity index was also conserved. Indeed, as expected, the more substituted $dexC_{16}$ forms more compact hydrophobic microdomains, such that the colloidal stability of nanoparticles is increased.

3.3.3 Weight of the dexC$_{16}$ self-aggregates

The nanoparticle weight (NP_w) and the second virial coefficient (A_2) of the dexC$_{16}$ self-aggregates were studied, for different degrees of substitution, using the Debye plot. The second virial coefficient (A_2) of the nanoparticles is positive, revealing stability in aqueous medium. The value obtained, divided by the molecular weight (M_w) of a single polymer chain, provide the number of polymer (dexC$_{16}$) molecules within a nanoparticle. Thus, using the aggregation number determined by quenching experiments, a comprehensive characterization of nanoparticle is possible, namely the estimation of the number of polymer molecules (molecules/NP) and hydrophobic moieties per nanoparticle (C_{16}/NP), number of hydrophobic molecules within one hydrophobic microdomain (N_{agg}) and number of hydrophobic microdomains (MD/NP). The results are presented in Table 3.1. As shown, dexC$_{16}$ used for the nanoparticle weight determination has not the same DS_{C16} as one used for N_{agg} determination (see Figure 3.5). Therefore, the values of N_{agg} used for nanoparticle characterization (Table 3.1) were obtained using the trend line shown in Figure 3.5.

Table 3.1. Nanoparticles characterization with different DSC$_{16}$.

DS_{C16} (%)	$\frac{C_{16}}{molecule}$	M_w dexC$_{16}$ (Da) (a)	NP_w (kDa) (b)	A_2 mL mol/g^2 (b)	$\frac{molecule}{NP}$ (b)	$\frac{C_{16}}{NP}$	N_{agg} calc (c)	$\frac{MD}{NP}$	$\frac{molecules}{MD}$
3.4	0.4	2231	336	4.75e-4	151	60	5	12	13
4.8	0.6	2278	346	4.95e-4	152	91	6	15	10
6.0	0.8	2318	411	3.82e-4	177	142	7	20	9
8.8	1.1	2412	418	4.93e-4	173	190	11	17	10
10.0	1.3	2452	530	2.53e-4	216	281	13	22	10

(a) $M_W(dexC_{16}) = 2106 + \left(\frac{\%DS_{C16}}{100} \times 258.1\right) + \left(\frac{\%DS_{VA}}{100} \times 54.1\right)$, assuming Mw(dextrin) = 2106Da, determined previously by chromatography.

(b) Determined by static light scattering.

(c) Determined by: $N_{agg}calc = 0.1094 \times (DS_{C16})^2 - 0.2206 \times DS_{C16} + 4.299$ (trend line equation in figure 3.5).

The nanoparticle weight determination (by SLS) allows an estimation of the number of polymer molecules, per nanoparticle, in the range 151-216 (Table 3.1), depending on the degree of substitution.

The N_{agg} value has been calculated under the assumption that all hydrophobes are involved in hydrophobic microdomains. This assumption might be true for polymers with higher degrees of substitution (Nichifor*, et al.*, 2004), where the density of the side alkyl chains is high enough. Therefore, N_{agg} corresponds to the maximum number of hydrophobes that can exist within microdomain.

From the experimental hydrodynamic radius (R_H) and NP_w values, one can calculate the average polymer density (ϕ_H) within a nanoparticle, as defined by Equation 3.5, where N_A is Avogadro´s number.

$$\phi_H = \left(\frac{NP_w}{N_A} \right) \left(\frac{4}{3} \pi R_H^{\,3} \right)^{-1} \qquad \text{(Equation 3.5)}$$

The average polymer density, for samples with DS_{C16} 4.8, 6.0, 8.8 and 10.0%, was 0.14, 0.17, 0.11 and 0.15 g/mL, respectively. These results indicate that the nanoparticles have about 85-90 wt% of water; they may be considered hydrogel-like structures.

3.3.4 Influence of pH, urea and ionic strength

The magnitude of the zeta potential gives an indication of the stability of the colloidal system. If particles in a suspension have a large zeta potential value, negative or positive, then they will repeal each other and the particles do not aggregate. However, if the particles have a low zeta potential value (close to zero), then there is no electrostatic force to prevent the particles to aggregate. The most important factor that affects zeta potential is pH. The variation of hydrodynamic diameter and zeta-potential of nanoparticles with the pH was studied.

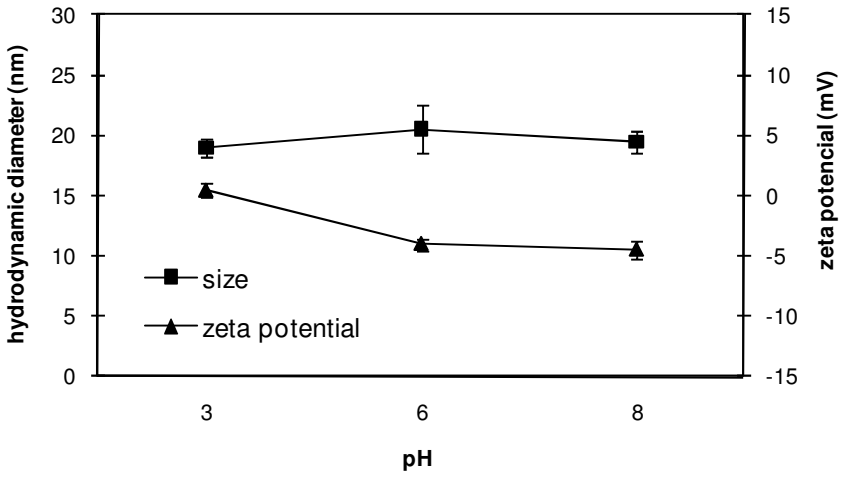

Figure 3.6. Particle size and zeta potential of nanoparticles with DS_{C16} 6.1% (0.1 g/dL) as a function of pH solution.

Figure 3.6 shows that the nanoparticles size is not sensitive to the pH medium. In the pH range studied, the zeta potential is almost constant and close to zero. Indeed, the polymer is made of glucose, and the hydroxyl glucose residues have a high p*K*a (12.35), and thus the material is expected to be poorly ionized in the analysed pH range. Although the low zeta potential, the nanoparticles are stable. The stability can be attributed to the solvation forces. Typically, solvation forces are ignored in colloidal analysis, because they are difficult to access and quantify. It has been noted that solvation forces can be comparable to, or greater than, van der Waals forces (Fichthorn*, et al.*, 2006).

In order to further understand the nature of the associations exhibited by $dexC_{16}$ in aqueous medium, the effects of urea and salt (NaCl) on nanoparticle size was studied.

Urea can produce twofold effects: firstly, urea may break intra-molecular hydrogen bond, an effect that may lead to the uncoiling of dextrin molecules, which would assume a more extended conformation. Secondly, urea can severely disturb the hydrophobic interactions. It was found that particle size slightly increases with the urea concentration. Using DS_{C16} 8.8% (0.1 g/dL), the nanoparticles size increase from 25.8 to 31.3 nm, corresponding to an urea concentration up to 7 M. Thus, urea seems to perturb the hydrophobic interactions inducing the nanoparticles to “swell”, although it is noticeable that the size increase is not dramatic. Indeed, the driving force for hydrophobic association in aqueous systems is partially attributed to the need for the hydrophobic moieties to minimize the surface area of contact with water, and consequently minimize

the amount of water that must be "structured" in order to solubilise them. The addition of urea to aqueous solutions disrupts the structuring ability of water, thereby weakening the hydrophobic interactions in the solution (Philippova*, et al.*, 2001). Therefore, urea may hinder the formation of hydrophobic domains, although it does not prevent the formation of nanoparticles.

The effect of NaCl concentration on the hydrodynamic diameter of nanoparticles obtained with DS_{C16} 9.0% (0.1 g/dL) was also studied. An increase of the average particle size, in the same range as observed with urea, may be observed. Nanoparticles size increase from 23.7 to 35.5 nm, corresponding to NaCl concentration in the range 0-0.6 M. Since nanoparticles bears a rather low charge, considering the zeta potential, the size increase is not likely to arise from the double layer compression and subsequent aggregation.

The interaction forces between colloidal nanoparticles determine the dispersion and stability of their suspensions. Electrostatic, van der Waals, depletion, and solvation forces exist between solid particles suspended in a liquid. However, for nanoparticles, the absolute and relative magnitudes of these forces are not well-known. It is difficult to measure forces acting upon nanoparticles, experimentally.

The general conclusion that may be drawn from these results is that the nanoparticles have a slightly higher size when prepared in buffer (irrespective of the pH), in the presence of a salt or urea (irrespective of the concentration). The rather high stability of these nanoparticles must be remarked.

3.4 Conclusions

In the present study we evaluated the influence of the degree of substitution on the self-assembly process of a hydrophobized dextrin polymer, $dexC_{16}$. The size of self-assembled hydrogel nanoparticles was evaluated as a function of DS_{C16}. The nanoparticles size is only slightly influenced by DS_{C16} or polymer concentration. The fluorescence quenching study reveals that the more substituted polymer forms more densely packed hydrophobic microdomains, such that colloidal stability (in water and PBS) of nanoparticles is increased. The nanoparticles are stable in the presence of urea and at different pH and ionic strength. Small size, low density and high stability of the

nanoparticles obtained can promote a stable entrapment of bioactive and hydrophobic molecules, and allow them to circulate in the blood long enough to reach the desired therapeutic effects.

Acknowledgments. This research was supported by Fundação para a Ciência e a Tecnologia under Grant SFRH/BD/22242/2005 and POCTI/BIO/45356/2002.

3.5 References

Akiyama, E.; Morimoto, N.; Kujawa, P.; Ozawa, Y.; Winnik, F.M.; Akiyoshit, K. Self-assembled nanogels of cholesteryl-modified polysaccharides: Effect of the polysaccharide structure on their association characteristics in the dilute and semidilute regimes. *Biomacromolecules* **2007**, *8*, 2366-2373.

Akiyoshi, K.; Deguchi, S.; Moriguchi, N.; Yamaguchi, S.; Sunamoto, J. Self-Aggregates of Hydrophobized Polysaccharides in Water - Formation and Characteristics of Nanoparticles. *Macromolecules* **1993**, *26*, 3062-3068.

Akiyoshi, K.; Sunamoto, J. Supramolecular assembly of hydrophobized polysaccharides *Supramolecular Science* **1996**, *3*, 157-163.

Chen, C.; Yu, C.H.; Cheng, Y.C.; Yu, P.H.F.; Cheung, M.K. Biodegradable nanoparticles of amphiphilic triblock copolymers based on poly(3-hydroxybutyrate) and poly(ethylene glycol) as drug carriers. *Biomaterials* **2006a**, *27*, 4804-4814.

Chen, C.; Yu, C.H.; Cheng, Y.C.; Yu, P.H.F.; Cheung, M.K. Preparation and characterization of biodegradable nanoparticles based on amphiphilic poly(3-hydroxybutyrate)-poly(ethylene glycol)-poly(3-hydroxybutyrate) triblock copolymer. *European Polymer Journal* **2006b**, *42*, 2211-2220.

Fichthorn, K.A.; Qin, Y. Molecular-dynamics simulation of colloidal nanoparticle forces. *Industrial & Engineering Chemistry Research* **2006**, *45*, 5477-5481.

Gaucher, G.; Dufresne, M.H.; Sant, V.P.; Kang, N.; Maysinger, D.; Leroux, J.C. Block copolymer micelles: preparation, characterization and application in drug delivery. *Journal of Controlled Release* **2005**, *109*, 169-188.

Gonçalves, C.; Martins, J.A.; Gama, F.M. Self-assembled nanoparticles of dextrin substituted with hexadecanethiol. *Biomacromolecules* **2007**, *8*, 392-398.

Kim, I.S.; Jeong, Y.I.; Kim, S.H. Self-assembled hydrogel nanoparticles composed of dextran and poly(ethylene glycol) macromer. *International Journal of Pharmaceutics* **2000**, *205*, 109-116.

Letchford, K.; Burt, H. A review of the formation and classification of amphiphilic block copolymer nanoparticulate structures: micelles, nanospheres, nanocapsules and polymersomes. *European Journal of Pharmaceutics and Biopharmaceutics* **2007**, *65*, 259-269.

Liang, H.F.; Chen, C.T.; Chen, S.C.; Kulkarni, A.R.; Chiu, Y.L.; Chen, M.C.; Sung, H.W. Paclitaxel-loaded poly(gamma-glutamic acid)-poly(lactide) nanoparticles as a targeted drug delivery system for the treatment of liver cancer. *Biomaterials* **2006**, *27*, 2051-2059.

Na, K.; Park, K.H.; Kim, S.W.; Bae, Y.H. Self-assembled hydrogel nanoparticles from curdlan derivatives: characterization, anti-cancer drug release and interaction with a hepatoma cell line (HepG2). *Journal of Controlled Release* **2000**, *69*, 225-236.

Nichifor, M.; Lopes, S.; Bastos, M.; Lopes, A. Self-aggregation of amphiphilic cationic polyelectrolytes based on polysaccharides. *Journal of Physical Chemistry B* **2004**, *108*, 16463-16472.

Philippova, O.E.; Volkov, E.V.; Sitnikova, N.L.; Khokhlov, A.R.; Desbrieres, J.; Rinaudo, M. Two types of hydrophobic aggregates in aqueous solutions of chitosan and its hydrophobic derivative. *Biomacromolecules* **2001**, *2*, 483-490.

Roux, M.; Perly, B.; Djedaini-Pilard, F. Self-assemblies of amphiphilic cyclodextrins. *European Biophysics Journal with Biophysics Letters* **2007**, *36*, 861-867.

Turro, N.J.; Yekta, A. Luminescent Probes for Detergent Solutions - Simple Procedure for Determination of Mean Aggregation Number of Micelles. *Journal of the American Chemical Society* **1978**, *100*, 5951-5952.

Vorobyova, O.; Lau, W.; Winnik, M.A. Aggregation number determination in aqueous solutions of a hydrophobically modified poly(ethylene oxide) by fluorescence probe techniques. *Langmuir* **2001**, *17*, 1357-1366.

4. Dextrin nanoparticles: Studies on the interaction with murine macrophages and blood clearance

Adapted from **Colloids and Surfaces B: Biointerfaces** (2010) 75, 483-489

The uptake of nanoparticles by cells of the mononuclear phagocytic system limits its use as colloidal drug carriers, reducing the blood circulation time and the ability to reach biological targets. In this work, the interaction between dextrin nanoparticles - recently developed in our laboratory - and murine bone marrow-derived macrophages was evaluated. Cytotoxicity and nitric oxide production were studied, using the MTT assay and the Griess method, respectively. Fluorescein-labelled nanoparticles were used to assess the phagocytic uptake and blood clearance after intravenous injection. The phagocytic uptake was analysed *in vitro* by confocal laser scanning microscopy and fluorescence activated cell sorting. The results show that the nanoparticles are not cytotoxic and do not stimulate the production of nitric oxide by macrophages, in the range of concentrations studied. Nanoparticles are phagocytosed by macrophages and are detected inside the cells, concentrated in cellular organelles. The blood clearance study showed that the blood removal of the nanoparticles occurs with a more pronounced rate in the first 3 h after intravenous administration, with about 30% of the material remaining in systemic circulation at this stage. Given the fairly high blood circulation time and biocompatibility, the dextrin nanoparticles are promising carriers for biomedical applications. Both applications targeting phagocytic, antigen-presenting cells (for vaccination purposes) and different tissues (as drug carriers) may be envisaged, by modulation of the surface properties.

4.1 Introduction

Many colloidal carriers, such as liposomes, nanocapsules and nanoparticles, have been developed as intravenous drug delivery systems. These systems may improve the absorption of poorly water-soluble pharmaceuticals, protect sensitive molecules against *in vivo* degradation, modify the distribution of drugs in the body and increase the patient`s compliance, by avoiding repeated injections. The rapid removal of intravenously administered colloidal drug carrier systems by the mononuclear phagocytic system (MPS) is an obstacle to the efficient targeting of solid tumours and inflammatory tissues (Mosqueira*, et al.*, 2001, Oyewumi*, et al.*, 2004). When nanoparticles enter the blood-stream, they instantly encounter a complex environment of plasma proteins and phagocytic cells. Opsonization promotes recognition and uptake by cells of the MPS, especially macrophages in the liver (the Kupffer cells), but also spleen and bone marrow macrophages (Stolnik*, et al.*, 1995). Recent research has focused on the modification of nanoparticles surface to avoid opsonization. In this context, poly(ethylene glycol) (PEG) was found to decrease the interactions of the particles with blood proteins, avoiding recognition by the MPS and thus increasing the circulation time in the blood (Zahr*, et al.*, 2006). As one of the most promising alternatives to PEG, polysaccharides have been widely investigated. The advantage of polysaccharide coating is the steric protection of nanoparticles against non-specific interactions with proteins, ensuring particle stability in blood circulation. Additionally, as polysaccharides offer reactive groups for modification, active targeting may be obtained by grafting ligands onto the nanoparticles surface (Lemarchand*, et al.*, 2004, Lemarchand*, et al.*, 2005, Lemarchand*, et al.*, 2006, Ma*, et al.*, 2008).

Knowledge on the interaction between macrophages and drug carriers is essential in the design of more effective therapeutic strategies using nanobiotechnological devices. Macrophages may be the therapeutic target, for the treatment of macrophage-associated pathologies or vaccination purposes, given their activity as antigen-presenting cells (Schroer*, et al.*, 1980, Underhill*, et al.*, 1999). Otherwise, when other targets are envisaged, phagocytic activity should ideally be avoided, providing the drug carrier time enough to reach the target. Macrophages are phagocytic cells that produce antimicrobial molecules, in the phagosome, and secrete a variety of substances, whose actions range from induction of cell growth to cell death, in addition to their role in antigen-presentation to T cells. These substances produced by macrophages, such as nitric oxide and cytokines, are involved in host defence against pathogenic micro-organisms, parasites or

tumour cells. The phagocytic process starts when macrophages recognize foreign particles or pathogens, becoming thereafter activated, a process that leads to the secretion of a number of chemical mediators of inflammation. These molecules are very aggressive, not only against foreign molecules or particles, but also to the host tissues. Among them, nitric oxide (NO) is a key marker of activation of inflammation (Fiorito*, et al.*, 2006).

After administration of colloidal carriers, the *in vivo* distribution largely depends on their particle size (Sonavane*, et al.*, 2008) and surface properties (Esmaeili*, et al.*, 2008). As referred above, in many instances it is desirable to increase the blood circulation time of the drug carriers. Elimination of the nanoparticles from systemic circulation can occur by different mechanisms: uptake by phagocytic cells, extravasation through endothelium and renal excretion. Nanoparticle uptake by the phagocytic cells may occur both in the bloodstream by monocytes and in tissues by resident phagocytes (e.g., Kupffer cells in the liver, dendritic cells in the lymph nodes, spleen macrophages). Nanoparticles can escape the circulation through the gaps, also called fenestrations, of the endothelial barrier. Fenestrations and the vasculature can undergo modifications under various pathological conditions. For instance, tumor growth induces the development of neovasculature characterized by discontinuous endothelium, with large fenestrations. Depending on the reports, the “ideal” size requirements for nanoparticles developed for cancer treatment vary from 70 to 200 nm. Larger particles can be rapidly taken up by the mononuclear phagocytic system cells (Gaumet*, et al.*, 2008). Small particles (<5.5 nm) are described to be rapidly and efficiently excreted in the urine (Choi*, et al.*, 2007).

In previous work, nanoparticles obtained by self-assembling of hydrophobized dextrin were developed and characterized in our laboratory. The nanoparticles obtained have high colloidal stability and spherical shape (Gonçalves*, et al.*, 2007). Size distribution obtained by dynamic light scattering showed two distinct populations, with 25 and 150 nm, the smaller being the predominant one (Gonçalves*, et al.*, 2008). In the present work, the ability of these nanoparticles to interact with bone marrow-derived macrophages (BMDMs) was analysed. The use of nanoparticles labelled with a fluorochromic probe allowed the detection of internalization by BMDM and the evaluation of the blood clearance profile. These are the major goals of this work: to ascertain whether the dextrin nanoparticles are effectively internalized by phagocytic cells (relevant for vaccination purposes) and estimate the blood circulation time (crucial for the development of drug delivery applications).

4.2 Experimental section

4.2.1 Materials

Dextrin-VA-SC_{16} (VA: vinyl acrylate, SC_{16}: alkyl chain) was synthesized as comprehensively described previously (Gonçalves*, et al.*, 2007). In this work, a sample of dextrin-VA-SC_{16} ($dexC_{16}$) with 13 acrylate groups (DS_{VA} 13%) and 6 alkyl chains (DS_{C16} 6%) per 100 dextrin glucopyranoside residues was used. Dimethyl-sulfoxide was purchased from Fluka. The chemicals 4',6-diamidino-2-phenylindole (DAPI), lipopolysaccharide (LPS), saponine and 3-(4,5-dimethylthiazol-2-yl)-2,5-diphenyltetrazolium bromide (MTT) were purchased from Sigma-Aldrich. SAMSA (5-((2-(and-3)-S-(acetylmercapto) succinoyl) amino) fluorescein was obtained from Invitrogen. IFN-γ was obtained from R&D systems. Sephadex G25 PD10 columns were obtained from Amersham Biosciences.

4.2.2 Animals

Eight-week-old female BALB/c mice, an inbred strain with high genetic homogeneity between individuals, obtained from Harlan Interfauna Ibérica (Barcelon, Spain), were housed under specific-pathogen-free conditions with food and water *ad libitum*. The experiments involving mice were conducted under the guidelines and approval of the Research Ethics Committee of the Life and Health Sciences Research Institute (Braga, Portugal) and of the governmental agency *Direcção Geral de Veterinária* (Lisbon, Portugal).

4.2.3 Culture of murine BMDM

Macrophages were obtained from the bone marrow, as previously described (Pedrosa*, et al.*,1994, Torrado*, et al.*,2007). This method allows the differentiation of a homogenous primary culture of macrophages that retains the morphological, physiological and surface marker characteristics of these phagocytes (Tushinski*, et al.*,1982, Warren*, et al.*,1985, Zhang*, et al.*,2008). Briefly, mice were sacrificed using CO_2, and the femurs were removed under aseptic conditions. Bones were flushed with 5 mL cold Hanks` balanced salt solution (HBSS; Gibco, Paisley, United Kingdom). The resulting cell suspension was centrifuged at 500 × g and resuspended in Dulbecco`s modified Eagle`s medium

(DMEM; Gibco), supplemented with 10 mM HEPES (Sigma, St. Louis, MO), 1 mM sodium pyruvate (Gibco), 10 mM glutamine (Gibco), 10% heat-inactivated fetal bovine serum (Sigma), and 10% L929 cell conditioned medium (complete DMEM [cDMEM]). To remove fibroblasts or differentiated macrophages, cells were cultured for a period of 4 h on cell culture dishes (Nunc, Naperville, IL) with cDMEM. Nonadherent cells were collected with warm HBSS, centrifuged at 500 × g, distributed in 24-well plates at a density of 5×10^5 cells /well, and incubated at 37 ºC in a 5% CO_2 atmosphere. On day 4 after seeding, 0.1 mL of L929 cell conditioned medium was added, and medium was renewed on the seventh day. After 10 days in culture, cells were completely differentiated into macrophages.

4.2.4 Preparation of self-assembled nanoparticles

Lyophilized dexC_{16} was dissolved in culture medium under stirring and further sonicated for 20 min. A stock solution (3 mg/mL) of nanoparticles was prepared. The nanoparticle concentration was adjusted by dilution of concentrated nanoparticle dispersion, with culture medium, in the wells. All solutions were sterilized by filtration through a 0.22 μm membrane. The nanoparticles formation was confirmed by dynamic light scattering and visualized in atomic force microscopy.

The size distribution was determined with a Malvern Zetasizer, MODEL NANO ZS (Malvern Instruments Limited, U.K.). A dispersion of nanoparticles was analysed at 25 ºC in a polystyrene cell, using a Helium-Neon laser - wavelength of 633 nm and a detector angle of 173º.

Tapping mode imaging was carried out on a Nanoscope IIIa Multimode (Digital Instruments, Veeco) scanning probe microscope. A silicon tip doped with phosphorus, with a radius curvature of less than 10 nm (RTESP, VEECO), was used. This tip has a typical resonance frequency of 288-328 kHz and a typical force constant of 20-80 N/m. A scan rate of 1.4-1.8 Hz was sufficient to maintain a good signal-to-noise ratio. A drop of nanoparticles dispersion was placed on new-cleaved HOPG surface, thoroughly rinsed with water and dried under a N_2 flux.

4.2.5 Cytotoxicity test

The cytotoxicity of the dextrin nanoparticles was evaluated, *in vitro*, using the 3-(4,5-dimethylthiazol-2-yl)-2,5-diphenyl-tetrazolium bromide (MTT) assay. The tetrazolium salt is widely used to quantify cytotoxicity, by colorimetry. The tetrazolium salts are metabolically reduced to highly coloured end products, formazans (Mosmann,1983). The colourless MTT is cleaved to formazan by the succinate-tetrazolium reductase system which belongs to the mitochondrial respiratory chain and is active only in viable cells.

Nanoparticles, at different concentrations, were incubated with cells, for 24 or 48 h. Then, MTT was added to the culture medium to a final concentration of 0.5 mg/mL. After 3 h of incubation, the insoluble formazan crystals were solubilized with DMSO, and the absorption was measured at 570 and 690 nm in an automated ELISA plate reader. For each sample, the background optical density (690 nm) was subtracted; the test was performed in triplicate.

4.2.6 Nitric oxide quantification

The nitric oxide production was evaluated by quantifying the nitrite accumulation in cell culture supernatants using the Griess method (Green*, et al.*,1982). Despite this method quantifies only nitrites, not nitrates, for the sake of the comparison carried out in this work it is sufficient. As a positive control, BMDM culture was challenged with lipopolysaccharide (LPS) and gamma interferon (IFN-γ). LPS is an endotoxin of the bacterial cell wall, well known to stimulate the release of different markers of inflammation by macrophage cells. It is used to stimulate macrophages in order to obtain a background of activation/inflammation, as it is usually done in studies concerning the inflammatory potential of different biochemical agents. IFN-γ is a cytokine produced by T-lymphocytes and NK cells which activates the antimicrobial mechanism of macrophages.

BMDM cells (5×10^5 cells /well) were incubated, at 37 ºC in a 5% CO_2 atmosphere, for 24 or 48 h, in the presence of different concentrations of nanoparticles (1.0, 0.5 and 0.1 mg/mL). Assays were carried out either with and without LPS (100 ng/mL) and IFN-γ (1 ng/mL). The final volume used was 1 mL per well. Then, 100 μL of Griess reagent was added to 100 μL of sample culture medium, and the absorbance was measured at 550 nm. Nitrite concentrations in the medium were finally determined by using standard solutions of sodium nitrite (0-100 μM).

4.2.7 Uptake of nanoparticles by the BMDM

4.2.7.1 Preparation of fluorescein-labelled nanoparticles

Fluorescein is a fluorescent probe quite commonly used in biological studies, owing to its biocompatibility. In order to label the nanoparticles with fluorescein, the following solutions were prepared: (1) Nanoparticle solution – 10 mg of dexC_{16} were dissolved in 1.3 mL of sodium phosphate buffer 0.1 M pH 7 and stirred for 30 min; (2) fluorescein solution - 5 mg of SAMSA fluorescein were dissolved in 0.5 mL of NaOH 0.1 M and stirred for 15 min. Afterwards, 7 µL of HCl 6 M and 0.1 mL of $NaPO_4$ buffer 0.5 M pH7 were added and stirred for 10 min. Finally, these two solutions were mixed up and stirred for 30 min. Unbound fluorescein was separated using a Sephadex G25 PD10 column equilibrated with PBS. Nanoparticles labelled with fluorescein were eluted with PBS and sterilized by filtration through a 0.22 µm membrane before use. Fluorescein labelling did not affect the properties of the nanoparticles, as estimated by dynamic light scattering.

4.2.7.2 Fluorescence studies

The assessment of phagocytosis, after incubating the fluorescent-labelled nanoparticles with murine macrophages, was attempted by spectrofluorimetry. In this study, Fluorescein-containing nanoparticles (1.0, 0.5 or 0.1 mg/mL) were added to BMDM cultures, which were pre-stimulated with LPS (100 ng/mL) and IFN-γ (1 ng/mL) on a 96-well plate. As a control, 0.5 mg/mL nanoparticles were incubated with cells without LPS and IFN-γ. Following incubation periods of 3 or 6 h, the culture medium was collected and cell monolayers were rinsed four times with PBS to remove the non-phagocytosed nanoparticles. Then, 200 µL culture medium and 2 µL saponine (10%) were added and the cell lysates collected 10 min after incubation. Fluorescence intensity was measured in both the cell lysate and the collected culture medium, using a spectrofluorimeter.

4.2.7.3 Confocal observation of the macrophages

In order to evaluate the phagocytic activity, macrophages (5×10^5 cells/well) were seeded on coverslips and stimulated with LPS (100 ng/mL) and IFN-γ (1 ng/mL). Then, the cell culture was incubated with or without fluorescein-containing nanoparticles (1.0 or 0.1 mg/mL) for 6 h. The cover glasses were washed twice with PBS and cells were fixed

with methanol absolute (-20ºC) for 10 min. Following PBS washing (twice), cells were labelled with DAPI (staining nucleous-blue) for 15 min. Vectashield was used as an anti-fading. Cover glasses were analysed using a laser scanning confocal microscope LEICA SP AOBS SE (Leica Microsystems, Germany), equipped with HC PL APO Lbl. Blue 63x / 140 Oil objective.

4.2.7.4 FACS analysis

Cells ($5x10^5$ cells/mL) were seeded in 96-well plates and incubated at 37 ºC and 5% CO_2. After removal of the growth medium, the cells were pre-stimulated with LPS (100 ng/mL) and IFN-γ (1 ng/mL) and treated with fluorescein-linked nanoparticles (1.0, 0.5 or 0.1 mg/mL), for 3 or 6 h. As a control, 0.5 mg/mL nanoparticles were incubated with cells not pre-stimulated with LPS and IFN-γ. After incubation, cells were washed four times with PBS and collected with 100 µL of cooled EDTA. Then cells were transferred to fluorescence activated cell sorting (FACS) tubes with 1 mL PBS and centrifuged at 500 × g for 10 min. After removal of the supernatant, cells were resuspended in 500 µL of FACS buffer (EDTA with 1% BSA).

Flow cytometric analysis was performed using a FACS Coulter Epics XL (Applied Cytometry Systems, United Kingdom). The cells were excited with a 488 nm laser and green fluorescence collected using a 530 ± 30 nm band pass filter. Data were analysed using EXPO32 software (Applied Cytometry Systems, United Kingdom), which statistical functions were used to quantify the proportion of cells with green fluorescence, corresponding to the percentage of macrophages with phagocytosed nanoparticles.

4.2.8 Blood clearance

On the day of experiments, mice were grouped (N = 3) according to pre-defined periods of time (0, 3, 5, 10 and 24 h). A solution of fluorescein-containing nanoparticles (100 µL, 0.3 mg/mL) was injected in the tail vein. The injections were well tolerated and no adverse effects were recorded during the observation period. After pre-defined periods following nanoparticles administration, blood was collected through tail cut. Blood was centrifuged (14,000 rpm, 40 min, 4 ºC) and the fluorescence of supernatant was analysed. The samples corresponding to the beginning of the experiment (0 h) were collected immediately after injection. Fluorescence measurements were performed on a VARIAN Cary Eclipse fluorescence spectrofluorometer using a quartz cell. The

fluorescein spectra were obtained using an excitation wavelength of 485 nm, and recording the emission over the range 500-590 nm, at a scan rate of 125 nm min^{-1}. The slit width was set at 5 nm for the excitation and 10 nm for the emission.

4.3 Results and discussion

Self-assembled nanoparticles were observed using dynamic light scattering (DLS) and atomic force microscopy after filtration through a 0.22 µm membrane. The AFM image (Figure 4.1a) shows that nanoparticles have spherical shape. The fundamental size distribution generated by DLS is an intensity distribution - quite sensitive to the presence of larger particles - which can be converted, using Mie theory, to a volume distribution. This volume distribution can also be further converted to a number distribution. The DLS analysis reveal two populations in the intensity distribution (Figure 4.1b), with roughly 20 and 100 nm. The conversion to number distribution (Figure 4.1c) highlights only the smaller population of nanoparticles, the predominant one. The nanoparticles size was not affected by the fluorescein labelling (data not shown).

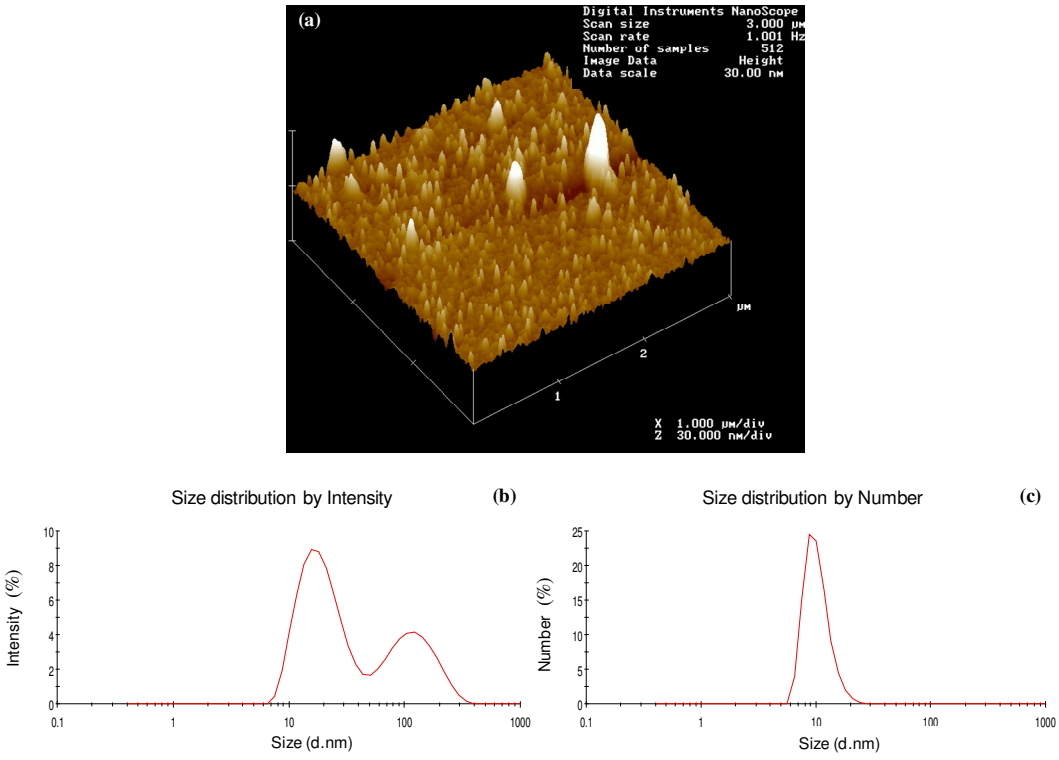

Figure 4.1. AFM image (a) and size distribution by intensity (b) and by number (c) of nanoparticles dispersion (1.0 mg/mL).

It should be remarked that the material used on the development of the nanoparticles, dextrin, is a very promising biomaterial, available in medical grade and accepted by FDA (Hreczuk-Hirst*, et al.*, 2001, Treetharnmathurot*, et al.*, 2009). However, in spite of its biocompatibility and availability on large amounts, it is under exploited in the biomedical field.

4.3.1 BMDM cultures: cytotoxicity and nitric oxide production

The nanoparticles toxicity was studied using BMDM cultures and the MTT assay. Figure 4.2a shows the results. The presence of nanoparticles, in the range of concentrations studied, does not affect cell viability as measured by the MTT assay. Cells treated with nanoparticles showed a optical density similar to the control (untreated cells). Furthermore, the cells exhibit normal morphology. Similar experiments performed with fibroblast cultures produced similar results (data not shown). It must be remarked that the concentration of nanoparticles used in these assays exceeds the values likely to be reached *in vivo*, therefore it may be concluded that the dextrin nanoparticles are not cytotoxic.

The nanoparticles effect on the nitric oxide production by cultured macrophages was analysed (Figure 4.2b). Cells were incubated for 48 h with nanoparticles alone and the production of nitric oxide was not detected in the conditions of the assay. Moreover, as expected, the addition of LPS and IFN-γ to the culture medium induced nitric oxide production. The effect of combining LPS and IFN-γ with different nanoparticles concentration was therefore studied. This analysis revealed that the release of nitric oxide was similar, irrespective of the presence of nanoparticles. The presence of the nanoparticles seems not to promote any inflammatory action or elicit a reactive response when in contact with macrophages.

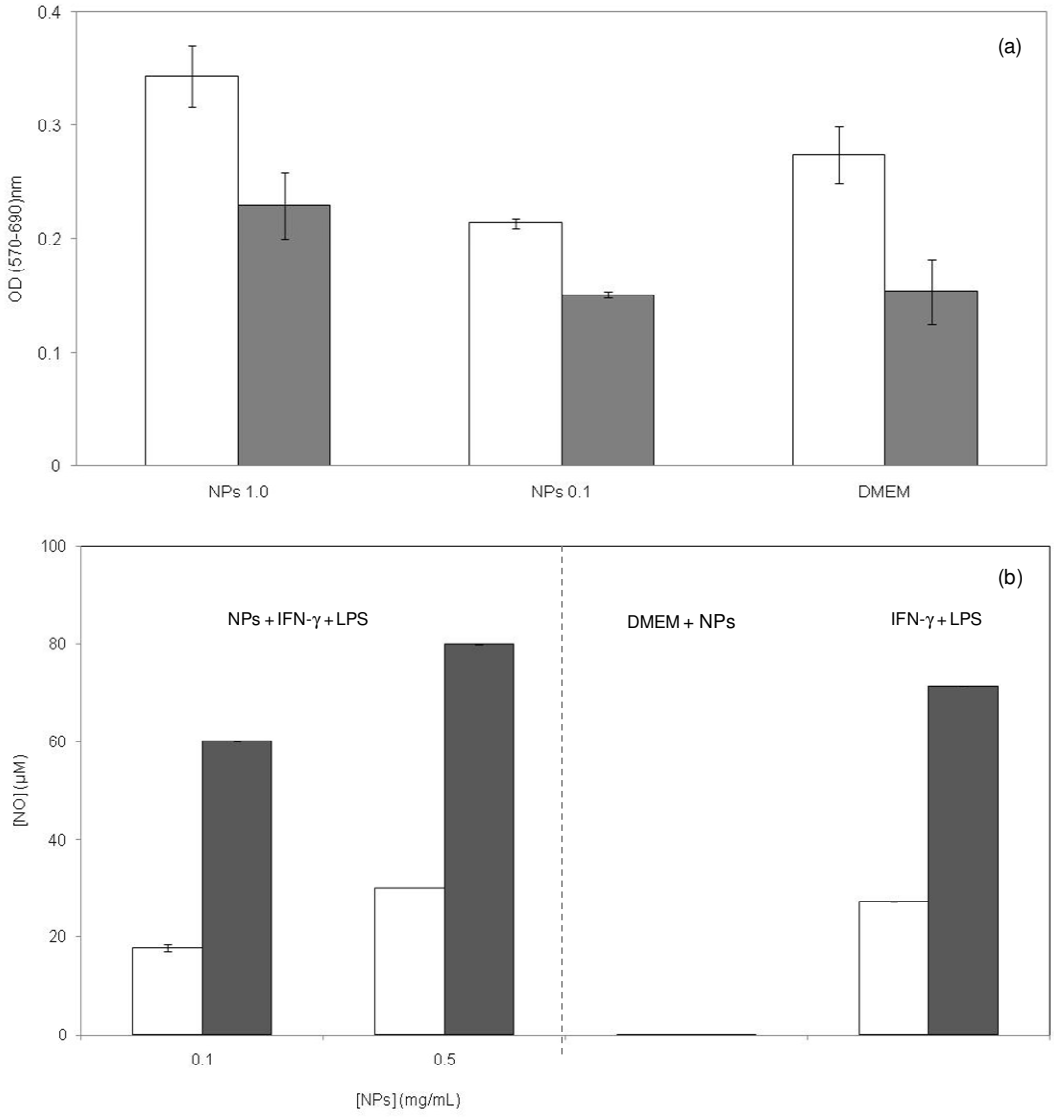

Figure 4.2. BMDM viability (a) with different nanoparticles concentrations (1.0 or 0.1 mg/mL) and nitric oxide production (b) using 0.5 or 0.1 mg/mL nanoparticles, after 24 h (□) or 48 h (■) of incubation. For nitric oxide assay BMDM were stimulated with LPS (100 ng/mL) and IFN-γ (1 ng/mL). For negative control cells were incubated only with nanoparticles. The error bar corresponds to the standard deviation.

4.3.2 Uptake of nanoparticles

Particle size is known to play a primary role in the interaction of nanoparticles with phagocytic cells. Larger particles are rapidly taken up by the mononuclear phagocytic system, and smaller ones have a minor chance of being sequestered by phagocytic cells.

Therefore, the size of the nanoparticles has a critical effect on their behavior in biological systems.

In order to detect the internalization of the nanoparticles by the macrophages, fluorescence intensity was measured before (0 h) and after 3 or 6 h of contact of fluorescein-labelled nanoparticles with BMDM, both in cell lysates and in the culture medium. The results are shown in Figure 4.3.

The fluorescence intensity was assessed in the macrophage culture medium, following incubation with the nanoparticles. No differences were seen throughout the periods of observation (Figure 4.3a), the majority of nanoparticles remaining outside the phagocytic cells. However, when lysates of BMDM cultivated in the presence of nanoparticles were analysed, an increased fluorescence intensity (Figure 4.3b) was detected at the higher concentrations tested. The variations in fluorescence intensity, although slight ones, suggest the occurrence of phagocytic processes. The hardly detectable variations in fluorescence intensity suggest that the nanoparticles concentration is far beyond the saturation of the cells. The cell activation does not affect the phagocytic activity of BMDM, since no significant difference was observed irrespective of the stimulation with LPS and IFN-γ (data not shown).

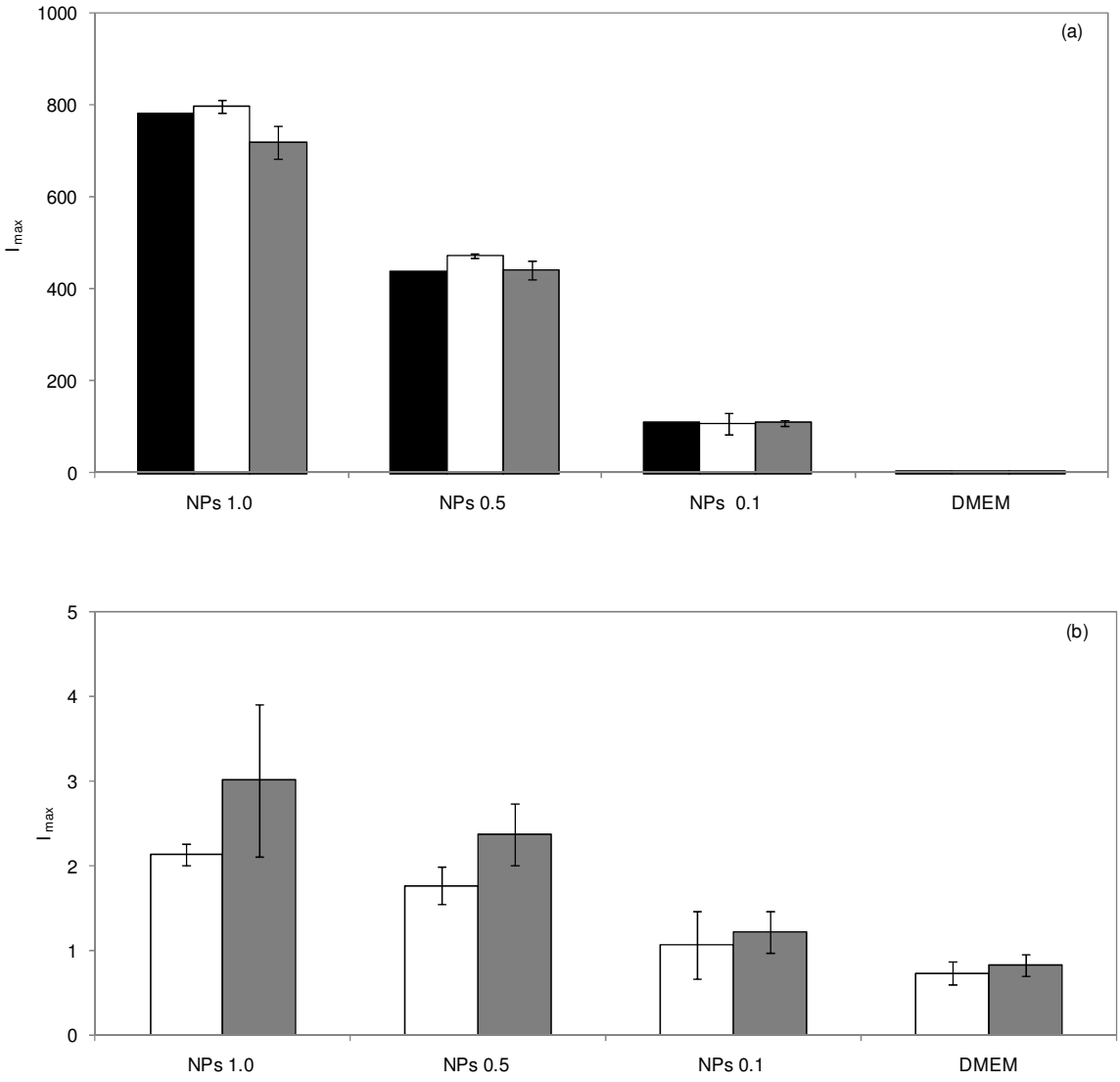

Figure 4.3. Fluorescence intensity of the fluorescein-labelled nanoparticles in the culture medium before (t = 0 h) and after (t = 3 h or 6 h) contact with cells (a) and for BMDM cell lysate (b) after incubation with 1.0, 0.5 or 0.1 mg/mL nanoparticles. Bars represent 0 h (■), 3 h (□) or 6 h (■). The error bar corresponds to the standard deviation.

Bocca, *et al.*, using the same methodology, reported substantial differences in the internalization of stealth and non-stealth solid lipid nanoparticles (average diameter 100 nm), the former undergoing the fastest uptake. The phagocytic uptake of stealth fluorescent nanoparticles was very low - as in this work, with the dextrin nanoparticles - corresponding to about 5% of the initial dose, after 90 min of incubation with murine macrophages (Bocca*, et al.*, 1998). Fang, *et al.* reported the influence of nanoparticles

size on macrophage uptake. The study was performed using poly methoxypolyethyleneglycol cyanoacrylate-co-n-hexadecyl cyanoacrylate (PEG-PHDCA) nanoparticles with different size (80, 170 and 240 nm). No significant uptake differences were observed in the first 0.5 h. However, after 2 h remarkable differences were observed and the uptake percentage was lower for nanoparticles with 80 nm (Fang*, et al.*, 2006). Again, as in this work, only a minor fraction of the nanoparticles are taken up by the cells.

Confocal microscopy was used to further examine the uptake of fluorescein-labelled nanoparticles by macrophages. In the control culture (Figure 4.4a) only nucleus stained with DAPI are visible. Cells incubated with nanoparticles show small green spots (Figure 4.4b and c), in the cytoplasm, that can be attributed to the fluorescein in the internalised nanoparticles. Fluorescent material is concentrated in cellular organelles, irrespective of the concentration used. The cell membrane is not visible, suggesting that the nanoparticles are not adsorbed on the cell surface, as confirmed by the FACS analysis (see below). Apparently, as suggested by the fluorescence depletion studies, the nanoparticles concentration seems to largely exceed the uptake ability of macrophages. Ongoing work focuses on the analysis of the nanoparticles intracellular trafficking.

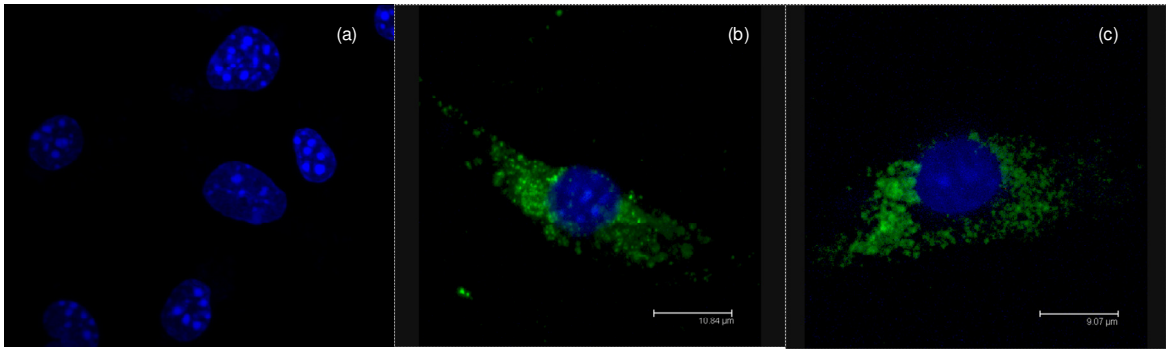

Figure 4.4. Fluorescence images of BMDM obtained by confocal microscopy, without nanoparticles contact (a), and with 6 h of incubation with fluorescein-containing nanoparticles, 0.1 mg/mL (b) or 1.0 mg/mL (c).

The results obtained by FACS analysis confirm the confocal microscopy observations. The cell viability was confirmed with propidium iodide. The percentage of fluorescent macrophages after incubation with labelled nanoparticles was very high, as shown in Figure 4.5. Furthermore, an additional assay using a cell-impermeable dye (trypan blue, a fluorescein quencher), was performed. Since the fluorescence was not reduced in the presence of trypan blue (data not shown), it may be concluded that the nanoparticles are

indeed concentrated inside the macrophages, as shown by confocal microscopy, and not just adsorbed on the cell membrane.

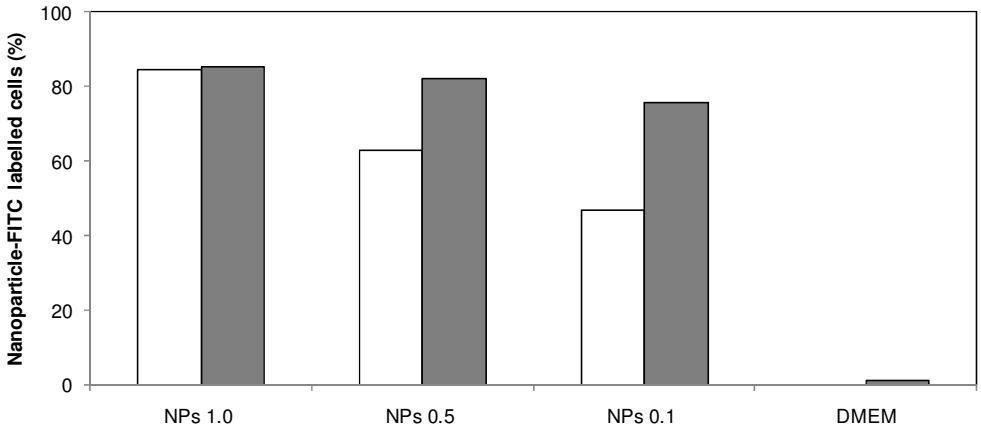

Figure 4.5. Percentage of macrophage cells that incorporated fluorescein-labelled nanoparticles (1.0, 0.5 or 0.1 mg/mL), after 3 h (□) or 6 h (■), measured by FACS analysis.

As suggested by the confocal microscopy images, shown in Figure 4.4, the amount of nanoparticles internalised is similar for the different concentrations used, suggesting that a saturation of the uptake ability of the cells occur in the range of concentrations tested. The phagocytic activity of BMDM cells is not affected by activation with LPS and IFN-γ, since no significant difference was observed (data not shown). The effective internalization suggests that the nanoparticles may be used for vaccination purposes, carrying synthetic antigens to phagocytic cells. Considering this possibility, ongoing work aims at clarifying the kinetics of the phagocytosis, the concentration dependence effects, and the intracellular fate of the nanoparticles.

4.3.3 Blood clearance

Long systemic circulation time is a highly demanded feature for nanoparticles-based drug delivery systems, providing the carriers enough time to reach their targets and to release their content in a continuous and controlled-way.

The fluorescein-labelled nanoparticles were used for blood clearance studies, after intravenous injection. The blood clearance profile for fluorescein-labelled nanoparticles is shown in Figure 4.6. The elimination of nanoparticles from systemic circulation is relatively fast in the first 3 h, then proceeding at lower rate. In the first period studied, 3 h, about 65% of the nanoparticles were removed from the bloodstream and in the next 2 h

another 15% fade away. At 24 h, only 5% of the injected dose is circulating in the bloodstream. The clearance rate of dextrin nanoparticles observed in the blood clearance profile may be related with the nanoparticles size distribution. The small nanoparticles should be small enough to cross the endothelial barrier or to be eliminated by renal clearance. Thus, the nanoparticles remaining longer periods may correspond to the population of larger nanoparticles. Further biodistribution studies by scintigraphy are being carried out in our laboratory, using nanoparticles labelled with radioactive samarium (complexed with quelating agent). Preliminary results show renal accumulation of the nanoparticles and consequent excretion in the urine, thus reinforcing the hypothesis of filtration of the smallest nanoparticles, at least in the kidney. Biodegradation by serum α–amylase is not likely to occur. Indeed, enzymatic hydrolysis of $dexC_{16}$ by α–amylase, *in vitro*, was not detected by dynamic light scattering or reducing sugar method (data not shown). We assume that the polymer modification with alkyl chains blocks the enzyme action: since the dextrin used has very low degree of polymerization – about 12 - every glucose residue is quite close to the alkylic graft, which is likely to avoid the amylase action.

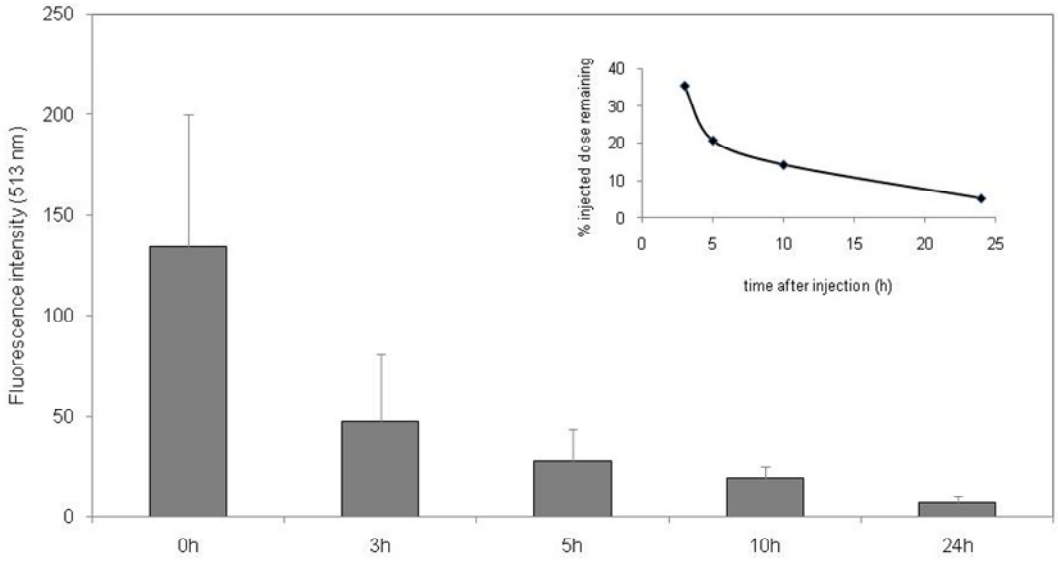

Figure 4.6. Blood clearance profile of fluorescein-labelled nanoparticles. Inset shows the percentage of the initial (0 h) fluorescence, remaining in the bloodstream at different time. The error bar corresponds to the standard deviation.

The blood clearance profile obtained is very similar to others reported for polymeric nanoparticles. Micelles prepared from conjugates of polyethylene glycol (PEG) and phosphatidylethanolamine (PE), with the size of 7-35 nm, have circulation half-lives from 1.2 to 2.1 h depending on the molecular size of PEG block (Lukyanov*, et al.*, 2002). A recent study evaluated the circulation kinetics and biodistribution of core-crosslinked (CCL) and non-crosslinked (NCL) micelles based on $mPEG_{5000}$ and *N*-(2-hydroxyethyl)methacrylamide-oligolactates (mPEG-*b*-p(HEMAm-Lac_n)). CCL and NCL micelles have the same size (57 nm). The NCL micelles were rapidly eliminated from the circulation and only 6% of the injected dose was present after 4 h, probably due to interactions with plasma proteins which lead to recognition by macrophages. Contrary to NCL assemblies, CCL micelles displayed significantly prolonged circulation times, and 50% of the injected dose was still present in the systemic circulation after 6 h. At 24 h post-injection, 5% of the injected dose was in the blood circulation and 10% and 1.7% were taken up by the liver and spleen, respectively. A relatively high accumulation in the abdominal skin was observed, attributed to extravasation into areas that experience pressure and/or micro-traumatised areas in the skin, which is allowed by long circulation time and small size (Rijcken*, et al.*, 2007).

4.4 Conclusions

In vitro studies with BMDM revealed that nanoparticles are non-cytotoxic and do not elicit a reactive response when in contact with macrophages. Moreover, FACS analysis and confocal observation demonstrated that BMDM internalize the nanoparticles. A saturation of the cells uptake ability is observed in the range of concentrations tested. The *in vivo* study showed that, after intravenous injection, a relatively fast removal of the nanoparticles occurs in the first 3 h, then continuing slowly up to 24 h. The blood clearance profile reveal a moderately long circulation time, compatible with drug delivery or diagnostic applications. Dextrin nanoparticles may also be used to address phagocytic cells. Ongoing work aims at modifying nanoparticles surface with PEG, intracellular trafficking analysis and scintigraphy-based biodistribution studies.

Acknowledgments. This research was supported by Fundação para a Ciência e a Tecnologia under grant SFRH/BD/22242/2005 and POCTI program. FACS analysis carried by Manuel Vilanova and Pedro Madureira, from ICBAS – Oporto University, is greatly acknowledged.

4.5 References

Bocca, C.; Caputo, O.; Cavalli, R.; Gabriel, L.; Miglietta, A.; Gasco, M.R. Phagocytic uptake of fluorescent stealth and non-stealth solid lipid nanoparticles *International Journal of Pharmaceutics* **1998**, *175*, 185-193.

Choi, H.S.; Liu, W.; Misra, P.; Tanaka, E.; Zimmer, J.P.; Itty Ipe, B.; Bawendi, M.G.; Frangioni, J.V. Renal clearance of quantum dots. *Nature Biotechnology* **2007**, *25*, 1165-1170.

Esmaeili, F.; Ghahremani, M.H.; Esmaeili, B.; Khoshayand, M.R.; Atyabi, F.; Dinarvand, R. PLGA nanoparticles of different surface properties: preparation and evaluation of their body distribution. *International Journal of Pharmaceutics* **2008**, *349*, 249-255.

Fang, C.; Shi, B.; Pei, Y.Y.; Hong, M.H.; Wu, J.; Chen, H.Z. In vivo tumor targeting of tumor necrosis factor-alpha-loaded stealth nanoparticles: effect of MePEG molecular weight and particle size. *European Journal of Pharmeutical Sciences* **2006**, *27*, 27-36.

Fiorito, S.; Serafino, A.; Andreola, F.; Bernier, P. Effects of fullerenes and single-wall carbon nanotubes on murine and human macrophages *Carbon* **2006**, *44*, 1100-1105.

Gaumet, M.; Vargas, A.; Gurny, R.; Delie, F. Nanoparticles for drug delivery: the need for precision in reporting particle size parameters. *European Journal of Pharmaceutics and Biopharmaceutics* **2008**, *69*, 1-9.

Gonçalves, C.; Gama, F.M. Characterization of the self-assembly process of hydrophobically modified dextrin. *European Polymer Journal* **2008**, *2008*, 3529-3534.

Gonçalves, C.; Martins, J.A.; Gama, F.M. Self-assembled nanoparticles of dextrin substituted with hexadecanethiol. *Biomacromolecules* **2007**, *8*, 392-398.

Green, L.C.; Wagner, D.A.; Glogowski, J.; Skipper, P.L.; Wishnok, J.S.; Tannenbaum, S.R. Analysis of nitrate, nitrite, and [^{15}N]nitrate in biological fluids. *Analytical Biochemistry* **1982**, *126*, 131-138.

Hreczuk-Hirst, D.; Chicco, D.; German, L.; Duncan, R. Dextrins as potential carriers for drug targeting: tailored rates of dextrin degradation by introduction of pendant groups. *International Journal of Pharmeutics* **2001**, *230*, 57-66.

Lemarchand, C.; Gref, R.; Couvreur, P. Polysaccharide-decorated nanoparticles. *European Journal of Pharmaceutics and Biopharmaceutics* **2004**, *58*, 327-341.

Lemarchand, C.; Gref, R.; Lesieur, S.; Hommel, H.; Vacher, B.; Besheer, A.; Maeder, K.; Couvreur, P. Physico-chemical characterization of polysaccharide-coated nanoparticles. *Journal of Controlled Release* **2005**, *108*, 97-111.

Lemarchand, C.; Gref, R.; Passirani, C.; Garcion, E.; Petri, B.; Muller, R.; Costantini, D.; Couvreur, P. Influence of polysaccharide coating on the interactions of nanoparticles with biological systems. *Biomaterials* **2006**, *27*, 108-118.

Lukyanov, A.N.; Gao, Z.; Mazzola, L.; Torchilin, V.P. Polyethylene glycol-diacyllipid micelles demonstrate increased acculumation in subcutaneous tumors in mice. *Pharmaceutical Research* **2002**, *19*, 1424-1429.

Ma, W.; Yuan, X.; Kang, C.; Su, T.; Yuan, X.; Pu, P.; Sheng, J. Evaluation of blood circulation of polysaccharide surface-decorated PLA nanoparticles *Carbohydrate Polymers* **2008**, *72*, 75-81.

Mosmann, T. Rapid colorimetric assay for cellular growth and survival: application to proliferation and cytotoxicity assays. *Journal of Immunological Methods* **1983**, *65*, 55-63.

Mosqueira, V.C.; Legrand, P.; Morgat, J.L.; Vert, M.; Mysiakine, E.; Gref, R.; Devissaguet, J.P.; Barratt, G. Biodistribution of long-circulating PEG-grafted nanocapsules in mice: effects of PEG chain length and density. *Pharmaceutical Research* **2001**, *18*, 1411-1419.

Oyewumi, M.O.; Yokel, R.A.; Jay, M.; Coakley, T.; Mumper, R.J. Comparison of cell uptake, biodistribution and tumor retention of folate-coated and PEG-coated gadolinium nanoparticles in tumor-bearing mice. *Journal of Controlled Release* **2004**, *95*, 613-626.

Pedrosa, J.; Florido, M.; Kunze, Z.M.; Castro, A.G.; Portaels, F.; McFadden, J.; Silva, M.T.; Appelberg, R. Characterization of the virulence of Mycobacterium avium complex (MAC) isolates in mice. *Clinical & Experimental Immunology* **1994**, *98*, 210-216.

Rijcken, C.J.; Snel, C.J.; Schiffelers, R.M.; van Nostrum, C.F.; Hennink, W.E. Hydrolysable core-crosslinked thermosensitive polymeric micelles: synthesis, characterisation and in vivo studies. *Biomaterials* **2007**, *28*, 5581-5593.

Schroer, J.; Rosenthal, A.S. Function of macrophages as antigen presenting cells. *Springer Seminars in Immunopathology* **1980**, *3*, 247-264.

Sonavane, G.; Tomoda, K.; Makino, K. Biodistribution of colloidal gold nanoparticles after intravenous administration: effect of particle size. *Colloids and Surfaces B: Biointerfaces* **2008**, *66*, 274-280.

Stolnik, S.; Illum, L.; Davis, S.S. Long circulating microparticulate drug carriers. *Advanced Drug Delivery Reviews* **1995**, *16*, 195-214.

Torrado, E.; Adusumilli, S.; Fraga, A.G.; Small, P.L.; Castro, A.G.; Pedrosa, J. Mycolactone-mediated inhibition of tumor necrosis factor production by macrophages infected with Mycobacterium ulcerans has implications for the control of infection. *Infection and Immunity* **2007**, *75*, 3979-3988.

Treetharnmathurot, B.; Dieudonne, L.; Ferguson, E.L.; Schmaljohann, D.; Duncan, R.; Wiwattanapatapee, R. Dextrin-trypsin and ST-HPMA-trypsin conjugates: enzyme activity, autolysis and thermal stability. *International Journal of Pharmeutics* **2009**, *373*, 68-76.

Tushinski, R.J.; Oliver, I.T.; Guilbert, L.J.; Tynan, P.W.; Warner, J.R.; Stanley, E.R. Survival of mononuclear phagocytes depends on a lineage-specific growth factor that the differentiated cells selectively destroy. *Cell* **1982**, *28*, 71-81.

Underhill, D.M.; Bassetti, M.; Rudensky, A.; Aderem, A. Dynamic interactions of macrophages with T cells during antigen presentation. The *Journal of Experimental Medicine* **1999**, *190*, 1909-1914.

Warren, M.K.; Vogel, S.N. Bone marrow-derived macrophages: development and regulation of differentiation markers by colony-stimulating factor and interferons. The *Journal of Immunology* **1985**, *134*, 982-989.

Zahr, A.S.; Davis, C.A.; Pishko, M.V. Macrophage uptake of core-shell nanoparticles surface modified with poly(ethylene glycol). *Langmuir* **2006**, *22*, 8178-8185.

Zhang, X.; Gonçalves, R.; Mosser, D.M. The isolation and characterization of murine macrophages. *Current Protocols in Immunology* **2008**, *Chapter 14*.

5. Dextrin nanoparticles as a curcumin delivery system; studies on the stability of self-assembled nanoparticles

Curcuma longa
(from Kochler´s Medicinal-Plants)

Curcumin is a natural polyphenol with anti-oxidative, anti-inflammatory and anti-cancer properties. Its therapeutic potential is substantially hindered by the rather low water solubility and bioavailability, hence the need for suitable carriers. In this study, we show that self-assembled nanoparticles – also called nanogels or macromolecular micelles – obtained from hydrophobically modified dextrin are effective curcumin nanocarriers. The stability and loading efficiency of curcumin in the dextrin nanoparticles depends on the polymer/curcumin ratio; higher stability is achieved in water than in PBS buffer, as analysed by dynamic light scattering. Fluorescence resonance energy transfer experiments were carried out to evaluate the spatial re-distribution/assembly of aqueous dispersions of dexC_{16} nanoparticles. The *in vitro* release of curcumin and cytotoxicity on HeLa cell cultures were estimated using the MTS assay.

5.1 Introduction

Curcumin is a multi-functional and pharmacologically safe natural agent. Chemically it is a low-molecular-weight polyphenol derivative, extracted from rhizomes of *Curcuma* species. Used as a food additive for centuries, it has been recently demonstrated that curcumin is highly pleiotropic, interacting physically with diverse molecular targets, which includes transcription factors, growth factors and their receptors, cytokines, enzymes, and genes regulating cell proliferation and apoptosis (Goel*, et al.*, 2008). Curcumin possess potent anti-inflammatory, anti-tumor and anti-oxidative (free radical scavenging activity) properties. Pre-clinical data shows that curcumin inhibits the formation of tumors in animal models of carcinogenesis, induce apoptosis in cancer cells of different tissues or organs, such as colon, breast, prostate and lung, acting on a variety of signal transduction pathways and molecular targets involved in the development of cancer (Lopez-Lazaro, 2008). The ability of curcumin to induce apoptosis in cancer cells, without cytotoxic effects on the healthy ones, is suggestive of a relevant anti-cancer potential. For instance, curcumin leads to apoptosis in scleroderma lung fibroblasts without affecting normal lung fibroblasts (Tourkina*, et al.*, 2004). Preferential uptake of curcumin by tumor cells compared to normal cells was also demonstrated.

Curcumin, being a lipophilic molecule, interacts with the cellular membrane and is subsequently internalized, probably by diffusion. The higher curcumin uptake by tumor cells, against normal ones, has been assigned to various hypothetic factors, including the different membrane structure, protein composition and larger size (Kunwar*, et al.*, 2006). The anti-oxidant activity of curcumin has been identified as the key mechanism by which this dietary phytochemical prevents cancer *in vivo*. Curcumin also allows reduction of oxidative and inflammatory stress in Alzheimer patients (Lim*, et al.*, 2001). Indeed, curcumin has also been shown to inhibit mediators of inflammation such as cyclo-oxygenase-2 and lipooxygenase (two enzymes involved in inflammation) (Huang*, et al.*, 1991), inducible nitric oxide synthase (enzyme that catalyzes the production of nitric oxide) (Chan*, et al.*, 1998), cytokines and NFκB.

Despite all these promising characteristics, a major problem with curcumin is the very low solubility in aqueous solutions, which limits bioavailability and clinical efficacy. Interest in the development of nanocarriers for curcumin therapy is emerging. Polymeric nanoparticles have gained attention due to several advantages, such as low toxicity, high stability and small size, which may allow passive targeting of solid tumor tissues by enhanced permeation and retention (EPR) effect. Being highly hydrophobic, curcumin is

insoluble in water but soluble in ethanol, dimethylsulfoxide and acetone. The encapsulation of a highly hydrophobic compound like curcumin in nanocarriers makes it readily soluble in aqueous systems, improving the ease of dosing and making intravenous administration possible. In a clinical study, after oral administration of 2 g kg^{-1} of curcumin to rats, a maximum serum concentration of 1.35±0.23 µg mL^{-1} was observed at time 0.83 h, whereas in humans the same dose of curcumin resulted in extremely low (0.006±0.005 µg mL^{-1} at 1 h) serum levels (Shoba*, et al.*, 1998).

In a previous work, we described the production and characterization of new dextrin nanoparticles - also called nanogels or macromolecular micelles - obtained by self-assembling of hydrophobically modified dextrin. The use of this material for curcumin solubilisation and delivery is now reported. Curcumin loading efficiency, stability and release profile were studied. The biocompatibility of nanoparticles and the bioactivity of the curcumin/nanoparticles formulation were evaluated using the (3-(4,5-dimethylthiazol-2-yl)-5-(3-carboxymethoxyphenyl)-2-(4-sulfophenyl)-2H-tetrazolium) (MTS assay) using HeLa cell cultures.

5.2 Experimental section

5.2.1 Materials

Dextrin-VA-SC_{16} ($dexC_{16}$) was synthesized as comprehensively described previously (Gonçalves*, et al.*, 2007). $DexC_{16}$ is composed by a hydrophilic dextrin backbone with grafted acrylate groups (VA - vinyl acrylate), which are partially substituted with long alkyl chains (SC_{16}). In this work, $dexC_{16}$ with a degree of substitution of dextrin with acrylate groups and alkyl chains was respectively 13.0% (DS_{VA}) and 6.0% (DS_{C16}). Curcumin was purchased from Fluka and (3-(4,5-dimethylthiazol-2-yl)-5-(3-carboxymethoxyphenyl)-2-(4-sulfophenyl)-2H-tetrazolium) (MTS) from Promega. SAMSA (5-((2-(and-3)-S-(acetylmercapto) succinoyl) amino) fluorescein (SAMSA-F) and QSY-7 amine hydrochloride (QSY-7) were obtained from Invitrogen. Ethanol was purchased from AppliChem.

5.2.2 Preparation of polymeric nanoparticles

Polymeric nanoparticles were obtained by dispersion of dexC_{16} in water, avoiding the use of any organic solvent. Lyophilized dexC_{16} was dispersed in water or phosphate-buffered saline (PBS) solution under stirring at 50ºC, until a clear solution was obtained. The solution was then filtrated through a 0.22 µm syringe filter. The polymer concentration must be higher than 0.008 mg/mL, previously identified as the critical micelle concentration (CMC) (Gonçalves*, et al.*, 2007) required for the amphiphilic polymer to self-assemble in water, originating nanostructures containing hydrophobic domains, allowing the solubilization of hydrophobic molecules.

5.2.2.1 SAMSA-F labelled nanoparticles

In order to label the nanoparticles with SAMSA fluorescein (SAMSA-F), the following solutions were prepared: (1) Nanoparticle solution – 10 mg of dexC_{16} were dissolved in 1.3 mL of sodium phosphate buffer 0.1 M pH 7 and stirred for 30 min; (2) fluorescein solution - 5 mg of SAMSA-F were dissolved in 0.5 mL of NaOH 0.1 M and stirred for 15 min. Afterwards, 7 µL of HCl 6 M and 0.1 mL of $NaPO_4$ buffer 0.5 M pH 7 were added and stirred for 10 min. Finally, these two solutions were mixed up and stirred for 30 min. Unbound fluorescein was separated using gel filtration in a sephadex G25 PD10 column equilibrated with PBS. SAMSA-F-labelled nanoparticles were eluted with PBS, sterilized by filtration through a 0.22 µm membrane and stored at 4ºC. SAMSA-F labelling did not affect the nanoparticles size distribution, as estimated by dynamic light scattering.

5.2.2.2 QSY-7 labelled nanoparticles

In order to label the nanoparticles with QSY-7, the following solutions were prepared: (1) Nanoparticle solution – 5 mg of dexC_{16} were dissolved in 2 mL DMSO; (2) QSY-7 solution - 5 mg of QSY-7 were dissolved in 1.0 mL of DMSO. Then, 246 µL of QSY-7 solution and nanoparticle solution were mixed up and 1 µL of TEA was added; the mixture was stirred overnight at room temperature, and dialysed for 48 h against frequently changed water. To guarantee total removal of unbound QSY-7, the labelled nanogel was further purified by gel filtration in a sephadex G25 PD10 column equilibrated with PBS. Nanoparticles labelled with QSY-7 were eluted with PBS, sterilized by filtration through a 0.22 µm membrane and stored at 4ºC. QSY-7 labelling did not affect the nanoparticles size distribution, as estimated by dynamic light scattering.

5.2.3 Curcumin loading, efficiency and stability

Curcumin has been loaded into the hydrophobic domains of nanoparticles. The physical entrapment of curcumin in the nanoparticles was performed following the nanoparticles formation, as described ahead. A stock solution of curcumin in ethanol with a concentration of 2.7 mM was prepared. The required volume of curcumin from this solution was added to the nanoparticles solution (final concentration of ethanol < 1%). The effect of polymer/curcumin ratio on the loading efficiency and stability of the formulation was studied. Different formulations were prepared by varying the curcumin (10, 30, 50 μM) and polymer (0.1, 0.25, 0.5, 1.0 or 2.0 mg/mL) concentrations. In order to evaluate the stability of the dispersion, the solutions were kept under stirring at 37ºC up to 8 days. The resultant solution was centrifuged at 4000 rpm (Sigma 4K-15 refrigerated centrifuge) and 4ºC, for 10 min, to remove the insoluble curcumin. The clear yellowish supernatant was carefully collected and analyzed spectrophotometrically. The quantification was carried out using a calibration plot obtained with curcumin concentrations between 0.3 and 30 μM. The entrapment efficiency was calculated by the Equation 5.1:

$$\text{Entrapment efficiency (\%)} = \frac{[CM]_{encapsulated}}{[CM]_{added}} \qquad \text{(Equation 5.1)}$$

The size distribution of loaded and unloaded nanoparticles was determined by dynamic light scattering (DLS) using a Malvern Zetasizer, MODEL NANO ZS (Malvern Instruments Limited, U.K.). The nanoparticles dispersion was analysed at 25ºC in a polystyrene cell, using a He-Ne laser - wavelength of 633 nm and a detector angle of 173º. The DLS analysis provides the characterization of a sample through the mean value (z-avg) for the diameter, and a width parameter known as the polydispersity index (PdI).

5.2.4 Curcumin release

In the present work, the release of curcumin from the nanoparticles was studied using sink conditions – sample in a dialysis membrane – and a closed system - sample in a flask. The curcumin loaded nanoparticles (30 μM of curcumin and 1.0 mg/mL of polymer in an aqueous solution) were maintained in a glass flask or transferred to a dialysis bag. The dialysis bag (molecular cut off of 10 kDa) was placed in 200 mL of distilled water or PBS, shaken under 500 rpm at 37ºC. At predefined timeframe (up to 24 h), a sample of

200 μL was withdrawn from each condition, centrifuged to guarantee removal of unentrapped curcumin and the supernatant was analyzed spectrophotometrically (Jasco V560). At the end of the assay, after 24 h, the size distribution of the nanoparticles was evaluated by DLS.

5.2.5 Fluorescence measurements

To understand the spatial re-distribution/assembly of distinct dispersions of dexC_{16} nanoparticles, after mixing, fluorescence resonance energy transfer (FRET) was used. FRET is a distance-dependent interaction between the electronic excited states of two dye molecules in which excitation is transferred from a donor molecule to an acceptor one without emission of a photon. Thus, FRET is a technique suitable for investigating a variety of biological phenomena that produce changes in molecular proximity. In this work, the pair fluorescein/QSY-7 was used as donor/acceptor. Non-fluorescent acceptors, such as QSY dyes, have the particular advantage of eliminating the potential problem of background fluorescence resulting from direct (i.e., nonsensitized) acceptor excitation. In this study, FRET is detected by quenching of donor fluorescence.

Nanoparticles with covalently attached SAMSA-F and those with the non-fluorescent acceptor QSY-7 were mixed; then, PBS solution was added for the system to reach the required final concentration of material. Steady-state as well as time resolved fluorescence studies were performed to evaluate the distribution/re-distribution of each population after mixing. Additional studies were performed with SAMSA-F labelled nanoparticles (0.115 mg/mL) diluted in distilled water or PBS, over time, using time resolved fluorescence to ascertain the occurrence of structural modifications.

The steady-state fluorescence measurements were performed with a Spex Fluolog 3 spectrofluorimeter at room temperature. All spectra were corrected for the instrumental response of the system. The excitation wavelength was set at 460 nm. The steady state quenching ratio was calculated using the emission spectra area of SAMSA-F labelled nanoparticles between 470 nm and 600 nm in the presence (I) and absence (I_o) of QSY-7 labelled nanoparticles.

The fluorescence decay times were determined using the frequency-doubled output of a Ti:Sa laser at 399 nm for excitation and measuring the emission at 540 nm. The decay curves were gained by Time Correlated Single Photon Counting (TCSPC) using a Becker & Hickl SPC-150 computer board collecting the photon detection events from a

Hamamatsu MCP R3809U-51 photon counting unit. The time resolution was 20 ps. Data fitting was done with the Picoquant Fluolog software by deconvolution of the Instrument Response Function (IRF), allowing the recovery of the average life time in the presence (τ) and absence (τ_0) of QSY-7 labelled nanoparticles.

5.2.6 Cell culture and cytotoxicity assay

The cytotoxicity of free or encapsulated curcumin was evaluated by MTS, a colorimetric assay that gives a measure of the mitochondrial metabolic activity. Human cervical cancer cells (HeLa) were counted and seeded at 1×10^4 cells/well into 24-well cell culture plates, in cDMEM medium with 10% fetal bovine serum, and allowed to adhere for 24 h at 37ºC and 5% CO_2 atmosphere. Afterwards, the culture medium was decanted and replaced with fresh culture medium or with the test conditions. Nanoparticles (0.10 or 0.25 mg/mL), free or encapsulated curcumin (30 µM) were tested. Then, plates were incubated for 24 or 48 h in triplicate, at 37ºC, 5% CO_2. The viability of the cells after treatment was determined by the MTS assay, as described ahead. The culture medium of each well was decanted and replaced with 100 µL of fresh culture medium. Then, 20 µL of "CellTiter 96® AQueous One Solution Reagent" was added into each well and the plates were incubated for 2 h at 37ºC, 5% CO_2. The amount of soluble formazan produced by cellular reduction of the MTS was measured at 490 nm. The absorbance at 490 nm is proportional to the cell number.

5.3 Results and discussion

5.3.1 Curcumin loading, efficiency and stability

The possibility of enhancing curcumin's solubility using polymeric nanoparticles as nanocarrier was investigated in this work. Soluble curcumin obtained in a suitable solvent such as ethanol (Figure 5.1) exhibits intense absorption in the wavelength range from 350 to 550 nm, with a maximum absorption at 428 nm. The addition of curcumin dissolved in ethanol to water (to a final concentration of ethanol < 1%), leads to curcumin precipitation. On the other hand, the addition of curcumin to aqueous solutions of nanoparticles results in a bright yellow solution (Figure 5.1a), suggesting the entrapment of curcumin, presumably into the hydrophobic domains within the nanoparticles. Indeed,

the UV-Vis spectra reveal an intense absorption at 428 nm, confirming the curcumin dissolution (Figure 5.1b).

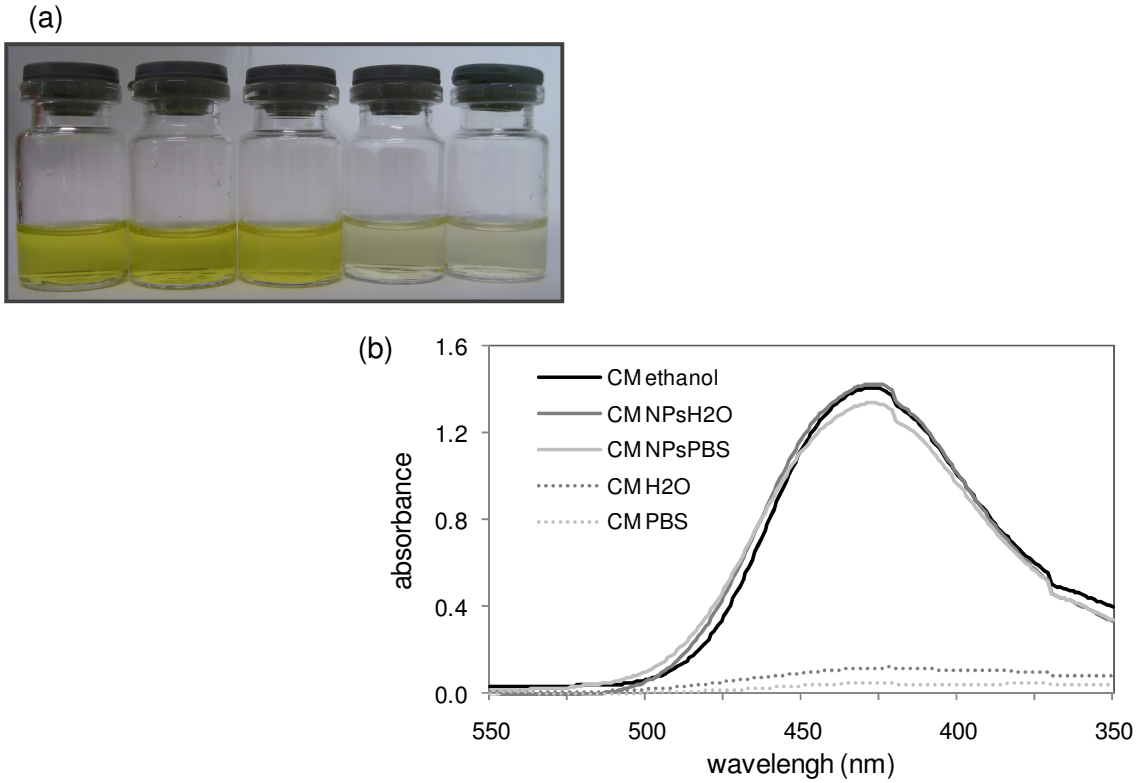

Figure 5.1. Supernatant of curcumin (a) dissolved in different solvents (from left: ethanol, aqueous solution of nanoparticles, PBS solution of nanoparticles, water and PBS solution) and (b) ultraviolet-visible absorbance spectra for each condition.

The size of the self-assembled nanoparticles, with or without curcumin, was determined by dynamic light scattering. The mean diameters (z-avg) of unload or curcumin-loaded nanoparticles were found to be 61.1 nm (PdI 0.243) and 74.6 nm (PdI 0.368) for water or 59.2 nm (PdI 0.209) and 90.9 nm (PdI 0.422) for PBS solution, respectively. The colloidal stability of nanoparticles (in water or PBS solution) has been previously assessed (Gonçalves*, et al.*, 2008) using dexC_{16} with a higher degree of substitution (DS_{C16} 8.7% vs 6.0% in this work), up to 7 days. High stability was observed in both water and PBS solution, since no aggregates were detected and a low polydispersity index was conserved. The more substituted polymer forms more densely packed hydrophobic domains, such that the colloidal stability of nanoparticles is increased. In this work, the stability of nanoparticles with DS_{C16} 6.0%, without curcumin, in water or PBS solution, was evaluated (Table 5.1), up to 12 days.

Table 5.1. Evaluation of mean hydrodynamic diameter (z-avg) and polydispersity index (PdI), of dexC_{16} (DS_{C16} 6.0%) dispersed in distilled water or PBS solution, up to 12 days.

	Water		PBS solution	
time	**z-avg (nm)**	**PdI**	**z-avg (nm)**	**PdI**
freshly prepared	61.1	0.243	59.2	0.290
3 days	62.3	0.304	72.2	0.312
5 days	61.0	0.270	79.1	0.285
12 days	58.7	0.244	100.0	0.247

A general conclusion may be drawn from the results: the nanoparticles prepared in a saline solution (buffer) present an increased size along with the incubation period, apparently associated to a swelling process when compared to those dispersed in water. A successful nanodelivery system should have a high drug-loading capacity, thereby reducing the quantity of carrier for administration. Additionally, drug-loaded nanoparticles should be able to retain the drug for a prolonged time in circulation, for effective targeting of tissues. In this work, different formulations were prepared to evaluate the effect of polymer/curcumin ratio on the loading efficacy and stability, using both distilled water or PBS solution as the dispersion medium. Figure 5.2 shows the concentration of curcumin obtained using different proportions of nanoparticles and curcumin.

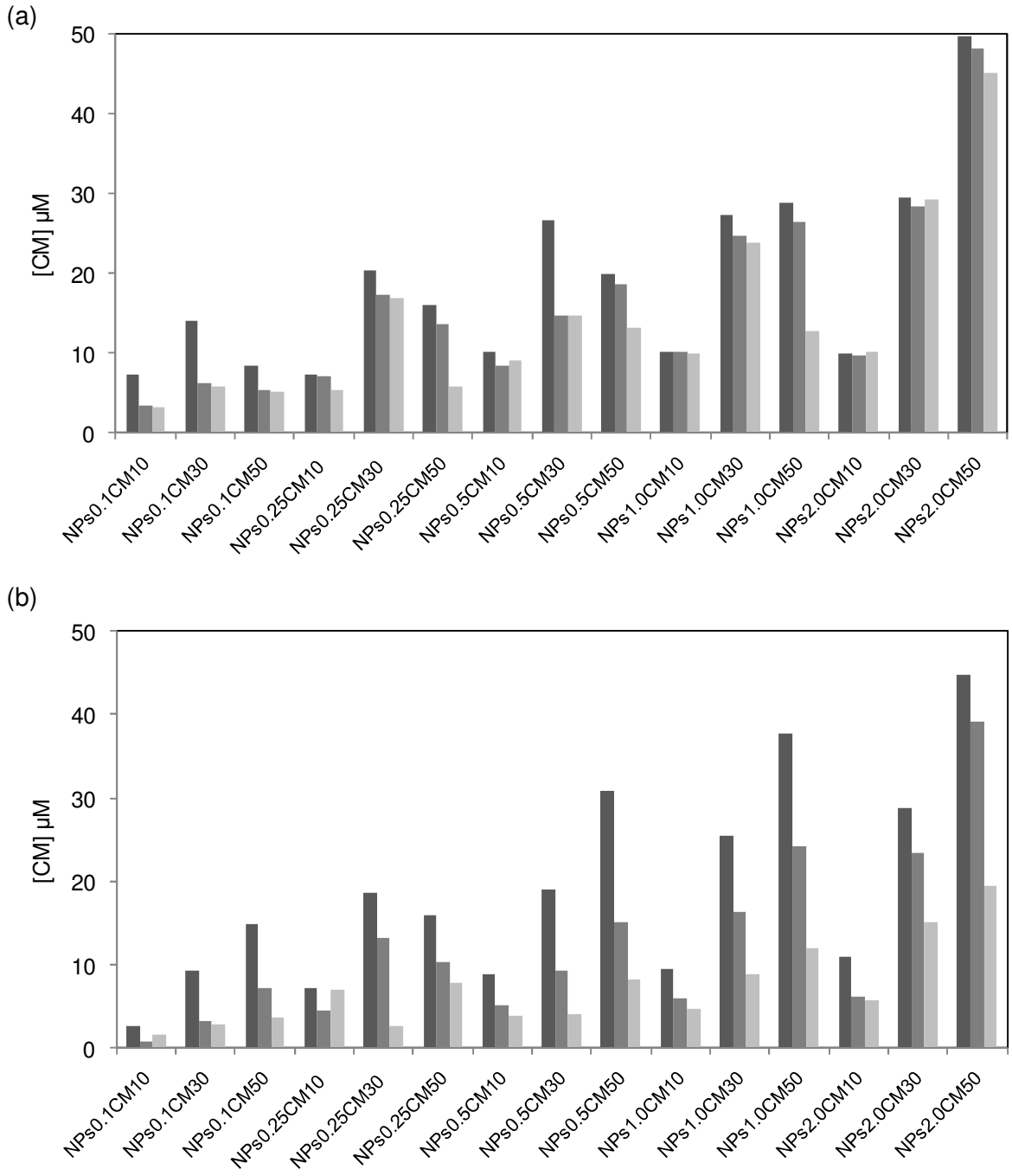

Figure 5.2. Curcumin loading into dextrin nanoparticles in (a) aqueous or (b) PBS solution of different formulations varying the curcumin (10, 30, 50 µM) and polymer (0.1, 0.25, 0.5, 1.0 or 2.0 mg/mL) concentrations, (■) 3 h, (■) 24 h or (■) 8 days after incubation.

The results of curcumin loading in aqueous solution (Figure 5.2a) show that for a constant polymer concentration, the higher curcumin loads results in lower stability over time. For instance, for the highest polymer concentration studied (2.0 mg/mL), 10 or 30

μM of curcumin remain stable until 8 days. The lower curcumin concentration tested (10 μM) is stabilized by a polymer concentration of 0.25 mg/mL. Increasing the curcumin concentration to 30 μM, requires a polymer concentration of at least 1.0 mg/mL. Thus, as could be expected, there is an optimal proportion of curcumin/nanoparticle that allows a stable system to be obtained; high loadings results in unstable systems. Curcumin loading in PBS solution (Figure 5.2b) shows similar results in the first period of observation (3 h). However, a relevant difference is noticeable for longer incubation time frames: curcumin solutions are unstable for every formulations studied.

To evaluate the spatial re-distribution/assembly of distinct dispersions of $dexC_{16}$ nanoparticles, after mixing, nanoparticles with covalently attached SAMSA-F and those with the non-fluorescent acceptor QSY-7 were mixed and fluorescence measurements were performed. Comparing the fluorescence intensity of SAMSA-F in the steady state, or the fluorescence decay time in the time resolved fluorescence, with or without acceptor dye, some differences are evident. Both steady state and time resolved fluorescence measurements show a quenching effect as can be concluded from $I_0/I > 1$ and $\tau_0/\tau > 1$ (Table 5.2). But as these ratios are different, we conclude that part of the quenching effect results from a non-fluorescent ground-state complex formation between SAMSA-F and QSY-7 labelled $dexC_{16}$ (Valeur, 2002).

Table 5.2. SAMSA-F fluorescence quenching by QSY-7.

[SAMSA-F NPs] = 0.115 mg/mL		[SAMSA-F NPs] = 0.080 mg/mL	
[QSY-7 NPs] = 0.20 mg/mL		[QSY-7 NPs] = 0.14 mg/mL	
I_o/I	1.26	I_o/I	1.24
τ_o/τ	1.18	τ_o/τ	1.20

The formation of ground-state complexes between SAMSA-F and QSY-7 implies a dynamic behavior of the nanoparticles, through an exchange of $dexC_{16}$ molecules among them. The quenching effects observed in the time resolved measurements ($\tau_0/\tau > 1$) indicate that there is also energy transfer from SAMSA-F to QSY-7 for the population of labelled $dexC_{16}$ not forming ground-state complexes (without influence on the fluorescence decay). The measurements were done few seconds after mixing and results

remained constant up to 30 min (data not shown) suggesting a rapid exchange of dexC_{16} between nanoparticles, upon mixing. The dilution of nanoparticles dispersion (concentration always kept above the CMC) does not change the quenching efficiency (Table 5.2). As FRET is a distance-dependent phenomenon, the nanoparticles dilution would result in a decrease of quenching efficiency if the energy transfer occurs between different particles (inter-nanoparticle) due to an increase of the average nanoparticles distance. So we conclude that this energy transfer takes place within the individual nanoparticle (intra-nanoparticle). Although we have not performed similar studies in water it is expected that a similar exchange occurs.

We then tried to see if SAMSA-F can report on the observed structural changes of nanoparticles with aging time, in line with the observed instability of curcumin in nanoparticles and with the observed growth of particle size. Figure 5.3 shows the SAMSA-F fluorescence decays for nanoparticles dispersed in distilled water or in PBS over time, up to 14 days. We can see that there is a systematic trend of faster decay of SAMSA-F with aging time in the case of nanoparticles in PBS but not in distilled water. This can be explained by assuming an alteration of the SAMSA-F environment with time from an initially more hydrophobic to a more hydrophilic pocket, as a nanoparticle enlargement would lead to a possibly increased exposure of SAMSA-F to water resulting in a decreased decay time.

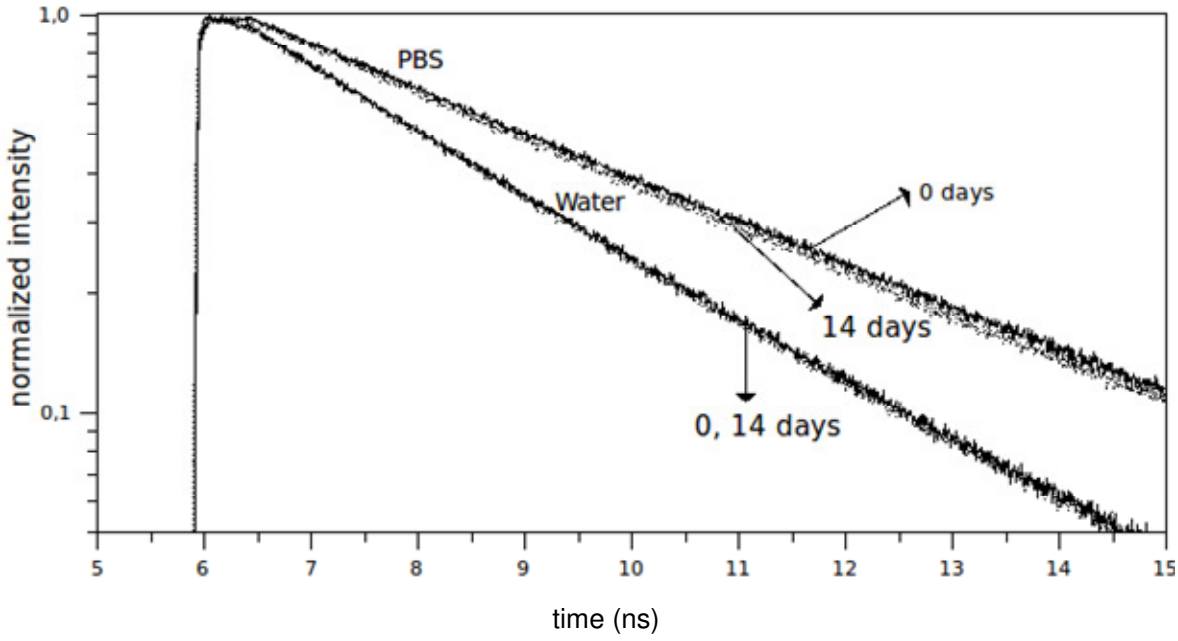

Figure 5.3. SAMSA fluorescence decays for nanoparticles dispersed in water or in PBS up to 14 days.

5.3.2 Curcumin release

To ascertain the suitability of dextrin nanoparticles as delivery systems for hydrophobic drugs such as curcumin, the *in vitro* release was studied. In the literature, different methods are reported to evaluate the release profiles using nanoparticles. Open (Shaikh*, et al.*, 2009) or closed systems (Das*, et al.*, 2009) have been described. In the former case (open system or sink conditions), dialysis membranes are often used. For closed systems, loaded-nanoparticles are incubated, enclosed in a flask, under agitation. In the present work, the release study of curcumin from nanoparticles was carried out using both approaches. At pre-defined time intervals, the soluble drug was quantified spectrophotometrically, after centrifugation. This method is based on the fact that unentrapped curcumin precipitates after centrifugation, only the entrapped curcumin being quantified.

The results obtained for closed systems show that curcumin remain stable within nanoparticles, up to 24 hours, confirming the high stability of the formulation in the conditions used. In our opinion, this method assesses curcumin stability instead of curcumin release. Using dialysis membrane method, a fast transfer of free curcumin across the dialysis bag provided evidence for the presence of sink condition under experimental conditions (inset Figure 5.4b). Using the sink method, a sustained release was observed for either release mediums. After 1 and 5 h of incubation, the fractions of curcumin released were respectively 51.7% and 26.1% using distilled water and 42.7% and 19.4% the PBS solution. The release profile without initial burst indicates the absence of curcumin adsorbed on the surface of nanoparticles (Mulik*, et al.*, 2009). The nanoparticles size distribution was evaluated at the end of dialysis process. The z-avg value remained constant during the dialysis process against water (74.7 nm) and slightly increased when using PBS solution (103 nm).

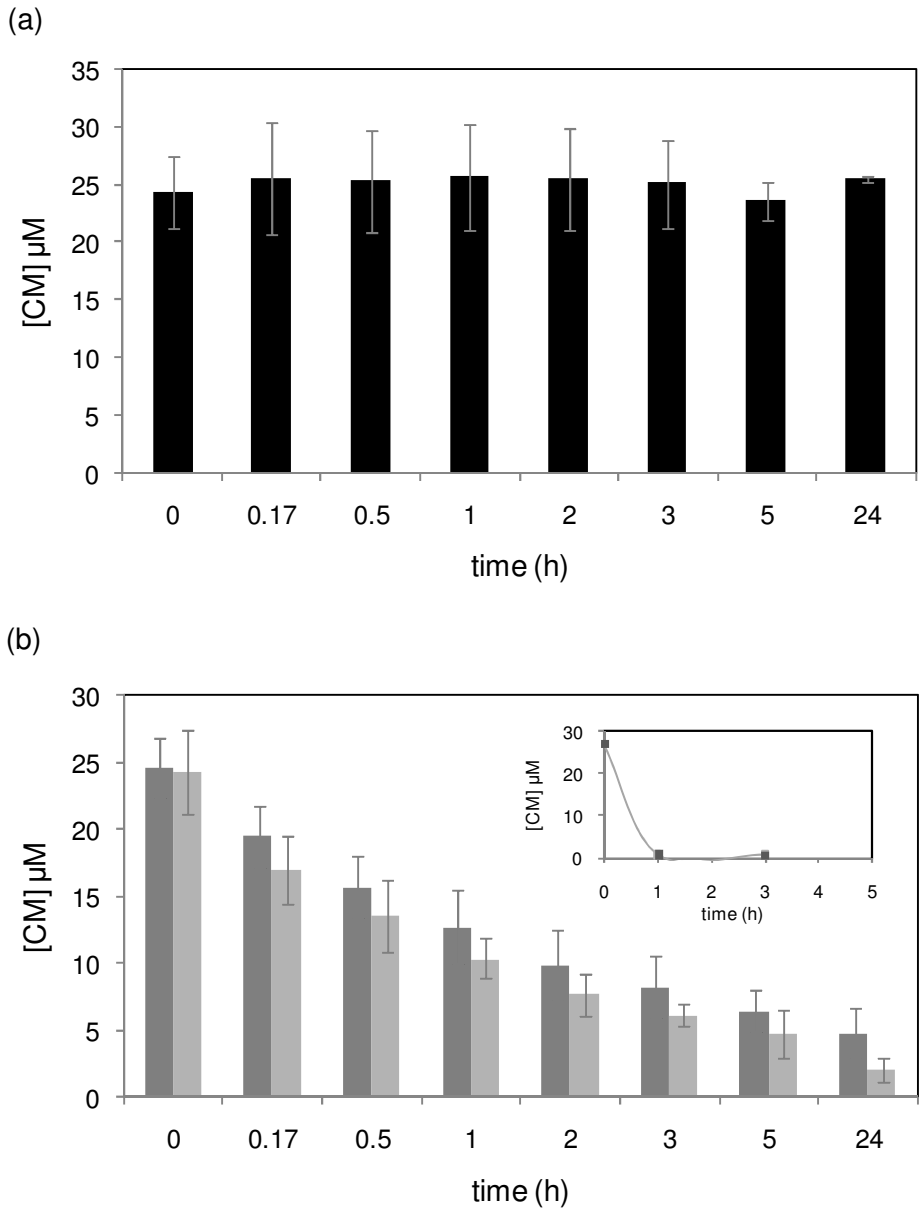

Figure 5.4. *In vitro* curcumin release from dextrin nanoparticles (1.0 mg/mL) using (a) closed system or (b) dialysis membrane. For dialysis membrane method, distilled water (■) or PBS solution (■) were used as release medium; free curcumin in ethanol was tested (inset).

It is well-known that drug release is affected by particle size. Smaller particles have a larger surface-to-volume ratio; therefore, most of the drug associated with small particles would be at or near the particle surface, leading to faster drug release. In contrast, larger particles have large cores, which allow more drug encapsulation per particle, providing a slower release. Thus, control of particle size provides a means of tuning the drug release

rates. In the current case, the fairly low size of the nanoparticles may explain the complete release of curcumin in a 24 h timeframe.

5.3.3 Cytotoxicity assay

An evaluation of the cytotoxicity of nanoparticles was carried out in a previous study, using murine bone marrow-derived macrophages: no significant toxicity was found for up to concentrations of 1.0 mg/mL (Gonçalves*, et al.*, 2010). In this work, the cytotoxicity of the nanoparticles and its formulations with curcumin were evaluated with the HeLa cell line. Previous studies on cytotoxicity of HeLa cells showed that the IC_{50} of free curcumin and complexed curcumin was 14.85 and 12.69 μM, respectively; otherwise, complexed curcumin showed a cytotoxic effect that was comparable to that of free curcumin (Sahu*, et al.*, 2008).

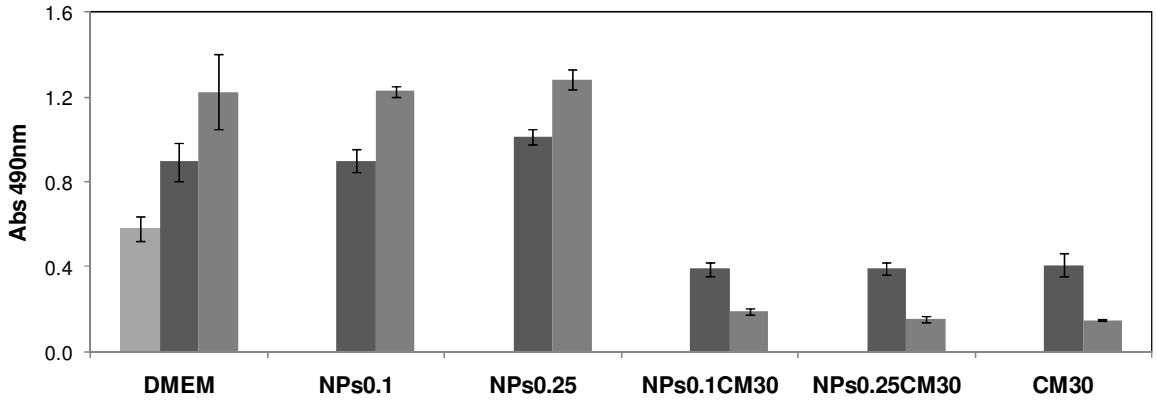

Figure 5.5. Cell viability of HeLa cells after (■) 0h, (■) 24h or (■) 48h of incubation with different concentrations of nanoparticles, nanoparticles-loaded curcumin or free curcumin. Empty nanoparticles were used to test the cytotoxicity of the nanocarrier.

In this study, as a positive control, HeLa cells were kept in the culture medium (DMEM) without any treatment. Nanoparticles concentration tested do not induce cell death up to 48 h, indeed the number of viable cells in contact with nanoparticles is similar to the control. The curcumin cytotoxicity (free or loaded on nanoparticles) was assessed. Nanoparticles (0.10 or 0.25 mg/mL) were loaded with curcumin (30 μM). When treated with curcumin, cells react to encapsulated curcumin (irrespective of the nanoparticles concentration) as effectively as free curcumin. The benefit of curcumin entrapment into

nanoparticles is to overcome the limited bioavailability after *in vivo* administration without any organic solvent use.

5.4 Conclusions

Dextrin nanoparticles served as an effective ‘‘nanocarrier’’ for the formulation of lipophilic curcumin by increasing its water solubility, improving its stability, and controlling its release profile. Incorporation of curcumin into nanoparticles did not compromise its cytotoxicity in HeLa cell line. Therefore, dextrin nanoparticles hold promise as delivery system for the development of an injectable formulation of curcumin for the treatment of human cancers. The small size of this system can be advantageous for passive targeting of tumor tissues by the EPR effect.

Acknowledgments. This research was supported by Fundação para a Ciência e a Tecnologia under Grant SFRH/BD/22242/2005.

5.5 References

Chan, M.M.; Huang, H.I.; Fenton, M.R.; Fong, D. In vivo inhibition of nitric oxide synthase gene expression by curcumin, a cancer preventive natural product with anti-inflammatory properties. *Biochemical Pharmacology* **1998**, *55*, 1955-1962.

Das, R.K.; Kasoju, N.; Bora, U. Encapsulation of curcumin in alginate-chitosan-pluronic composite nanoparticles for delivery to cancer cells. *Nanomedicine* **2009**.

Goel, A.; Kunnumakkara, A.B.; Aggarwal, B.B. Curcumin as "Curecumin": from kitchen to clinic. *Biochemical Pharmacology* **2008**, *75*, 787-809.

Gonçalves, C.; Gama, F.M. Characterization of the self-assembly process of hydrophobically modified dextrin. *European Polymer Journal* **2008**, *44*, 3529-3534.

Gonçalves, C.; Martins, J.A.; Gama, F.M. Self-assembled nanoparticles of dextrin substituted with hexadecanethiol. *Biomacromolecules* **2007**, *8*, 392-398.

Gonçalves, C.; Torrado, E.; Martins, T.; Pereira, P.; Pedrosa, J.; Gama, M. Dextrin nanoparticles: studies on the interaction with murine macrophages and blood clearance. *Colloids and Surfaces B: Biointerfaces* **2010**, *75*, 483-489.

Huang, M.T.; Lysz, T.; Ferraro, T.; Abidi, T.F.; Laskin, J.D.; Conney, A.H. Inhibitory effects of curcumin on in vitro lipoxygenase and cyclooxygenase activities in mouse epidermis. *Cancer Research* **1991**, *51*, 813-819.

Kunwar, A.; Barik, A.; Pandey, R.; Priyadarsini, K.I. Transport of liposomal and albumin loaded curcumin to living cells: an absorption and fluorescence spectroscopic study. *Biochimica et Biophysica Acta* **2006**, *1760*, 1513-1520.

Lim, G.P.; Chu, T.; Yang, F.; Beech, W.; Frautschy, S.A.; Cole, G.M. The curry spice curcumin reduces oxidative damage and amyloid pathology in an Alzheimer transgenic mouse. The *Journal of Neuroscience* **2001**, *21*, 8370-8377.

Lopez-Lazaro, M. Anticancer and carcinogenic properties of curcumin: considerations for its clinical development as a cancer chemopreventive and chemotherapeutic agent. *Molecular Nutrition & Food Research* **2008**, *52 Suppl 1*, S103-127.

Mulik, R.; Mahadik, K.; Paradkar, A. Development of curcuminoids loaded poly(butyl) cyanoacrylate nanoparticles: Physicochemical characterization and stability study. *European Journal of Pharmaceutical Sciences* **2009**, *37*, 395-404.

Sahu, A.; Kasoju, N.; Bora, U. Fluorescence study of the curcumin-casein micelle complexation and its application as a drug nanocarrier to cancer cells. *Biomacromolecules* **2008**, *9*, 2905-2912.

Shaikh, J.; Ankola, D.D.; Beniwal, V.; Singh, D.; Kumar, M.N. Nanoparticle encapsulation improves oral bioavailability of curcumin by at least 9-fold when compared to curcumin administered with piperine as absorption enhancer. *European Journal of Pharmaceutical Sciences* **2009**, *37*, 223-230.

Shoba, G.; Joy, D.; Joseph, T.; Majeed, M.; Rajendran, R.; Srinivas, P.S. Influence of piperine on the pharmacokinetics of curcumin in animals and human volunteers. *Planta Medica* **1998**, *64*, 353-356.

Tourkina, E.; Gooz, P.; Oates, J.C.; Ludwicka-Bradley, A.; Silver, R.M.; Hoffman, S. Curcumin-induced apoptosis in scleroderma lung fibroblasts: role of protein kinase cepsilon. *American Journal of Respiratory Cell and Molecular Biology* **2004**, *31*, 28-35.

Valeur, B. *Molecular Fluorescence*; Wiley-VCH: Germany, 2002; *Chapter 4*.

6. Studies on the biodistribution of dextrin nanoparticles

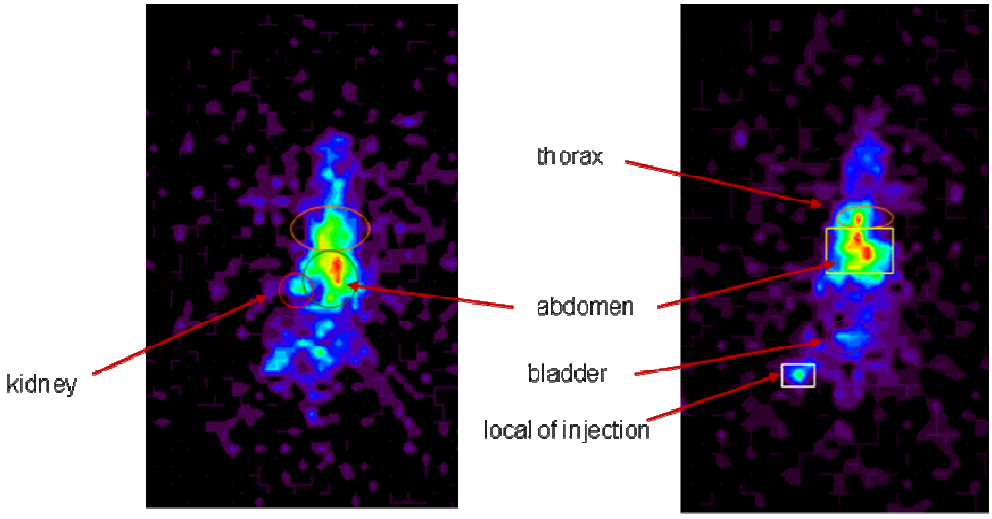

The characterization of biodistribution is a central requirement in the development of biomedical applications based on the use of nanoparticles, in particular for controlled drug delivery. The blood circulation time, organ biodistribution and rate of excretion must be well characterized in the process of product development. In this work, the biodistribution of recently developed self-assembled dextrin nanoparticles is addressed. Functionalization of the dextrin nanoparticles with a DOTA-monoamide-type metal chelator, via *click* chemistry, is described. The metal chelator-functionalized nanoparticles were labelled with the γ-emitting $^{153}Sm^{3+}$ radioisotope and the blood clearance rate and organ biodistribution of the nanoparticles were obtained. The effect of PEG surface coating on the blood clearance rate and organ biodistribution of the nanoparticles was also studied.

6.1 Introduction

Nanomedicine has emerged in recent years as an exciting area for chemists, materials scientists, engineers and medical doctors, converging in the development of new tools for diagnostics and therapeutics (Fernandez-Montesinos*, et al.*, 2009) (Leary*, et al.*, 2006) (Farokhzad*, et al.*, 2006). A rather large number of nanostructures have been developed over the past few decades. Well-defined polymeric nanostructures, on the same size-scale as proteins and cellular structures, are promising *vehicles* for diagnostics and drug-delivery (Weinstein*, et al.*, 2010). The capability to carry and release a therapeutic payload in a controlled way, coupled to imaging ability opens the way to theragnostics (Shubayev*, et al.*, 2009). A major limitation in the use of (polymeric) nanoparticles *in vivo* is their premature elimination from the circulatory system by the mononuclear phagocyte system (MPS), which prevents the nanoparticles from reaching their target (Owens*, et al.*, 2006). The disposal of particles through the MPS begins with the adsorption of serum proteins (opsonins) onto the surface of the nanoparticles, followed by macrophage recognition, phagocytosis, and subsequent sequestration in the liver, spleen, and/or bone marrow. To address these limitations, several methods have been developed to mask or camouflage nanoparticles from the MPS. Among these, the preferred one is the grafting of poly(ethylene glycol) (PEG) onto the surface of nanoparticles (Peracchia*, et al.*, 1999a). The purpose of the PEG chains is to block the adhesion of opsonins present in the blood serum, such that the particles remain invisible to phagocytic cells. Using transmission electron microscopy, it has been possible to visualise the protein rejecting capabilities of PEGylated surfaces (Peracchia*, et al.*, 1999b). PEG 5,000 has proved to be a threshold for maximum reduction of protein adsorption (Gref*, et al.*, 2000) and lower uptake in the liver (Pressly*, et al.*, 2007).

In recent years, the Michael addition of thiols to acrylates, acrylamides and vinylsulfones has acquired the status of a *click reaction*: it can be performed selectively under mild (aqueous) conditions. The major disadvantage of this reaction in comparison to the dipolar addition of azides to terminal alkynes is the possibility of thiol oxidation to disulfide and its inherent lack of bio-orthogonality, deriving from many endogenous thiols (Hiemstra*, et al.*, 2007, Van Dijk*, et al.*, 2009). Recently, our research group has reported the preparation of the acrylate ester functionalized dextrin: dexVA. The Michael addition of hexadecanethiol to dexVA generates an amphiphilic material, dexC_{16}, which self-assembles in water into well defined nanoparticles, stable macromolecular micelles (nanogel) (Gonçalves*, et al.*, 2007). Importantly, the dexC_{16} nanoparticles can be loaded

with a hydrophobic cargo, e.g., curcumin (anti-cancer drug), for drug delivery purposes (Bisht*, et al.*, 2007, Shaikh*, et al.*, 2009).

To evaluate the potential of the $dexC_{16}$ nanogel for drug delivery purposes, the nanogel was labelled, *via* Michael addition of a thiol-functionalized fluorescent probe to the acrylate groups, and its blood clearance was studied in BALB/c mice (Gonçalves*, et al.*, 2010). Although the blood clearance of the nanogel could be readily followed by fluorescence measurements, its organ distribution profile could not be evaluated, possibly due to quenching effects of the fluorescent probe in the organ´s homogenates. It is widely accepted that the physical and chemical properties of the nanoparticles, including particle size, surface charge, and surface hydrophilicity, are important parameters determining their biological fate after intravenous administration (Li*, et al.*, 2008). It is, therefore, crucial to devise a labelling methodology that conserves the native nanoparticle properties. To obtain the biodistribution profile of the nanoparticles in experimental animals, we envisaged labelling the nanogel with a radioactive label. With this goal, we have synthesized a new ω-thiol functionalized DOTA-monoamide type metal chelator (DOTA=1,4,7,10-tetraazacyclododecanetetraacetic acid) for covalent functionalization (via Michael addition) and labelling (complexation) of a suitable Ln^{3+} (e.g., $^{153}Sm^{3+}$) radioisotope. DOTA-like chelators are well known to form lanthanide (III) chelates of high thermodynamic and kinetic stability, which is of crucial importance for *in vivo* applications (Port*, et al.*, 2008).

In the present study, the biodistribution and blood clearance of dextrin nanoparticles labelled with $^{153}Sm^{3+}$-DOTA-type chelates has been studied in experimental animals after intravenous administration. The effect of surface decoration with PEG on the biodistribution was also evaluated.

6.2 Experimental section

6.2.1 Materials

Dextrin-VA (dexVA) and dextrin-VA-SC_{16} ($dexC_{16}$) were synthesized as comprehensively described before (Gonçalves*, et al.*, 2007). DexVA is the dextrin backbone with grafted acrylate ester groups (VA - vinyl acrylate). $DexC_{16}$ is composed by

the hydrophilic dextrin backbone with grafted VA groups, which are partially substituted with long alkyl hexadecanethioalkyl chains (SC_{16}). In this work, dexC_{16} with 13 acrylate groups (DS_{VA} 13%) and 6 hexadecanethioalkyl chains (DS_{C16} 6%) per 100 dextrin glucopyranoside residues was used.

O-[2-(3-Mercaptopropionylamino)ethyl]-*O'*-methylpolyethylene glycol 5,000 (PEG-SH), europium (III) chloride hexahydrate 99.99%, samarium (III) chloride hexahydrate 99% ($SmCl_3$), dimethyl sulfoxide (DMSO), triethylamine (TEA) and deuterium oxide (D_2O) were purchased from Aldrich. Regenerated cellulose tubular membranes, with 3500 MWCO, were obtained from Membrane Filtration Products.

$^{153}SmCl_3$ was produced at the Instituto Tecnológico e Nuclear, Lisbon, Portugal with a specific radioactivity of > 5 GBq/mg. For this purpose, $^{153}Sm_2O_3$ was prepared from a 98% ^{152}Sm enriched Sm_2O_3 target, sealed into a quartz vial and welded into an aluminum can, by neutron irradiation using a thermal flux of $2.3X10^{13}$ n/cm^2.s. After irradiation, the sample was opened, dissolved in 1 M HCl, and the final $^{153}SmCl_3$ solution was brought to a stock concentration of $1.9\ X10^{-3}$ M.

6.2.2 Synthesis of ω-thiol functionalized metal chelator

Synthesis of tris-tert-butyl 2,2',2''-(10-(2-((2-(4-mercaptobutanamido)ethyl)amino)-2-oxoethyl)-1,4,7,10-tetraazacyclododecane-1,4,7-triyl)triacetate **(3)** (Scheme 6.1): to a solution of compound **2** (430 mg, 0.70 mmol) in methanol (30 cm^3) was added triethylamine (0.17 cm^3, 1.2 mmol) and γ-butyrothiolactone (0.61 g, 6.0 mmol). The reaction mixture was stirred at 50 ºC under nitrogen atmosphere for 6 hours and left stirring at room temperature overnight. The reaction mixture was concentrated under reduced pressure and the residue was purified by a flash chromatography (100% CH_2Cl_2 → CH_2Cl_2/EtOH (70:30)) to afford the title compound **(3)** as a colorless oil (0.162 g, 32%). ^{1}H NMR (300 MHz, D_2O): δ = 1.46 (s, 27H, tert-Bu), 1.97 (m, 2H, C(O)CH_2*CH_2*CH_2SH), 2.49 (m, 2H, C(O)C*H_2*CH_2CH_2SH), 2.57 (m, 2H, C(O)CH_2*C*H_2C*H_2*SH), 2.20-3.80 (broad, overlapped signals with a integration corresponding to approximately 28 H, N(*CH_2*)$_2$N, NC*H_2*C(O) and C(O)NHC*H_2*C*H_2*NHC(O)), 8.2 and 8.6 (broad signals, C(O)*NH*C*H_2*C*H_2**NH*C(O)).

Synthesis of 2,2',2''-(10-(2-((2-(4-mercaptobutanamido)ethyl)amino)-2-oxoethyl)-1,4,7,10-tetraazacyclododecane-1,4,7-triyl)triacetic acid **(4)**: compound **(3)** (162 mg, 226 μmol) was dissolved in a mixture ethanol/aqueous HCl 6 M (1/1 v/v; 20 cm^3) and left to

stirring overnight at room temperature. The solution was concentrated under reduced pressure and further dried under vacuum to afford the title compound **(4)**, in the hydrochloride form, as a white vitreous solid (121 mg). ^{1}H NMR (300 MHz, D_2O): δ = 1.88 (m, 2H, *J* = 7.5 Hz, C(O)CH_2CH_2C$H_2$$CH_2$SH), 2.38 (t, 2H, *J* = 7.5 Hz, C(O)C$H_2$$CH_2CH_2$SH), 2.54 (t, *J* = 6.9 Hz, 2H, C(O)CH_2CH_2CH_2SH), 3.00-3.70 (broad, overlapped signals with a integration corresponding to approximately 28 H, N(CH_2)$_2$N, NCH_2C(O) and C(O)NHCH_2CH_2NHC(O)). ^{13}C NMR (75.4 MHz, D_2O): 24.82 (C(O) CH_2C$H_2$$CH_2$SH), 34.34 (C(O) C$H_2$$CH_2CH_2$SH), 37.12 (C(O) CH_2CH_2CH_2SH), 38.61 (CH_2), 38.83 (CH_2), 39.88 (CH_2), 41.74 (CH_2), 48.21 (CH_2), 48.84 (CH_2), 50.54 (CH_2), 51.30 (CH_2), 51.57 (CH_2), 53.49 (CH_2), 55.71 (CH_2), 55.83 (CH_2), 56.50 (CH_2), 170.66 (C(O)OH), 173.25 (C(O)OH), 174.92 (C(O)NH), 176.42 (C(O)NH). MS (ESI-LR): m/z (%): 577.5 (18), 571.5 (66.5) $[M+Na]^+$, 549.5 (100) $[M+Na]^+$, 447.5 (5).

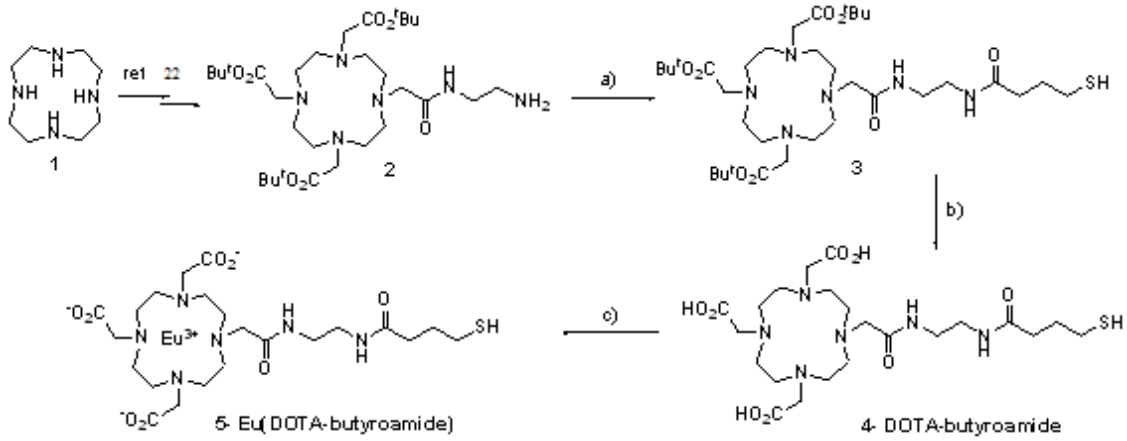

Scheme 6.1.Synthesis of the ω-thiol functionalized metal chelator DOTA-butyroamide (4) and its Eu^{3+} complex (5): a) γ-butyrothiolactone/TEA/MeOH; b) HCl/EtOH; c) $EuCl_3.6H_2O$

6.2.3 Preparation of DOTAdexC$_{16}$ or DOTAdexC$_{16}$PEG materials

In the first step dexVA was reacted with the ω-thiol-functionalized metal chelator **(4)** to afford the metal chelator-grafted material. In the second step, hexadecanethiol was added to the former material to afford the DOTAdexC$_{16}$ material **(9)**. Finally, a thiol-functionalized PEG molecule was added to produce the DOTAdexC$_{16}$PEG material **(11)**.

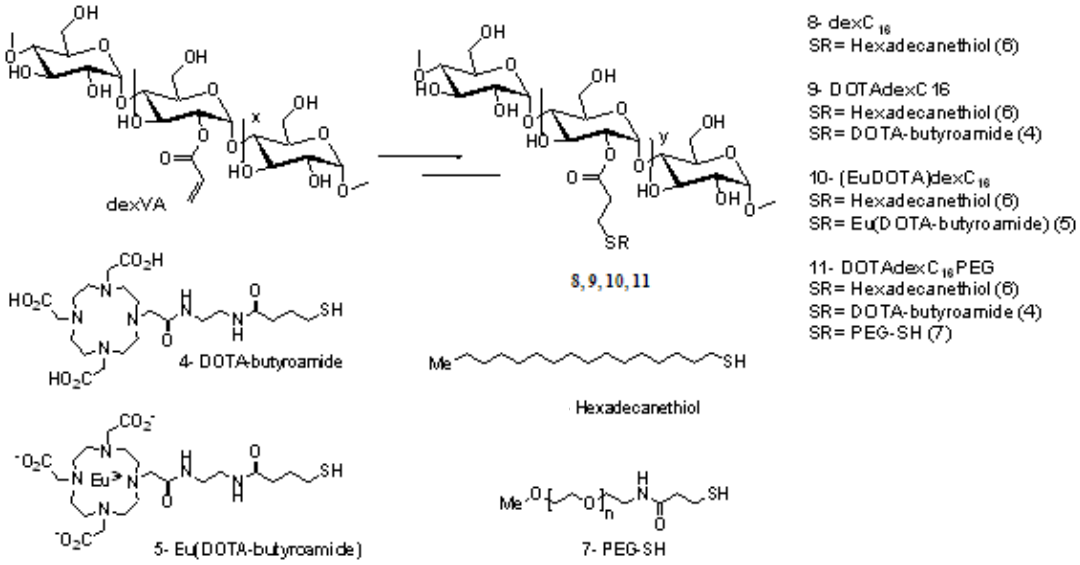

Scheme 6.2. Synthesis of the DOTAdexC$_{16}$ and DOTAdexC$_{16}$PEG and its Eu^{3+} complexes.

DexVA is the dextrin backbone with grafted acrylate ester groups (Scheme 6.2). For the sake of simplicity, the grafted acrylate groups are represented at position 2 of the glucopyranoside ring (major regioisomer), although grafting in position 3 (minor regioisomer) can be detected by ^{1}H NMR, as reported before (Carvalho*, et al.*, 2007). DexC$_{16}$ is composed by the hydrophilic dextrin backbone with grafted VA groups, which are partially substituted with hexadecanethiol chains (SR = hexadecanethiol). In this work, dexC$_{16}$ **(8)** with 13 acrylate groups (DS$_{VA}$ 13%) and 6 hexadecanethiol chains (DS$_{C16}$ 6%) per 100 dextrin glucopyranoside residues was used. For the sake of clarity the unreacted VA ester groups are not shown on the materials (only substituted VA ester groups are represented). DexVA (50 mg, DS$_{VA}$ 13%, 38.45 µmol equivalent VA) was dissolved in DMSO (0.931 cm^3). To this solution was added a solution of compound **4** (11 mg, 19.23 µmol, 50% mol to VA groups) and triethylamine (16 µL, 0.115 mmol, 3 molar equivalents to VA groups). The medium was stirred for 24 h, at 50 ºC. In the second step the addition of hexadecanethiol **(6)** was performed as previously reported (Gonçalves*, et al.*, 2007). Briefly, hexadecanethiol (7.95 mg, 30.76 µmol, 80 % relatively to VA groups) and triethylamine (11 µL, 38.45 µmol, 1 mol equivalent to VA groups) were added to the reaction mixture. The medium was stirred for 24 h, at 50 ºC. The mixture was dialysed for 48 h against water, with frequent water changes. After freezedrying, material **(9)** was obtained as a white *candyfloss-like* material and stored at room temperature.

DOTAdexC_{16}PEG **(11)** was obtained by dissolving DOTAdexC_{16} **(9)** (15 mg, 12.2 μmol equivalent VA), PEG-SH **(7)** (18 mg, 3.66 μmol, 30% mol to VA groups) and triethylamine (3.4 μL, 24.4 μmol, 2 mol equivalent to VA groups) in DMSO (0.295 cm^3). The mixture was stirred for 24 h, at 50 ºC and then dialysed for 48 h against water, with frequent water changes. After freezedrying, the product was obtained as a white *candyfloss-like* material and stored at room temperature.

6.2.4 Complexation of Eu^{3+} with ω-thiol functionalized chelator and DOTAdexC_{16} materials

In order to ascertain the success of DOTA coupling to dexC_{16} and its chelating capacity, DOTAdexC_{16} **(9)** was complexed with Eu^{3+} as a model metal ion. The [Eu(DOTAdexC_{16})] **(10)** complex was prepared by mixing a solution of $EuCl_3.6H_2O$ with a solution of DOTAdexC_{16} in D_2O. A slight excess (5%) of Eu^{3+} was used in relation to the amount of metal chelator used in the synthesis of the DOTAdexC_{16} material. The reaction mixture was adjusted to pH 5.5 by adding aqueous NaOD (0.1 mM) and was allowed to react for 24 h at 50 ºC. The reaction mixture was adjusted to pH 7.0, filtered through a 0.2 μm filter and characterized by ^{1}H NMR, DLS and zeta potential measurements.

The number of DOTA groups attached to the polymer backbone was estimated by back titration of excess (uncomplexed) Eu^{3+} metal with EDTA in the presence of the complexometric indicator, xylenol orange (Brunisholz*, et al.*, 1959). The amount of chelator agent grafted to the dexC_{16} material was estimated 0.152 μmol of DOTA chelator units/mg DOTAdexC_{16} material.

6.2.5 Preparation of [^{153}Sm(DOTAdexC_{16})] and [^{153}Sm(DOTAdexC_{16}PEG)] chelates for biodistribution studies

To a dispersion of DOTAdexC_{16} or DOTAdexC_{16}PEG (5 mg) in sodium acetate buffer (400 μL, 0.4 M, pH 5) $^{153}SmCl_3$ (1 mCi) was added. Each solution was stirred at 80 ºC for 5 h. After that, cold $SmCl_3$ was added to each solution in order to obtain an equimolar Sm^{3+}:DOTA ratio. The final solution was heated at 80 ºC for 2 h and stayed overnight at room temperature. The radiolabelled nanoparticles were purified using a Sephadex G-25 column eluted with 0.4 M acetate buffer. The nanoparticle dispersions were concentrated by centrifugal filtration (centricons, MWCO 10 kDa) to afford the pure radioligands. The complexation yield is ca 50 % in both cases.

6.2.6 Size distribution and zeta potential

The size distribution and zeta potential of nanoparticles were determined with a Malvern Zetasizer, NANO ZS (Malvern Instruments Limited, UK), using a Helium-Neon laser (wavelength of 633 nm) and a detector angle of 173º. Nanoparticles dispersion (1 mL) was analysed at 25 ºC and 1.0 mg/mL. The DLS analysis provides the characterization of a sample through the mean value (z-avg) for the size and a width parameter known as the polydispersity or polydispersity Index (PdI). The z-avg is the mean hydrodynamic diameter, determined from the intensity of scattered light, which can be converted to other distributions. In the present work, the z-avg is considered the best approach to the actual nanoparticles size. Nanoparticles dispersion was analysed in a polystyrene cell or in a folded capillary cell, for size distribution or zeta potential measurements, respectively. The zeta potential values were calculated using the Smoluchowski equation (Hunter, 1981). Repeated measurements were performed for each analysis (3 times) and the values reported are average values.

6.2.7 ^{1}H NMR

Nanoparticles were dispersed in deuterium oxide (10.0 mg/mL). Dispersions were transferred to 5 mm NMR tubes. 1D ^{1}H NMR measurements were performed with a VARIAN UNITY Plus 300 spectrometer operating at 299.94 MHz. 1D ^{1}H NMR spectra were measured at 298 K with 80 scans, a spectral width of 4800 Hz, a relaxation delay of 1 s between scans and an acquisition time of 3.75 s.

6.2.8 Blood clearance and biodistribution studies

The biodistribution of dextrin nanoparticles labelled with $^{153}Sm^{3+}$ was evaluated following intravenous administration in Wistar rats. Groups of four animals were anesthetized and injected in the femoral vein with ca 100 µl (20-100 µCi) of the nanoparticles mixture. After pre-defined periods of time, the rats were sacrificed and their tissues (liver, spleen, lungs, bone (femur of left hind leg), intestines (small and large), kidney, heart and brain were excised, weighed and tissue radioactivity measured in a γ well-counter. Blood samples were obtained at appropriate periods of time, weighted and radioactivity counted. The same procedure was used to evaluate the influence of the presence of PEG chains in the nanoparticles biodistribution: a group of four animals was injected in the femoral vein with the radiolabelled DOTAdexC_{16}PEG and sacrificed 2 h

later for organs collection. The national regulations for the care and use of laboratory animals have been observed in this study.

6.3 Results and discussion

6.3.1 Synthesis of ω-thiol functionalized metal chelator

We have previously described the synthesis of the bifunctional metal prochelator **(2)** bearing a functional amine group ready for conjugation to (bio)molecules (André*, et al.*, 2004). In this work, we have used γ-butyrothiolactone as a protected activated ω-thiol carboxylic acid equivalent (Scheme 6.1). This procedure allows performing the amide coupling without coupling reagents, avoiding potential purification problems related to the removal of the urea biproducts and auxiliary nucleophiles. Acidic deprotection of the ω-thiol functionalized prochelator **(3)** afforded the chelator **(4)**, in the hydrochloride form, in an aggregate 31% yield over two steps. DOTA-monoamide type metal chelators and its conjugates form Ln^{3+} complexes of high thermodynamic and kinetic stability, as required for *in vivo* studies, given the toxic effects of free (unchelated) Ln^{3+} ions.

6.3.2 Preparation of DOTAdexC_{16} or DOTAdexC_{16}PEG materials

With the ω-thiol functionalized DOTA *synthon* **(4)** on hand, one can envisage two pathways for the synthesis of the DOTAdexC_{16} material: either, performing first the Michael addition of the ω-thiol functionalized metal chelator to the acrylate-functionalized dextrin (dexVA), followed by the Michael addition of hexadecanethiol, or by reversing the addition order. We have noted before, during the synthesis of the dexC_{16} material, that even using a large molar excess of hexadecanethiol in relation to the acrylate groups does not give a full acrylate addition. Some acrylate groups are much less reactive, reflecting possibly their grafting position on the glucopyranoside ring and/or some degree of steric hindrance. By grafting first the metal chelator to the acrylate-functionalized dextrin allows using a large excess of hexadecanethiol (cheap, commercially available reagent) in the second step in order to push the degree of substitution towards the optimal value. We have established previously that the dexC_{16} material with DS_{VA} 13% and DS_{C16} 6% is suitable for forming stable nanoparticles within a narrow size range. In the ^{1}H NMR spectrum of the dexC_{16} material (Figure 6.1a) signals assigned to the

hexadecane moiety (δ = 0.75–1.75 ppm) are clearly visible. The ^{1}H NMR spectrum of the DOTAdexC$_{16}$ material (Figure 6.1c) displays a set of new broad low intensity signals assigned to the grafted DOTA-butyroamide chelator (e.g., δ =1.9, 2.4 and 2.7 ppm, assigned to the methylene groups of the terminal mercaptobutyl moiety) as can be inferred from the ^{1}H NMR spectrum of the DOTA chelator **(4)** (Figure 6.1b). Importantly, signals assigned to unreacted acrylate groups on the dextrin backbone (δ = 6.0–6.6 ppm) can also be seen in Figure 6.1a and 6.1c. The unreacted acrylate groups allow further functionalization of the nanogel with thiol-functionalized PEG molecule (Figure 6.1d). PEG grafting was confirmed by disappearance of the signals assigned to unreacted acrylate ester groups and the appearance of a new intense signal (δ = 3.6 ppm) assigned to the methylene groups of the grafted PEG molecule. The ^{1}H NMR spectrum of the DOTAdexC$_{16}$PEG material (Figure 6.1d) displays new signals assigned to the PEG moiety (δ = 3.4 and 3.6 ppm) confirming the PEGylation of the nanoparticles.

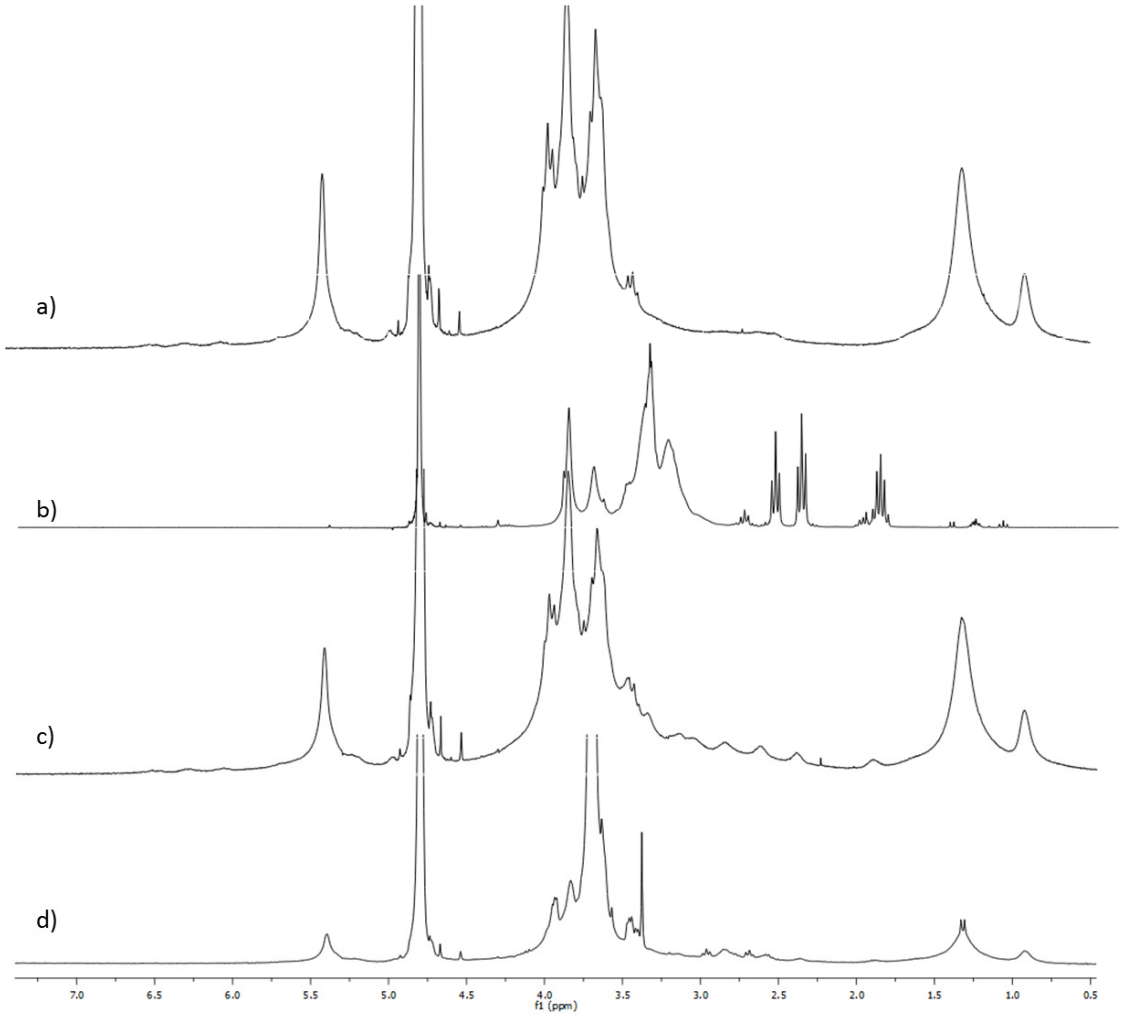

Figure 6.1. ^{1}H NMR spectra of (a) dexC$_{16}$, (b) DOTA-butyroamide, (c) DOTAdexC$_{16}$ and (d) DOTAdexC$_{16}$PEG.

6.3.3 Characterization of the nanoparticles

The DOTA coupling to the dextrin nanoparticles was used as a tool to obtain a Ln^{3+} chelate which could be used as (radioactive) label for biodistribution studies. The high detection sensitivity of γ-emitting radioisotopes, e.g., $^{153}Sm^{3+}$, ensures that a low degree of substitution on metal chelate allows sensitive detection, as required for biodistribution studies. Moreover, the formation of neutral Ln^{3+}-DOTA-monoamide complexes ensures that the labelling procedure does not substantially changes the structure and/or the overall (neutral) charge of the original (unlabelled) nanoparticles, and therefore is not expected to interfere in the biodistribution studies.

The size distribution and the zeta potential of the nanoparticles from different materials were determined by dynamic light scattering measurements (Table 6.1).

Table 6.1. DLS analysis of the nanoparticles from different materials in aqueous dispersion (1.0 mg/mL), pH 7.0.

Material	z-avg (nm)	PdI	Zeta Potential (mV)
$dexC_{16}$	23.9	0.388	-4.02
$dexC_{16}PEG$	32.4	0.442	-8.59
$DOTAdexC_{16}$	25.3	0.341	-17.8
$[Eu(DOTAdexC_{16})]$	--	--	-1.35
$DOTAdexC_{16}PEG$	37.1	0.275	--

As can be seen from Table 6.1, the functionalization of the nanoparticles with the DOTA metal chelator does not have a substantial effect on the mean diameter of the nanoparticles. For $dexC_{16}$ the nanoparticles size increased from 23.9 nm to 25.3 nm, after coupling of the metal chelator. For $dexC_{16}PEG$ a similar increase was observed, from 32.4 nm to 37.1 nm. In contrast, the PEG functionalization increases substantially the hydrodynamic diameter of the nanoparticles. Figure 6.2 shows the size distribution obtained by DLS for the nanoparticles from the $dexC_{16}$ and $dexC_{16}PEG$ materials. PEG decoration does not change the nanoparticle population distribution, only a shift to larger sizes is observed, suggesting that PEGylation does not change the nanoparticles structure. This is consistent with the formation of an exterior hydrophilic PEG corona

projecting into the aqueous media. The observed increase in nanoparticle´s size is similar to that observed for other types of nanoparticles (e.g. gold nanoparticles) following grafting with PEG 5,000 (Zhang*, et al.*, 2009).

The surface functionalization of the dexC_{16} nanoparticles with PEG is expected to affect its interaction with proteins and cells, and thus its fate *in vivo*. The PEG hydrophilic corona may avoid the recognition and uptake of the nanoparticles by the organs of the MPS increasing the blood circulation half-live, as reported by other authors working on different nanoparticulate materials (Shan*, et al.*, 2009).

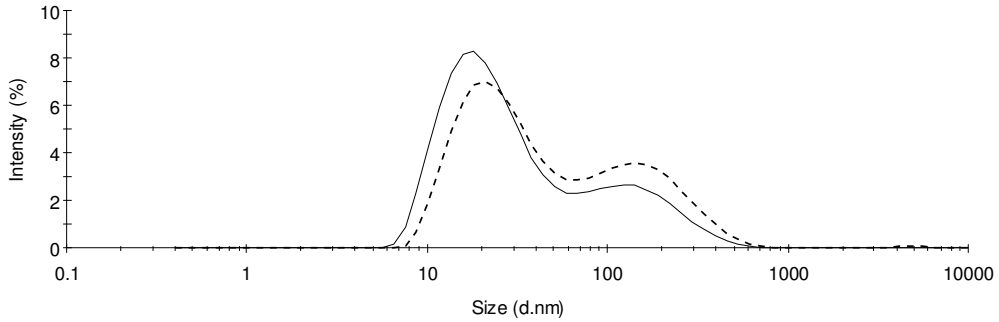

Figure 6.2. Size distribution in intensity (%) of (–) dexC_{16} or (---) dexC_{16}PEG in aqueous dispersion (1.0 mg/mL).

Zeta potential measurements were carried out to evaluate the nanoparticles surface charge. The change of the zeta potential of the dexC_{16} nanoparticles, from a near neutral value (-4.02 mV) to a negative value (-17.8 mV) at pH 7.0, following functionalization with the metal chelator, confirms the grafting of the metal chelator. The grafted DOTA-monoamide macrocycle is expected to bear an overall negative charge at pH 7.0. Moreover, after complexation of the DOTAdexC_{16} nanoparticles with Eu^{3+}, the zeta potential value returns to a near neutral value, similar to that of the original dexC_{16} nanoparticles (Gonçalves*, et al.*, 2008), consistent with the formation of neutral [Eu(DOTAdexC_{16})] complexes.

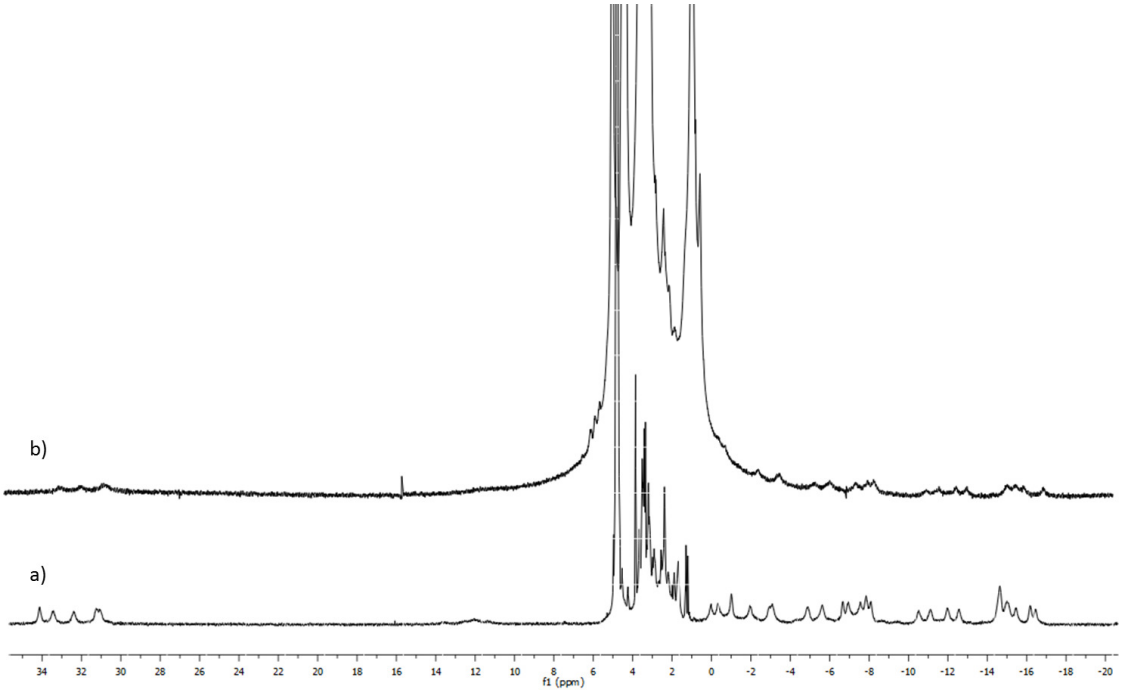

Figure 6.3. ^{1}H NMR spectra of (a) Eu(DOTA) and (b) [Eu(DOTAdexC$_{16}$)].

The ^{1}H NMR spectrum of the [Eu(DOTAdexC$_{16}$)] material (Figure 6.3b) confirms that the Eu^{3+} complexation effectively occurred. In the NMR spectra of the Eu(DOTA-butyroamide) chelate **(5)** and [Eu(DOTAdexC$_{16}$)] material (Figure 6.3) the CH_2 ressonances within the macrocycle and pendant acetate display strong paramagnetic shifts as reported before for glycoconjugates of Eu(DOTA-monoamide) chelates (André*, et al.*, 2004). The amount of metal chelator grafted to the dexC$_{16}$ material was estimated by back titration of excess Eu^{3+} with EDTA in the presence of the complexometric indicator xylenol orange: circa 0.152 µmol of DOTA-butyroamide per mg of DOTAdexC$_{16}$ material. The Eu^{3+} complexation was used as model system for the labelling of the nanoparticles with the radioisotope $^{153}Sm^{3+}$ for biodistribution studies. These studies confirm that nanoparticles features (size and surface potential) are conserved after labelling. Consequently, the biodistribution of the labelled nanoparticles is expected to be representative of the original (unlabelled) nanoparticles

6.3.4 Blood clearance and biodistribution studies

We have attempted previously to perform biodistribution studies of the dexC$_{16}$ nanoparticles, using fluorescein-labelled dextrin nanoparticles (Gonçalves*, et al.*, 2010). Although succeeding in evaluating the nanoparticles blood clearance, we failed in the

attempts to characterize the organ accumulation. In the present work, labelling the nanoparticles with $^{153}Sm^{3+}$ effectively allowed to study the nanoparticles blood clearance and to obtain the biodistribution profile *in vivo*.

The blood clearance profile of $^{153}Sm^{3+}$-labelled nanoparticles in Wistar rats, after intravenous injection, is shown in figure 6.4. The clearance of the nanoparticles from the systemic circulation is relatively fast in the first hour, proceeding afterwards at a lower rate. In the first 15 min, about 23% of the nanoparticles were removed from the bloodstream. At 1 h after injection, 47% of the injected dose is still detected in the bloodstream, followed by a further reduction 2 h later to about 30%. The blood clearance profile obtained is very similar to the one previously reported, using fluorescein-labelled dextrin nanoparticles (Gonçalves*, et al.*, 2010).

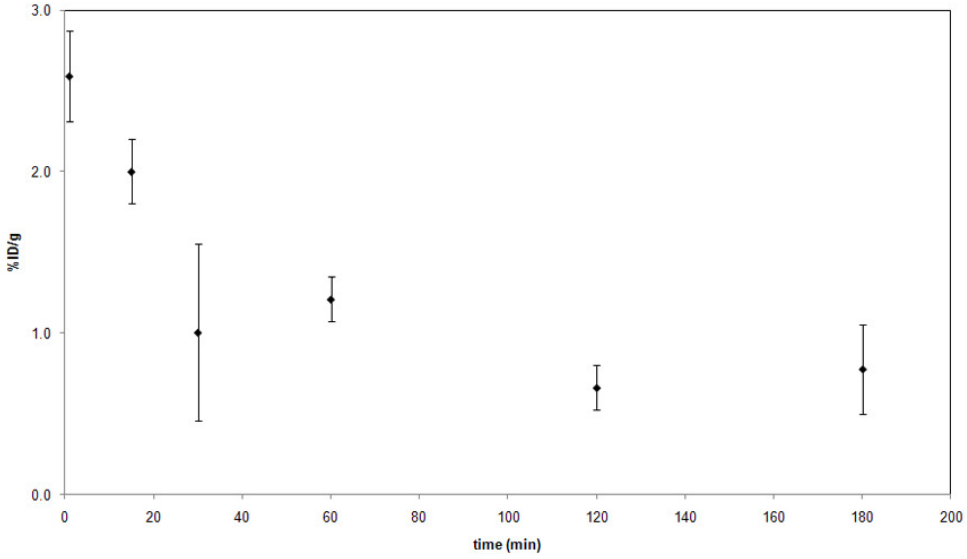

Figure 6.4. Blood clearance profile of radio-labelled nanoparticles. The error bars correspond to the standard deviation (N=4).

The organ biodistribution of the [^{153}Sm(DOTAdexC$_{16}$)] in Wistar rats was evaluated at different time points. Figure 6.5 shows representative data stated as percentage of the injected dose per gram of tissue (%ID/g).

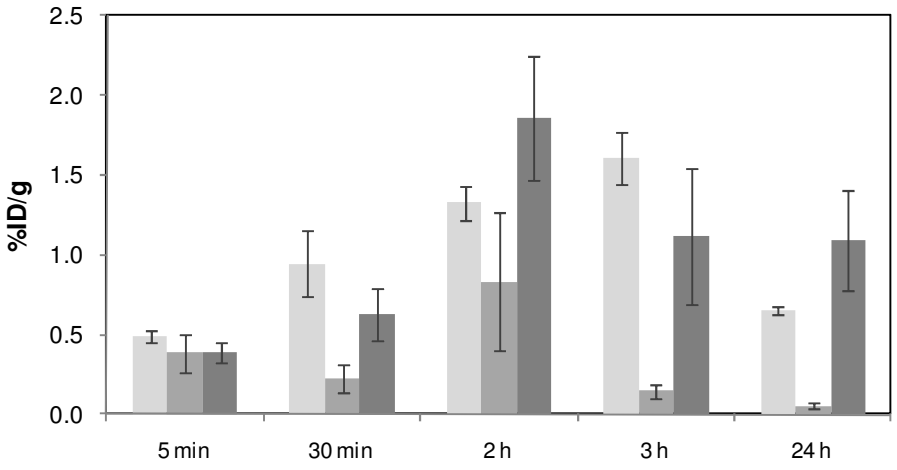

Figure 6.5. Biodistribution in (▫) liver, (▪) kidney and (■) spleen of Wistar rats 5 min, 30 min, 2 h, 3 h, 24 h after i.v. injection of [153Sm(DOTAdexC16)] stated as percentage of injected dose per gram of organ (%ID/g). Results are the mean of four animals.

The radioactivity was located mainly in the liver, spleen and kidneys (Figure 6.5), with low %ID/g found in the other organs (data not shown), in the time frame analysed in the experiment. These results suggest that the removal of nanoparticles occur by phagocytosis, since liver and spleen are macrophage-rich organs, consistently with the previous observation of *in vitro* internalization of nanoparticles by macrophages (Gonçalves*, et al.*, 2010). The maximum activity detected in the liver and spleen gradually increases from the first data obtained (5 minutes), reaching its maximum 2 h after injection, paralleling the decreasing profile of the blood activity (see above). The reduction of activity observed after 2 h suggests that the material does not accumulate in the organs, presumably being metabolized and excreted. As can be seen in Figure 6.5 there is some renal uptake of nanoparticles, and excretion in the urine was detected (data not shown), thus reinforcing the hypothesis of kidney filtration of the smallest nanoparticles. Zhang, *et al.*, reported that 20 nm pegylated gold nanoparticles are also excreted through renal filtration (Zhang*, et al.*, 2009). They assumed that the samples of gold nanoparticles contained a small fraction of nanoparticles with diameters < 5 nm, which could be excreted via the urinary system. In the current case, small dextrin nanoparticles are also likely to be present in the fairly polydisperse materials. Furthermore, it may be hypothesized that the self-assembled material is flexible enough to cross the renal filtration system, which would be expected to exclude rigid nanoparticles of the same size range. It must be remarked that only few studies are

available reporting the biodistribution of self-assembled polymeric nanoparticles; furthermore, the existing studies do not include nanoparticles in the size range used in this study.

To avoid a rapid blood clearance, the nanoparticles should retard opsonization and macrophage recognition, which results in sequestration by the MPS organs. The decoration with PEG was tested in this work with the purpose of improving the circulation time. Figure 6.6 compares the 2 h organ distribution of labelled nanoparticles, coated or not with PEG.

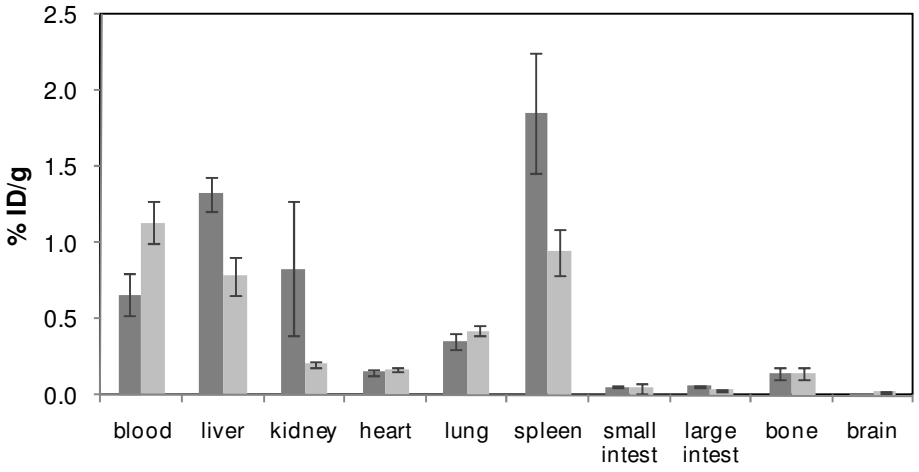

Figure 6.6. Comparison of the biodistribution in Wistar rats 2 h after i.v. injection of (■) [^{153}Sm(DOTAdexC$_{16}$)] or (■) [^{153}Sm(DOTAdexC$_{16}$PEG)]. Results are the mean of four animals.

The results obtained confirm the well documented stealth effect: PEG reduces opsonisation, presumably by steric and hydration effects, improving blood circulation time and reducing the accumulation in the liver and spleen (Shan*, et al.*, 2009).

The decoration with PEG increases significantly the hydrodynamic diameter of the nanoparticles. Although larger particles have been reported as being taken up faster by the MPS (Gaumet*, et al.*, 2008), the increased size is, in the current case, effectively counterbalanced by the the PEG steric and hydration effects, overall resulting in reduction of the uptake rate. In general, pegylated nanoparticles were found to have longer circulation time than the non-pegylated ones.

6.4 Conclusions

Functionalization of dextrin nanoparticles with a metal chelator allows the radioactive labelling of the nanoparticles. The labelling process has no significant effect on the nanoparticles size and surface charge; hence the biodistribution profile obtained in Wistar rats following intravenous administration is considered representative of the unmodified nanoparticles. This strategy is appropriate for *in vivo* studies, combining a high sensitive detection technique with minor nanoparticle modifications. The dexC_{16} nanoparticles display a characteristic biodistribution profile, being mainly taken up by the organs of the MPS- liver and spleen. The blood circulation time extends to several hours, although the concentration is halved in about 1 hour. The functionalization of the nanoparticles with PEG 5,000 in this formulation improves their circulation time in the bloodstream and reduces the accumulation in the liver and spleen.

Acknowledgments. The authors wish to acknowledge funding through the FCT/POCTI program (project PTDC/QUI/70063/2006).

6.5 References

André, J.P.; Geraldes, C.F.G.C.; Martins, J.A.; Merbach, A.E.; Prata, M.I.M.; Santos, A.C.; de Lima, J.J.P.; Toth, E. Lanthanide(III) complexes of DOTA-glycoconjugates: A potential new class of lectin-mediated medical imaging agents. *Chemistry- A European Journal* **2004**, *10*, 5804-5816.

Bisht, S.; Feldmann, G.; Soni, S.; Ravi, R.; Karikar, C.; Maitra, A. Polymeric nanoparticle-encapsulated curcumin ("nanocurcumin"): a novel strategy for human cancer therapy. *Journal of Nanobiotechnology* **2007**, *5*, 3.

Brunisholz, G.; Randin, M. Sur la séparation des terres rares à l'aide de l'acide éthylènediamine-tétraacétique. IX. Procédé en cycle pour le fractionnement des terres yttriques. *Helvetica Chimica Acta* **1959**, *42*, 1927-1938.

Carvalho, J.; Goncalves, C.; Gil, A.M.; Gama, F.M. Production and characterization of a new dextrin based hydrogel. *European Polymer Journal* **2007**, *43*, 3050-3059.

Farokhzad, O.C.; Langer, R. Nanomedicine: developing smarter therapeutic and diagnostic modalities. *Advanced Drug Delivery Review* **2006**, *58*, 1456-1459.

Fernandez-Montesinos, R.; Castillo, P.M.; Klippstein, R.; Gonzalez-Rey, E.; Mejias, J.A.; Zaderenko, A.P.; Pozo, D. Chemical synthesis and characterization of silver-protected vasoactive intestinal peptide nanoparticles. *Nanomedicine (Lond)* **2009**, *4*, 919-930.

Gaumet, M.; Vargas, A.; Gurny, R.; Delie, F. Nanoparticles for drug delivery: the need for precision in reporting particle size parameters. *European Journal of Pharmaceutics and Biopharmaceutics* **2008**, *69*, 1-9.

Gonçalves, C.; Gama, F.M. Characterization of the self-assembly process of hydrophobically modified dextrin. *European Polymer Journal* **2008**, *44*, 3529-3534.

Gonçalves, C.; Martins, J.A.; Gama, F.M. Self-assembled nanoparticles of dextrin substituted with hexadecanethiol. *Biomacromolecules* **2007**, *8*, 392-398.

Gonçalves, C.; Torrado, E.; Martins, T.; Pereira, P.; Pedrosa, J.; Gama, M. Dextrin nanoparticles: studies on the interaction with murine macrophages and blood clearance. *Colloids and Surfaces B: Biointerfaces* **2010**, *75*, 483-489.

Gref, R.; Luck, M.; Quellec, P.; Marchand, M.; Dellacherie, E.; Harnisch, S.; Blunk, T.; Muller, R.H. 'Stealth' corona-core nanoparticles surface modified by polyethylene glycol (PEG): influences of the corona (PEG chain length and surface density) and of the core composition on phagocytic uptake and plasma protein adsorption. *Colloids and Surfaces B: Biointerfaces* **2000**, *18*, 301-313.

Hiemstra, C.; van der Aa, L.J.; Zhong, Z.Y.; Dijkstra, P.J.; Feijen, J. Novel in situ forming, degradable dextran hydrogels by Michael addition chemistry: Synthesis, rheology, and degradation. *Macromolecules* **2007**, *40*, 1165-1173.

Hunter, R.J. *Zeta Potential in Colloid Science*; Academic Press: New York, 1981.

Leary, S.P.; Liu, C.Y.; Apuzzo, M.L. Toward the emergence of nanoneurosurgery: part II--nanomedicine: diagnostics and imaging at the nanoscale level. *Neurosurgery* **2006**, *58*, 805-823.

Li, S.D.; Huang, L. Pharmacokinetics and biodistribution of nanoparticles. *Molecular Pharmacology* **2008**, *5*, 496-504.

Owens, D.E., 3rd; Peppas, N.A. Opsonization, biodistribution, and pharmacokinetics of polymeric nanoparticles. *International Journal of Pharmaceutics* **2006**, *307*, 93-102.

Peracchia, M.T.; Fattal, E.; Desmaele, D.; Besnard, M.; Noel, J.P.; Gomis, J.M.; Appel, M.; d'Angelo, J.; Couvreur, P. Stealth PEGylated polycyanoacrylate nanoparticles for intravenous administration and splenic targeting. *Journal of Controlled Release* **1999a**, *60*, 121-128.

Peracchia, M.T.; Harnisch, S.; Pinto-Alphandary, H.; Gulik, A.; Dedieu, J.C.; Desmaele, D.; d'Angelo, J.; Muller, R.H.; Couvreur, P. Visualization of in vitro protein-rejecting properties of PEGylated stealth polycyanoacrylate nanoparticles. *Biomaterials* **1999b**, *20*, 1269-1275.

Port, M.; Idee, J.M.; Medina, C.; Robic, C.; Sabatou, M.; Corot, C. Efficiency, thermodynamic and kinetic stability of marketed gadolinium chelates and their possible clinical consequences: a critical review. *Biometals* **2008**, *21*, 469-490.

Pressly, E.D.; Rossin, R.; Hagooly, A.; Fukukawa, K.; Messmore, B.W.; Welch, M.J.; Wooley, K.L.; Lamm, M.S.; Hule, R.A.; Pochan, D.J.; Hawker, C.J. Structural effects on the biodistribution and positron emission tomography (PET) imaging of well-defined (64)Cu-labeled nanoparticles comprised of amphiphilic block graft copolymers. *Biomacromolecules* **2007**, *8*, 3126-3134.

Shaikh, J.; Ankola, D.D.; Beniwal, V.; Singh, D.; Kumar, M.N. Nanoparticle encapsulation improves oral bioavailability of curcumin by at least 9-fold when compared to curcumin administered with piperine as absorption enhancer. *European Journal of Pharmaceutical Science* **2009**, *37*, 223-230.

Shan, X.; Liu, C.; Yuan, Y.; Xu, F.; Tao, X.; Sheng, Y.; Zhou, H. In vitro macrophage uptake and in vivo biodistribution of long-circulation nanoparticles with poly(ethylene-glycol)-modified PLA (BAB type) triblock copolymer. *Colloids and Surfaces B: Biointerfaces* **2009**, *72*, 303-311.

Shubayev, V.I.; Pisanic, T.R.; Jin, S.H. Magnetic nanoparticles for theragnostics. *Advanced Drug Delivery Reviews* **2009**, *61*, 467-477.

van Dijk, M.; Rijkers, D.T.; Liskamp, R.M.; van Nostrum, C.F.; Hennink, W.E. Synthesis and applications of biomedical and pharmaceutical polymers via click chemistry methodologies. *Bioconjugate Chemistry* **2009**, *20*, 2001-2016.

Weinstein, J.S.; Varallyay, C.G.; Dosa, E.; Gahramanov, S.; Hamilton, B.; Rooney, W.D.; Muldoon, L.L.; Neuwelt, E.A. Superparamagnetic iron oxide nanoparticles: diagnostic magnetic resonance imaging and potential therapeutic applications in neurooncology and central nervous system inflammatory pathologies, a review. *Journal of Cerebral Blood Flow and Metabolism* **2010**, *30*, 15-35.

Zhang, G.; Yang, Z.; Lu, W.; Zhang, R.; Huang, Q.; Tian, M.; Li, L.; Liang, D.; Li, C. Influence of anchoring ligands and particle size on the colloidal stability and in vivo biodistribution of polyethylene glycol-coated gold nanoparticles in tumor-xenografted mice. *Biomaterials* **2009**, *30*, 1928-1936.

7. Conclusions and Perspectives

The main purpose of the present work has been the development and characterization of self-assembled dextrin nanogels. Its potencial for biomedical applications was also accessed. The results obtained lead to the following main conclusions:

Dextrin can be modified by grafting long alkyl chains (16 carbons), an amphiphilic polymer (dexC_{16}) being obtained; the degree of substitution with hydrophobic chains can be controlled. DexC_{16} with DS_{C16} 7% has a critical micelle concentration around 0.01 mg/mL. A DS_{C16} in the range of 6.0-8.0% was assumed as ideal, since a lower DS_{C16} corresponds to a high CMC and a higher DS_{C16} does not facilitate the material manipulation, due to the low solubility. The aqueous dispersion of dexC_{16} results in spontaneous formation of nanoparticles colloidally stable (over 2 months), when the concentration of the polymer is higher than its critical micelle concentration. Nanoparticles have about 85–90 wt% of water and may thus be considered hydrogel-like structures: nanogels. The size distribution of self-assembled nanoparticles was evaluated by dynamic light scattering, after filtration through a 0.22 μm membrane. A general conclusion is achieved: two populations exist after self-assembly, with diameters of roughly 20 and 100 nm. Depending on which is the predominant one, the average diameter obtained vary between 20-60 nm.

The hydrophobic domains within dextrin nanoparticles, dispersed in water, allow curcumin dissolution with high entrapment efficiency and stability, using the appropriate polymer/curcumin ratio. Nanoparticles served as an effective ‘‘nanocarrier’’, by controlling curcumin release profile. Incorporation of curcumin into nanoparticles did not compromise its cytotoxicity in HeLa cell line. Therefore, dextrin nanoparticles hold promise as delivery system for the development of an injectable formulation of curcumin for the treatment of human cancers.

The study of interactions between macrophages and dextrin nanoparticles revealed that nanoparticles are non-cytotoxic and do not elicit a reactive response when in contact with macrophages. Otherwise nanoparticles are internalized by macrophages being concentrated in cellular organelles.

The blood clearance of dextrin nanoparticles studied after intravenous injection of fluorescein-labelled nanoparticles in BALB/c mice or radioactively labelled nanoparticles in Wistar rats showed that a relatively fast removal of the nanoparticles occurs in the first

3 h, then continuing slowly up to 24 h. For fluorescein-labelled nanoparticles, although the blood clearance of dextrin nanoparticles could be readily followed by fluorescence measurements, its organ distribution profile could not be evaluated, possibly due to quenching effects of the fluorescent probe in the organ´s homogenates. Functionalization of dextrin nanoparticles with a metal chelator allows the radioactive labelling of the nanoparticles. The labelling process has no significant effect on the nanoparticles size and surface charge; hence the biodistribution profile obtained is considered representative of the unmodified nanoparticles. This strategy combines a high sensitive detection technique with minor nanoparticle modifications. The dexC_{16} nanoparticles display a characteristic biodistribution profile, being mainly taken up by the organs of the mononuclear phagocytic system- liver and spleen. The surface coating of the nanoparticles with PEG 5,000 improves the circulation time in the blood and reduces the accumulation in the liver and spleen.

Therefore, dexC_{16} nanoparticles may be used to target phagocytic cells or antigen presenting cells for the treatment of macrophage-associated pathologies or vaccination purposes. Otherwise, when other targets are envisaged, dexC_{16} nanoparticles coated with PEG avoid phagocytic activity, improving the circulation time in the bloodstream therefore the probability to reach the target.

The following goals are proposed for future work:

- Subcutaneous injection of dextrin nanoparticles to evaluate accumulation in lymph nodes for vaccination purposes;
- Chemical crosslinking of dextrin nanoparticles using PEG dithiol to improve the mechanical stability;
- Explore the small size of dextrin nanoparticles for passive targeting of tumor tissues by the enhanced permeability and retention effect in xenografs rats;
- Incorporation of therapeutic proteins; it has been demonstrated that proteins are stabilized in the interior of the nanogels, therefore a comprehensive study of the interaction protein/nanogel is required;
- Analysis of the intracellular trafficking of nanoparticles, which will determine the kind of applications in the field of drug delivery.